**ISTANBUL TECHNICAL UNIVERSITY ★ GRADUATE SCHOOL**

# MODELING AND SENSITIVITY ANALYSIS THE THERMAL BEHAVIOUR OF MASS CONCRETE WITH FINITE VOLUME METHOD

**M.Sc. THESIS**

**Farzad DANAEI**

**Department of Civil Engineering**

**Structural Engineering Programme**

**MAY 2023**

**ISTANBUL TECHNICAL UNIVERSITY ★ GRADUATE SCHOOL**

# MODELING AND SENSITIVITY ANALYSIS THE THERMAL BEHAVIOUR OF MASS CONCRETE WITH FINITE VOLUME METHOD

**M.Sc. THESIS**

**Farzad DANAEI**
**(501201013)**

**Department of Civil Engineering**

**Structural Engineering Programme**

**Thesis Advisor: Prof. Dr. Yilmaz Akkaya**

**MAY 2023**

**İSTANBUL TEKNİK ÜNİVERSİTESİ ★ LİSANSÜSTÜ EĞİTİM ENSTİTÜSÜ**

# SONLU HACİM YÖNTEMİ İLE KÜTLE BETONUN ISIL DAVRANIŞININ MODELLENMESİ VE HASSASİYET ANALİZİ

**YÜKSEK LİSANS TEZİ**

**Farzad DANAEI**
**(501201013)**

**İnşaat Mühendisliği Anabilim Dalı**

**Yapı Mühendisliği Programı**

**Tez Danışmanı: Prof. Dr. Yilmaz Akkaya**

**Mayıs 2023**

Farzad DANAEI, a M.Sc. student of ITU Graduate School student ID 501201013 successfully defended the thesis entitled "MODELING AND SENSITIVITY ANALYSIS THE THERMAL BEHAVIOUR OF MASS CONCRETE WITH FINITE VOLUME METHOD", which he/she prepared after fulfilling the requirements specified in the associated legislations, before the jury whose signatures are below.

| | | |
|---|---|---|
| **Thesis Advisor :** | **Prof. Dr. Yilmaz Akkaya**<br>Istanbul Technical University | ..... |
| **Jury Members :** | **Prof. Dr. Öğr. Üyesi Oguz GUNES**<br>Istanbul Technical University | ..... |
| | **Prof. Dr. Öğr. Üyesi Tayfun Altuğ SÖYLEV**<br>Gebze Technical University | ..... |
| | | ..... |

**Date of Submission :** **08 July 2023**
**Date of Defense :** **16 June 2023**

***To my lovely mother, supportive father, and fantastic brother.***

## FOREWORD

I am pleased to present this thesis, which was written for my master's degree in Structural Engineering at the Istanbul Technical University with a focus on construction materials. In order to predict the temperature profile within concrete elements, the main goal of this research is to model the thermal behavior of mass concrete. The objective is to create a straightforward model that can make early predictions about the temperature of concrete over time using readily available inputs. For those conducting research or working in the construction industry who want to comprehend and predict the thermal behavior of concrete, this study will be essential. It will open the door for more thorough modeling using other data inputs by gaining preliminary insights. Additionally, a sensitivity analysis was carried out to provide a clearer understanding of the impact of various variables on the thermal behavior of mass concrete elements. I would like to use this chance to convey my sincere gratitude to everyone who has helped me along the way. First of all, let me express my sincere gratitude to Prof. Dr. Yilmaz Akkaya for his assistance, insightful reviews, and helpful suggestions. His knowledge and commitment played a key role in the development of this study. Additionally, I want to express my appreciation to Bursa Beton Factory for kindly giving their experimental data, which was crucial to the development of this thesis. I' would also like to mention my family and thank them for their tireless support and encouragement. They have consistently inspired me to overcome obstacles and persevere throughout this difficult academic effort because they have faith in my talents.

18 May 2023 Farzad DANAEI

**TABLE OF CONTENTS**

**ABBREVIATIONS**

| | |
|---|---|
| **SCMs** | **:** Supplementary Cementitious Materials |
| **GGBFS** | **:** Ground Granulated Blast-Furnace Slag |
| **GGBS** | **:** Ground Granulated Blast Slag |
| **HPC** | **:** High Performance Concrete |
| **ACI** | **:** American Concrete Institute |
| **C-S-H** | **:** Calcium Silicate Hydrate |
| **C2S** | **:** Dicalcium Silicate |
| **C3S** | **:** Tricalcium Silicate |
| **C3A** | **:** Tricalcium Aluminate |
| **C4AF** | **:** Tetracalcium Aluminoferrite |
| **MHPC** | **:** Moderate Heat Portland Cement |
| **LHPC** | **:** Low Heat Portland Cement |
| **GU** | **:** General Used Cement |
| **HE** | **:** High Early Strength Cement |
| **ASTM** | **:** American Society for Testing and Materials |
| **AASHTO** | **:** American Association of Highway and Transportation Officials |
| **XRD** | **:** X-Ray Diffraction |
| **EPS** | **:** Expanded Polystyrene Insulation |
| **XPS** | **:** Extruded Polystyrene Insulation |
| **APDL** | **:** Algorithmic Processor Description Language |

## SYMBOLS

| | |
|---|---|
| **w/c** | : Water to cement ratio |
| $\mathbf{H_{cem}}$ | : Total heat of hydration of portland cement |
| $\mathbf{H_u}$,$\mathbf{Q_u}$ | : Torque Components |
| $\rho$ | : Density |
| **c**, $\mathbf{C_p}$ | : Specific heat capacity |
| $\rho$**c** | : Volumetric specific heat |
| **T** | : Temperature |
| **t** | : Time |
| $\dot{Q}$ | : Transfer heat rate |
| **P** | : Losted heat |
| **M** | : Maturity |
| $\mathbf{T_r}$ | : Average concrete temperature during the $\Delta T$ |
| $\mathbf{T_0}$ | : Datum temperature |
| **K(T)** | : Rate constant |
| $\mathbf{E_a}$ | : Activation Energy |
| **R** | : The gas constant |
| $\mathbf{t_e}$, $\tau_{\mathbf{ns}}$ | : Equivalent age |
| $\mathbf{T_i}$ | : Average concrete temperature for the period of $\Delta T_i$ |
| $\mathbf{T_r}$ | : Reference temperature |
| $\mathbf{f_E}$ | : Activation energy modification factor |
| $\alpha$ | : Degree of hydration |
| $\mathbf{H_t}$,$\mathbf{Q_t}$ | : Total generated heat until time t |
| $\alpha_{\mathbf{u}}$ | : Ultimate degree of hydration |
| $\tau$ | : Time parameter |
| $\beta$ | : Slope paramete |
| $Q\prime$ | : Total generated heat until time t |
| **k** | : Thermal conductivity of conctere |
| $\mathbf{k_r}$ | : Thermal conductivity of soil |
| $\delta_{\mathbf{t}}$ | : Time period |
| $\mathbf{h_f}$ | : Equivalent convection coefficient |
| $\mathbf{h_a}$ | : Convection coefficient |
| $\mathbf{T_a}$,$\mathbf{T_A}$ | : Ambient temperature |
| $Q\prime_{\mathbf{M}}$ | : Maturity heat rate |
| $Q\prime_{\mathbf{t}}$ | : Temporal heat rate |
| $\gamma$**(T)** | : Affinity ratio |
| **q(t)** | : Generated heat rate at time t |
| $\mathbf{q_a}$ | : Convective heat flow per unit area between concrete and air |
| **v** | : Wind speed |
| $\mathbf{T_c}$ | : Surface temperatures of the concrete |
| $\mathbf{h_r}$ | : Radiation exchange coefficient |
| $\varepsilon$ | : Emissivity parameter |
| $\mathbf{t_w}$ | : The time when the minimum temperature occurs |

## LIST OF TABLES

## LIST OF FIGURES

**MODELING AND SENSITIVITY ANALYSIS**
**THE THERMAL BEHAVIOUR OF MASS CONCRETE**
**WITH FINITE VOLUME METHOD**

## SUMMARY

Concrete is one of the most widely used materials in the world, second only to water. As the population grows and available land becomes limited, there is a growing need for large structures such as dams and bridges and towers to meet the demands of water management, transportation, and accommodation. To ensure the strength and durability of these structures, high-performance concrete is often used. However, a major challenge in such concrete structures is thermal cracking, which occurs due to temperature gradients within the concrete.

Concrete has low thermal conductivity, meaning that heat does not dissipate quickly throughout the material. As a result, the outer layer of concrete cools faster than the inner layer, creating thermal gradients. These temperature differences cause differential thermal expansion, if there is no restriction for these movements, there is no problem. But as soon as these movements are stopped by internal or external restrictions, the development of stress will start. When these stresses exceed the tensile strength of the concrete, cracks form. These cracks can result in issues such as water penetration, reduced structural integrity, durability problems (such as corrosion of embedded reinforcement), and aesthetic concerns. Different standards define limitations on the maximum temperature reached within concrete and the maximum temperature gradient within concrete elements, in Turkish standards (TS 13515 ) these limitations are 65 C and 25 C respectively. These specifications are designed to minimize the risk of thermal cracking by ensuring that concrete structures are maintained within safe temperature ranges throughout their service life.

The finite volume modeling technique is used in the current model, which was developed in Python. The concrete element is separated into nodes in this manner, and for each node, a control volume according to its location is considered. Convection and conduction are taken into account as boundary conditions in the model, with the flexibility to include other heat transfer processes such as radiation and solar loads. Additionally, an equivalent convection coefficient is derived and employed in the model to account for the impact of formwork and insulation using the analogy of electrical resistance. The governing equation, which is developed from energy balance principles, is then applied to each node. This energy balance takes into consideration all of the energy that enters, is produced, is lost, and is stored inside the concrete. The present model is capable of accepting the ambient temperature using a predictive method, or it may also take actual temperature-time histories as input to improve its accuracy and dependability.

The model incorporates the concept of maturity and calculates the heat generated during cement hydration using the Arrhenius maturity function. To simulate the

heat generation, Schindler's S-shaped function is employed, requiring curve fitting techniques to determine two important hydration parameters: the slope parameter and time parameter. Unlike previous models that use a single set of hydration parameters, which fails to capture the behavior of blended cement, the current model addresses this limitation by utilizing the superposition of two S-shaped functions. This approach accurately catch all the points on the released heat curve for blended cement. By considering the behavior of blended cement, the model effectively captures the heat generation characteristics. From the S-shaped function, the generated heat rate function can be easily obtained. Additionaly, the model has the capability to accept the generated heat rate as an input. Accurately determining the generated heat rate function is crucial in simulating the thermal behavior of mass concrete, ensuring that the model accurately represents the actual heat generation process.

During the experimental phase, data obtained from the Bursa Beton factory was employed. In Chapter 3 of the thesis, the experiment setup is described in detail, and the resulting outcomes are presented. This particular chapter focuses on investigating the impact of insulation on the temperature gradient within the concrete, as well as the influence of different concrete mixtures. The analysis of the collected data revealed noteworthy findings. When a thick layer of insulation was applied around the concrete, the temperature development recorded by the thermocouples placed inside the concrete exhibited similar behavior on both the right and left sides. However, in cases where no insulation was present and the concrete samples were exposed to the environment, distinct temperature profiles were observed between the right and left side sensors. This disparity in temperature can be attributed to the microclimate effect, which includes factors such as wind speed and solar loading on the concrete surface. It is worth noting that this effect has often been overlooked in previous models.

The model has been developed in both 2-D and 3-D. The 3-D version is validated by simulating Bursa Beton samples and comparing the findings with experimental data, whereas the 2-D model is validated by comparing its results with the Ballims model. The 3-D model is additionally validated using data from a study carried out at West Virginia University. The model constantly exhibits sufficient accuracy in every validation instance, creating trust in its abilities and allowing sensitivity analysis to be carried out.

Additionally, a sensitivity analysis is carried out to examine the impact of different variables on the temperature profile of mass concrete. The initial temperature of the concrete, the size of the concrete element, and the usage of supplemental cementitious materials (SCMs) in place of cement in blended cement are among the changes that have been taken into consideration. The results of the analysis show that the final temperature profile is significantly influenced by both the initial temperature and the size of the concrete part. However, the addition of SCMs to the concrete mixture lessens this sensitivity, especially when fly ash is used instead of some part of cement. Furthermore, when considering the utilization of different replacement levels of supplementary cementitious materials (SCMs), the findings demonstrate significant reductions in both the maximum temperature and maximum temperature gradient within the concrete. The results indicated that the usage of fly ash led to a greater reduction in the maximum temperature and temperature gradient compared to using

GGBFS. Additionally, the presence of GGBFS resulted in a delay in the time required for the concrete to reach its maximum temperature. This suggests that adding fly ash to mass concrete lessens its sensitivity to changes in size while at the same time reducing the maximum temperature and thermal gradient inside the concrete.

Furthermore, the degree of hydration affects the thermal properties of concrete, including its thermal conductivity and specific heat capacity. As the hydration reaction advances, the amount of available water or moisture inside the concrete drops, which causes a decrease in thermal conductivity and specific heat capacity. In earlier models, these thermal properties were frequently assumed to have constant values. A sensitivity analysis comparing the modeling results with constant thermal properties to those considering variations with hydration reveals that assuming constant specific heat capacity significantly impacts the final results. However, assuming a constant thermal conductivity does not cause substantial changes.

In conclusion, the developed model offers a simple yet effective approach to predict the temperature distribution within concrete elements using the finite volume method. It accounts for various boundary conditions, considers the generation of heat during cement hydration, and incorporates the behavior of blended cement using a superposition of S-shaped functions. The model's accuracy is validated through comparisons with experimental data and existing models. Sensitivity analysis provides insights into the influence of different parameters and variations on the temperature profile. By addressing the thermal cracking issue, the model contributes to ensuring the safety, durability, and cost-effectiveness of concrete structures.

# SONLU HACİM YÖNTEMİ İLE KÜTLE BETONUN ISIL DAVRANIŞININ MODELLENMESİ VE HASSASİYET ANALİZİ

## ÖZET

Beton, su hariç dünyada en yaygın kullanılan malzemelerden biridir. Nüfus arttıkça ve kullanılabilir arazi sınırlı hale geldikçe enerji, ulaştırma ve iskan gibi talepleri karşılamak için barajlar, köprüler, gökdelenler gibi büyük yapılar için giderek daha fazla ihtiyaç duyulmaktadır. Bu yapıların dayanıklılığını ve sağlamlığını sağlamak için genellikle yüksek performanslı beton kullanılır. Ancak, bu tür beton yapıların önemli bir sorunu beton içindeki sıcaklık farklarından kaynaklanan ısıl çatlaklardır.

Betonun ısıl iletkenliği düşüktür, bu da ısıyı malzeme içinde hızlı bir şekilde dağıtamadığı anlamına gelir. Sonuç olarak, betonun dış yüzeyi iç kısıma göre daha hızlı soğur ve bu da ısıl farklar oluşturur. Bu sıcaklık farkları, betonun içindeki hareketi kısıtlayan iç veya dış kısıtlar olmadığı sürece diferansiyel ısıl genleşmeye neden olur. Bu gerilmeler, kısıtlanmış haldeki betonun çekme dayanımını aştığında çatlaklar oluşur. Bu çatlaklar su girişi, yapısal bütünlük, dayanıklılık (gömülü donatının korozyonu gibi) ve estetik endişelere neden olabilir. Farklı standartlar, beton içinde maksimum sıcaklığı ve beton elemanları içindeki maksimum sıcaklık farklarını sınırlamak için çeşitli kısıtlamalar belirler. TS 13515 standartına göre, bu sınırlamalar sırasıyla 65 °C ve 25 °C'dir. Bu özellikler, beton yapıların hizmet ömrü boyunca güvenli sıcaklık aralıklarında tutulmasını sağlayarak ısıl çatlamaların riskini en aza indirmek için tasarlanmıştır.

Kullanılan hesaplamalı yöntem, Python'da geliştirilmiş olan sonlu hacim modelleme tekniğine dayanmaktadır. Beton eleman, düğüm noktalarına ayrılır ve her düğüm için konumuna bağlı olarak bir kontrol hacmi dikkate alınır. Sınır koşulları olarak konveksiyon ve iletkenlik dikkate alınırken, modelde radyasyon ve güneş yüklerini de içeren diğer ısı transfer süreçlerini eklemek mümkündür. Ayrıca, bir eşdeğer konveksiyon katsayısı türetilir ve modelde kalıp ve yalıtımın etkisi, elektrik direnci benzeşimi kullanılarak hesaba katılabilir. Enerji dengesi prensiplerinden geliştirilen yönetici denklem daha sonra her düğüme uygulanır. Bu enerji dengelemesi, betonun içine giren, üretilen, kaybedilen ve depolanan tüm enerjiyi dikkate alır. Mevcut model, tahmini bir yöntem kullanarak ortam sıcaklığını varsayım olarak kabul edebilme özelliğine sahiptir. Gerçek sıcaklık-zaman verisi girilerek doğruluk ve güvenilirlik artırabilir.

Model, olgunlaşma kavramını içerir ve Arrhenius olgunlaşma fonksiyonunu kullanarak çimento hidrasyonu sırasında oluşan ısıyı hesaplar. Isı oluşumunu simüle etmek için Schindler'in S-şekilli fonksiyonu kullanılır ve iki önemli hidrasyon parametresini belirlemek için eğri uydurma teknikleri gerektirir: eğim parametresi ve zaman parametresi. Daha önceki modellerde genellikle tek bir set hidrasyon

parametresi kullanıldığından, bu, katkılı çimento davranışını yakalamada başarısız olur. Mevcut model, iki S-şekilli fonksiyonun süperpozisyonunu kullanarak bu kısıtlamayı ele alır. Bu yaklaşım, katkılı çimentonun serbest bırakılan ısı eğrisindeki tüm noktaları doğru bir şekilde yakalar. S-şekilli fonksiyondan elde edilen ısı hızı fonksiyonu kolayca elde edilebilir ve model ayrıca oluşturulan ısı hızını giriş olarak kabul etme yeteneğine sahiptir. Oluşturulan ısı hızı fonksiyonunu doğru bir şekilde belirlemek, kütle betonunun termal davranışını simüle etmek için önemlidir ve modelin gerçek ısı oluşum sürecini doğru bir şekilde temsil etmesini sağlar.

Deneysel aşamada, Bursa Beton tesislerinden elde edilen veriler kullanılmıştır. Tezin 3. bölümünde deney kurulumu detaylı bir şekilde açıklanmış ve elde edilen sonuçlar sunulmuştur. Bu bölüm, beton içindeki sıcaklık gradyanı üzerinde yalıtımın etkisini ve farklı beton karışımlarının etkisini araştırmaya odaklanmaktadır. Toplanan verilerin analizi dikkate değer bulgular ortaya koymuştur. Beton etrafına kalın bir yalıtım tabakası uygulandığında, beton içine yerleştirilen ısıl-çiftler tarafından kaydedilen sıcaklık gelişimi, elemanın sağ ve sol tarafında benzer bir davranış sergilemiştir. Bununla birlikte, yalıtımın olmadığı durumlarda ve beton örnekleri çevre koşullarına maruz kaldığında, sağ ve sol taraftaki sensörler arasında belirgin sıcaklık profilleri gözlemlenmiştir. Bu sıcaklık farkı, beton yüzeyindeki rüzgar hızı ve güneş yükü gibi faktörleri içeren mikro iklim etkisine bağlı olabilir. Bu etki, daha önceki modellerde de sıklıkla göz ardı edilmiştir.

Model, 2-D ve 3-D olarak geliştirilmiştir. 3-D versiyon, Bursa Beton örneklerinin simülasyonunu yaparak eldeki deneysel verilerle karşılaştırılarak doğrulanmıştır, 2-D model ise Ballims modeliyle sonuçlarını karşılaştırarak doğrulanmıştır. 3-D model ayrıca West Virginia Üniversitesi'nde yapılan bir çalışmanın verileri kullanılarak doğrulanmıştır. Model her doğrulama örneğinde yeterli doğruluk sergilemektedir, bu da modelin yeteneklerine güven oluşturur ve hassasiyet analizinin yapılmasını sağlar.

Ayrıca, farklı değişkenlerin kütle betonunun sıcaklık profili üzerindeki etkisini incelemek için bir hassasiyet analizi yapılmıştır. Betonun başlangıç sıcaklığı, beton elemanının boyutu ve çimentonun yerine ek mineral katkı maddeleri kullanma gibi değişiklikler dikkate alınan değişiklikler arasındadır. Analizin sonuçları, son sıcaklık profili üzerinde hem başlangıç sıcaklığının hem de beton parçasının boyutunun önemli ölçüde etkili olduğunu göstermektedir. Ancak, beton karışımında çimento yerine mineral katkıların eklenmesi bu duyarlılığı azaltmaktadır. Özellikle bir kısım çimentonun yerine uçucu kül kullanıldığında bu durumla karşılaşılmaktadır. Ayrıca, farklı takviye düzeylerinin kullanımını dikkate aldığımızda, sonuçlar maksimum sıcaklık ve beton içindeki maksimum sıcaklık farkında önemli azalmalar göstermektedir. Özellikle uçucu kül ve yüksek fırın cürufunun kullanımı dikkate değer etkiler ortaya çıkarmıştır. Sonuçlar, uçucu kül kullanımının maksimum sıcaklık ve sıcaklık gradyanında daha büyük bir azalmaya yol açtığını göstermiştir. Ayrıca, yüksek fırın cürufunun varlığı, betonun maksimum sıcaklığa ulaşması için gereken sürenin gecikmesine neden olmuştur.

Sonuç olarak, geliştirilen ısıl beton davranış modeli, beton yapıların ısıl performansını analiz etmek için kullanılabilir ve ısıl çatlakların riskini azaltmak için tasarım ve yapım süreçlerinde rehberlik sağlar. Ayrıca, farklı değişkenlerin ısıl davranış üzerindeki etkisini değerlendirmek ve optimize etmek için kullanılabilir. Bu model, beton

yapıların dayanıklılığını artırmaya ve uzun ömürlü olmalarını sağlamaya yönelik daha iyi tasarım ve inşaat yöntemleri geliştirme çabalarını desteklemektedir.

# 1. INTRODUCTION

## 1.1 Background

Concrete has become an indispensable material in Turkey, particularly in recent years, as the country witnesses a significant surge in infrastructure projects. The construction industry relies heavily on the use of concrete due to its versatility, durability, and cost-effectiveness. With the growing need for new buildings, bridges, roads, and other structures such as dams, Demand for concrete with high strength and remarkable durability has significantly increased, indicating a growing need across the country. To address these issues, high-performance concrete (HPC) mixtures have become prevalent in the construction industry. HPC mixes often incorporate supplementary cementing materials (SCMs) and are composed of optimized mix designs, high-quality ingredients, and produced according to industry requirements. These mixes typically have higher strengths than normal concretes, making them suitable for applications requiring high strength, durability, and performance requirements such as abrasion resistance, permeability, and high early strength. However, the increased utilization of HPC mixes also poses design challenges, such as the need for strict curing procedures and large amounts of chemical admixtures that can lead to issues such as loosing slump or early-age cracking due to the high heat generated during the hydration process. Furthermore, HPC mixes are prone to early-age cracking because of the temperature gradient within the concrete element during the hydration process. Overall, the successful implementation of HPC in construction projects requires careful attention to mix design and adherence to industry standards. [8]

According to recent studies, thermal stresses that were previously only a concern for designers of large concrete dams are now considered a major cause of early-age cracking in high-performance concrete (HPC) structures. This is particularly problematic for HPC structures such as concrete pavements, roller compacted concrete,

and large concrete elements and foundations, as they generate high levels of heat during the early stages of development to achieve high strength quickly. Heat generation can produce temperature gradients inside the structure, resulting in internal tensile strains that, if not handled properly, might cause cracking. If left ignored, such cracks can significantly reduce the long-term durability and performance of the structure, leading to substantial costs for the contractor if the affected section must be fully replaced. This may be the case for concrete highways and bridge decks and any kind of concrete element which faces these kinds of problems.

A significant temperature difference between the center and surface can be produced by the external heat loss from the surface of the element and generated heat inside the concrete body which can not be dissipated easily. Due to non-uniform thermal expansion, the temperature difference can result in significant tensile strains on the concrete surfaces. The term "thermal stresses" or "thermally induced stresses" is frequently used to describe these surface tensile stresses. When the concrete strength is not fully developed, the thermal stress can be greater than the tensile strength and result in thermal cracking (Figure 1.1)

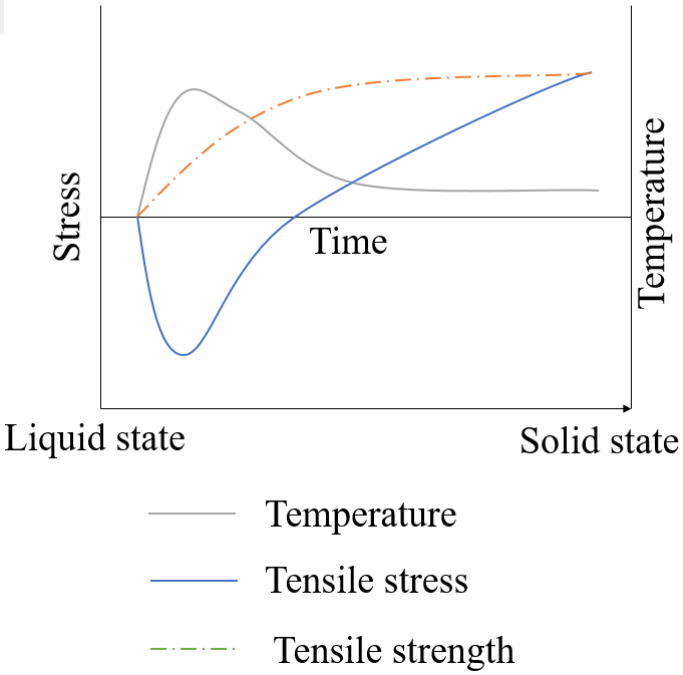


**Figure 1.1 :** Generalized temperature and stress development in early-age concrete [1]

Mass concrete is a term used for larger concrete members that are prone to heat cracking. Defining the minimum size of mass concrete is a significant challenge because thermal stress is unpredictable. When concrete undergoes temperature variations, it undergoes expansion and contraction. Thermal stresses are generated when these movements are restricted due to either internal volume restraint or external restraint. External restraint occurs when there is friction between new concrete and an existing block or when a long wall structure is anchored to the ground, and any thermal cracking that occurs near it is typically caused by external restraint (Figure 1.2). However, in larger concrete members, the effect of internal volume restraint may be more prominent due to different hardening speeds in various parts of the element. The American Concrete Institute ACI 207 defines mass concrete as any concrete volume large enough to require measures to minimize cracking due to heat generation from cement hydration and attendant volume change, without providing any specific dimensions for mass concrete. [9]

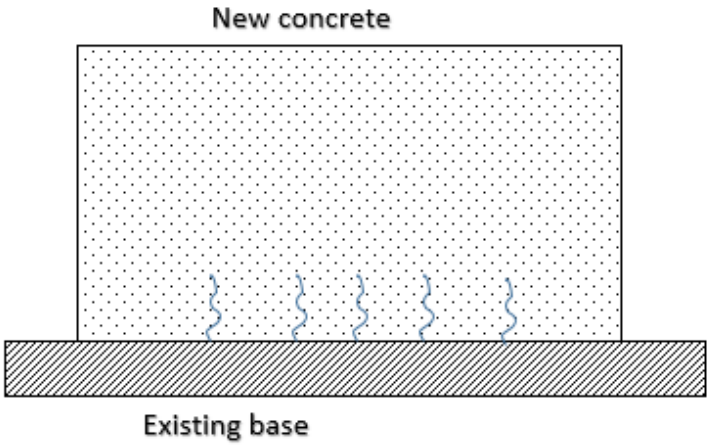


**Figure 1.2 :** External restraint.

To address these issues, engineers have developed innovative techniques to monitor and control the temperature gradient during the curing process. One such technique involves using cooling pipes or heat exchangers to remove excess heat from the concrete [10]. These systems can help prevent temperature gradients from forming and reduce the risk of thermal cracks. Another technique is to use low-heat cement, which generates less heat during the hydration process than traditional cement [9]. Another approach to lowering the maximum temperature in concrete is through the use

of pre-cooling techniques, which can reduce the maximum temperature of the concrete mixture.

Other techniques used in Turkey include monitoring the temperature of the concrete during the curing process and using insulation materials to help regulate the temperature gradient [11]. To monitor the temperature of the concrete, engineers use embedded temperature sensors or thermal imaging cameras. Insulation materials such as polystyrene foam or straw can be used to cover the surface of the concrete and reduce the heat loss from the surface, which helps to reduce temperature gradients.

In conclusion, while mass concrete is a valuable construction material, it presents unique challenges in hot and dry climates such as those found in Turkey. The temperature gradient control during the curing process is of utmost importance to prevent thermal cracks and ensure the durability and safety of the structure. With the development of innovative techniques and continued research, it is likely that these challenges will be overcome, and the use of mass concrete will continue to be a popular and effective choice for large-scale infrastructure projects in Turkey and beyond.

## 1.2 Purpose of Thesis

The necessity for an accurate prediction of the interior temperature increase of a concrete structure before the construction stage is the key problem that this work seeks to address. The predictions should be based on knowledge of the materials employed, as well as the placement and curing situation to which the structure will be subjected. The model should also be quick and accessible to a wide variety of users, regardless of their level of technical skill.

The goal of this research is to provide a straightforward thermal modeling program that may be employed to foresee the rise in temperature inside concrete constructions. The theoretical model that Dr. Anton Schindler created and Dr. Kevin Folliard subsequently improved will serve as the foundation for this concept. Real-world test results and comparisons with earlier 2-D and 3-D models will both be used to verify the model. Data from semi-adiabatic heat conduction calorimetry will be used in the testing procedure.

There are several software options available to analyze the temperature within concrete elements, including Concrete Works. However, a lot of these solutions might be challenging to use and need for in-depth understanding of the underlying concepts. Furthermore, there exist models that rely on finite element software like ANSYS or ABAQUS, which necessitate a drawing phase and the manual creation of elements, resulting in a time-intensive modeling process. [12] This project with the help of Python and an easy process aims to create a user-friendly simulation that provides an approximate estimate of the expected results with simple inputs. It can help users determine the temperature within the concrete element over time and identify potential solutions. Its goal is to give customers a simple tool to help them decide whether a more in-depth investigation is required rather than to replace already available solutions.

The simulation was developed using Python 3.10.10 with six main design objectives in mind. These objectives were set to guide and define the scope of the simulation's development, and include:

1. Regardless of a user's level of technical expertise, the simulation should be easy to use and accessible to a wide variety of users.

2. The results of the simulation should be consistent with the results of more detailed thermal analysis programs.

3. The simulation should be capable of performing a sensitivity analysisto see how changing the input parameters would affect the outcomes.

4. The simulation should be flexible enough to allow for the analysis of concrete elements with different sizes, however, it is not suitable for analyzing different shapes of elements.

5. The simulation should be able to handle changes in temperature conditions during the curing period.

6. The simulation should be able to consider the effects of external heat sources and heat losses from the concrete element's surface, also it should be ready to accept any kind of boundary conditions.

Simulations developed using MATLAB and Excel have been useful in predicting temperature variations in concrete structures. However, these simulations have limitations that can reduce their accuracy. For instance, two-dimensional modeling may not accurately represent the complexities of three-dimensional construction projects. Furthermore, simplifying assumptions are often made in previous simulations, which fail to capture the real-world behavior of concrete structures. An example of such simplification is the averaging of temperature at corner nodes in previous models, which may not accurately represent the actual behavior of concrete structures. To address these limitations, a new simulation approach has been developed that considers three-dimensional modeling and includes the real-world complexities of concrete construction projects, without increasing the computational time. This approach avoids extra simplifying assumptions and considers real situations at each point, including corner nodes, to provide more accurate predictions of temperature variations during the construction process.

In conclusion, The aim of this work is to overcome the limitations of previous simulations and improve the design and construction of concrete structures by providing more precise temperature predictions. The simulation is based on a theoretical model developed by Dr.Schindler and Dr.Folliard. The four major design goals for the simulation include providing estimates of maximum internal concrete temperature, having a simplified set of inputs, allowing the user to override inputs, and providing aid in interpreting results. The end-users for the simulation are cement and concrete manufacturing companies as well as consulting engineers. The development of the model will take into consideration these goals and end-users to ensure it meets the goals of the project.

## 2. LITERATURE REVIEW

According to [13], concrete cracking due to early-age thermal stresses has been a persistent issue since the early 1900s, leading to significant research into the problem over the years. Yoshida made the first attempt to estimate the hydration temperatures of concrete in 1921, and Rastrup created one of the earliest hydration simulations in the 1950s that took temperature and hydration level into account. In the late 1960s, efforts were made to quantify the level of generated thermal stresses in relation to the development of concrete's early tensile strength, as stated by [14]. However, these predictions faced two major challenges. Firstly, Measuring thermal stress in concrete during its early stages, when it undergoes the transition from a semi-liquid to a solid form, poses challenges. In addition, conventional methods were unable to determine the restraint stresses, resulting in a lack of data to confirm the stress calculations.

In recent time, a lot of study has been done on the possibility of thermal cracking in concrete elements and the prediction of heat rise. The impact of additional cementing ingredients on the hydration of concrete has been the subject of numerous studies, as this topic has not previously received much attention. Other research has proposed hydration models that allow for detailed thermal analyses of concrete elements, using various computer-based techniques. Furthermore, the temperature sensitivity of cementitious systems has been widely discussed, with numerous papers on the increasing use of calorimetry for hydration analysis.

To predict heat rise in concrete elements, three critical factors must be considered. First, it's important to understand the element's overall heat of hydration generation and its speed of occurrence. Second, it's important to understand how the concrete mix develops its strength. Finally, the element's physical configuration, size, and boundary conditions must all be taken into consideration. While this explanation is simplified, each factor is much more complex than its brief description suggests. Nonetheless, they provide a useful framework for organizing discussions on the topic.

## 2.1 Portland Cement Hydration process

According to Neville (1995), when cement is mixed with water, a complex series of exothermic reactions known as cement hydration occurs, releasing up to 500 Joules of energy per gram of cement. This can create high thermal gradients due to concrete's poor heat conductivity. The primary reactions involve the dicalcium and tricalcium silicates, which react with water to form calcium silicate hydrates (C-S-H) and hydrated lime. The resulting C-S-H paste makes up around %50 to %60 of the hydrated paste's volume and plays a crucial role in determining concrete's strength and durability. The exact composition of the C-S-H paste can vary depending on several factors, but it is not considered critical for the purpose of this thesis.

Reaction 1 : $C_2S + Water \rightarrow C-S-H + Ca(OH)_2$

Calcium hydroxide can react with fly ash to form more C-S-H paste, which results in denser concrete.

Reaction 2 : $Ca(OH)_2 + Flyash + Water \rightarrow C-S-H + (Otherreactionproducts)$

Secondary reactions involving tricalcium aluminate and tetracalcium aluminoferrite can act as catalysts but may cause flash sets without proper control. Ettringite is produced when tricalcium aluminate reacts with gypsum and water, while mono sulfate is formed when ettringite is converted entirely.

Reaction 3 : $C_3A + Gypsum + Water \rightarrow Ettringite$

Reaction 4 : $C_3A + Ettringite + Water \rightarrow Monosulfate$

Any remaining tricalcium aluminate will react with water to form calcium aluminate hydrate (C-A-H). [3]

Reaction 5: $C_3A + Water \rightarrow C-A-H$

### 2.1.1 Reaction Stages

The reactions in concrete occur in five stages, which are depicted in Figure 2.1. These stages have been identified and discussed by researchers such as D'Aloia and Mindess et al. [15] [16], in terms of heat release and temperature development, stage three is the most critical of them.

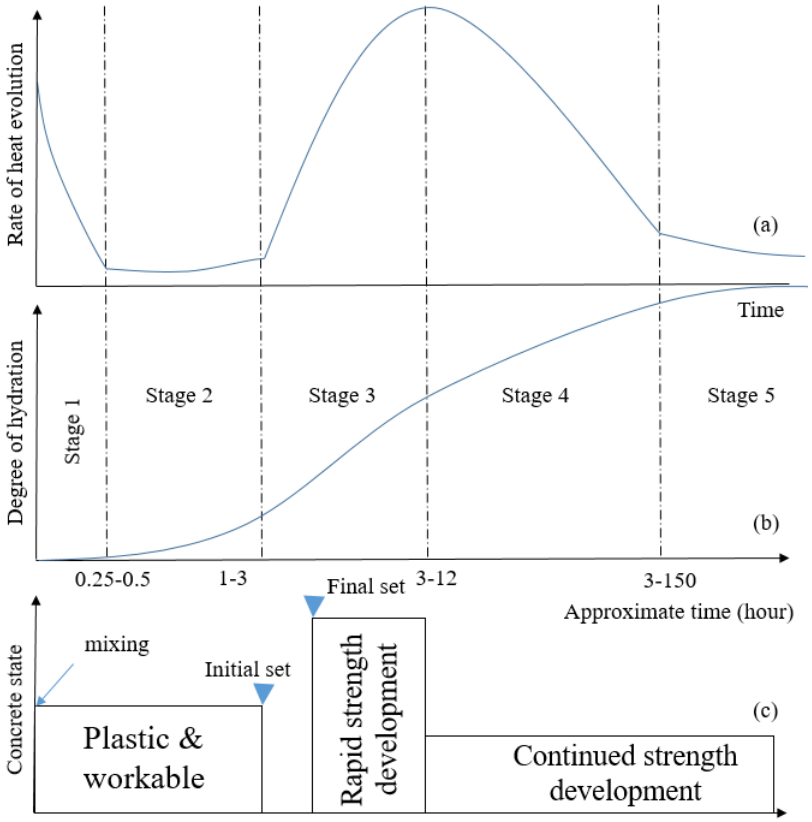


**Figure 2.1 :** Reaction phases of the hydration of cement. [2]

The initial phase of the usual concrete reaction series begins immediately after the cementitious materials are mixed with water. This phase is distinguished by a rapid evolution of heat, which is accompanied by a short-lived but significant increase in the speed of heat rise. The primary reason for this heat is the interaction between $C3A$ and gypsum, as illustrated by *Reaction*4. The formation of ettringite decreases when the amount of accessible gypsum is used up, causing the start of the inactive phase. While the $C2S$ and $C_3S$ also start to react during this stage, their impact on heat production is relatively minimal.

The temperature of the concrete may be significantly affected by this initial phase of fast heat evolution. However, because the reactions happen quickly, this stage often occurs in a ready-mix truck or concrete batch mixer, and therefore mainly affects the placement temperature of the concrete rather than its long-term properties [2].

Stage two is marked by a comparatively slow reaction rate, commonly known as the onset time, during which the concrete remains workable and can be placed. Throughout this stage, the concentration of calcium and hydroxide ions gradually

increases until it reaches a critical value. Once this key value is attained, The transition to stage three can be detected by the quick reaction between $C3S$ and $C3A$. Stage three typically lasts one to three hours at usual placing temperatures and is characterized by the process's maximum rate of hydration. $C_3A$ reacts again, producing additional ettringite until all the gypsum is consumed. After the start of stage three, the concrete sets quickly, which leads to a period of fast strength growth. However, the concrete is now too immature and brittle to withstand heavy loads without endangering the $C-S-H$ matrix. Stage three might take anywhere from three to twelve hours or more, depending on the mix.

During stage four, the rate of hydration slows down significantly compared to the previous stage, resulting in a slower rate of heat evolution. This is because most of the $C_3S$ and $C_3A$ have already reacted, and the remaining $C_2S$ reaction is slower. This stage is characterized by ongoing strength gain as the $C-S-H$ gel continues to densify and the concrete gains compressive strength. The rate of strength gain during this stage is much slower than during stage three, and it can take up to several days for the concrete to reach its final strength. The length of this stage depends on the composition of the concrete and the curing conditions, with higher temperatures and increased moisture accelerating the process.

The fifth and final stage of the hydration process represents the establishment of a stable condition in the concrete matrix. At this point, the majority of the materials that undergo hydration have reacted, leaving only the slower pozzolanic reactions to produce additional $C-S-H$ from calcium hydroxide. This phase will result in some further strength gain, and the concrete is going to continue to strengthen and acquire resistance to external forces. [2].

## 2.2 Factors Influencing Hydration

The amount and kind of cement used, the water-cement ratio, the curing temperature and exposure, and the use of SCMs are only a few of the variables that affect how well concrete hydrates. Another crucial element is the fresh concrete's temperature at the time of placement. While the temperature of the mix can be adjusted through various methods, such as using ice chips, cooling the aggregate, or applying liquid nitrogen,

most of the other factors are predetermined and addressed through modifications to the mix design. [2] In the subsequent sections, we will focus on three of the primary factors that impact concrete hydration in greater detail.

### 2.2.1 Cement Type

The type of cement used has a significant impact on the amount of heat generated during hydration. The various calcium compounds present in cement have different reactions, leading to a difference in the overall heat of hydration which is explained more in section 2.3. About two-thirds of the total heat of hydration in ordinary kinds of cement is produced by the hydration of $C_3S$. This is largely due to the demand for high early strengths in the construction industry, which has led to high $C_3S$ content in modern cement. $C_3A$ is the second-largest contributor to the overall heat of hydration. Figures 2.22 and Figure 2.3, respectively, depict the impact of $C_3S$ and $C_3A$ content on heat development. Additionally, the usual trend of the heat of hydration for various types of cement is shown in Figure 2.4. Therefore, selecting cement with lower concentrations of $C_3S$ and $C_3A$ and higher concentrations of $C_2S$ can aid in reducing heat from hydration.

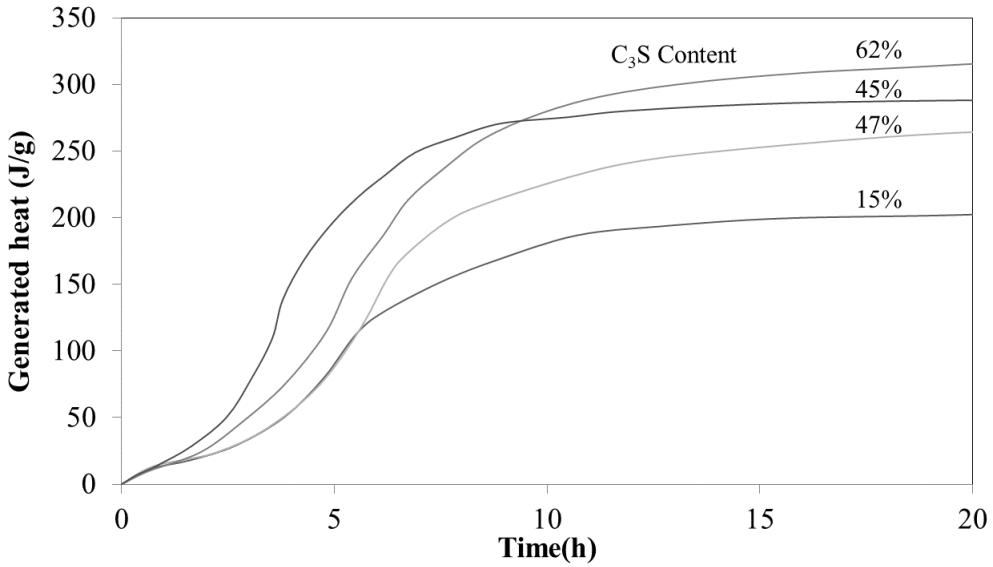


**Figure 2.2 :** Effect of the concentration of $C_3S$ on heat development [3]

As per the Standards, there are two cement types designed to address the issue of excessive heat generation during the hydration process: Low Heat Portland Cement

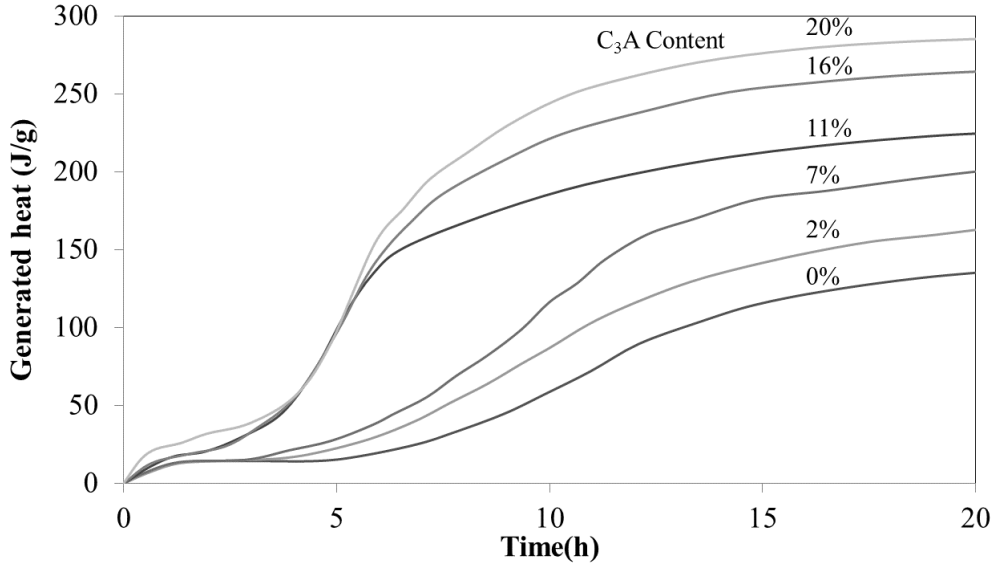


**Figure 2.3 :** Effect of the concentration of $C_3A$ on heat development [3]

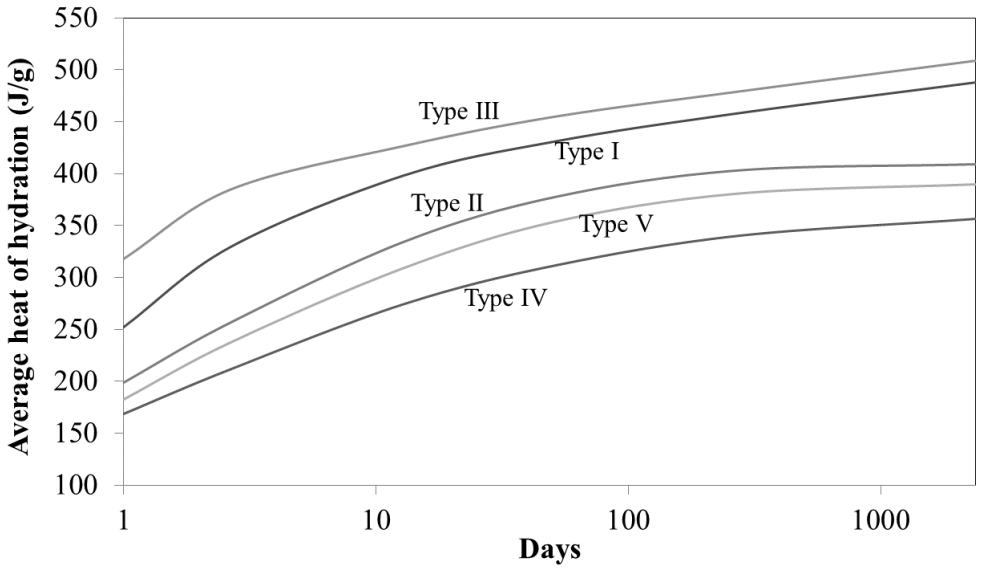


**Figure 2.4 :** Different types of cement' heats of hydration (cured at 21°C, w/c = 0.4) [3]

(LHPC) and Moderate Heat Portland Cement (MHPC). The primary difference between the two is the maximum allowed concentration of $C_3S$ and $C_3A$ in their composition. LHPC has a lower maximum limit for both compounds, resulting in a slower heat generation rate during hydration, making it suitable for large concrete structures. MHPC, on the other hand, has a slightly higher maximum limit for both compounds, allowing it to produce more heat during hydration, resulting in a faster strength gain, making it a preferred choice for precast and pre-stressed concrete

applications. However, both cement types require specific curing techniques to achieve optimal performance.

The heat generated during concrete hydration can also be affected by the specific surface area of the cement, which is a measure of its fineness. A higher specific surface area allows for more available particle surface area, resulting in faster reaction rates and higher heat generation. Increasing the fineness of the cement or supplementary cementitious materials (SCMs) can cause a higher temperature rise because the rate of hydration within the cement increases, while the rate of heat loss to the environment remains constant. The Blaine Fineness Apparatus is a tool that determines the fineness of Portland cement, following the standards set by ASTM and AASHTO. The degree of fineness is quantified by calculating the total surface area of the cement in square centimeters per gram or square meters per kilogram. In accordance with Canadian regulations, Type GU cement normally has a fineness value between 385 and 415 $m^2/kg$, although Type HE and silica fume mixes may have a fineness value greater than 605 $m^2/kg$ [17]. By only raising the final product's fineness, HE cement can be made from identical clinker as a type GU cement made of. The influence of fineness on the total heat is seen in Equation 2.16. However, while increasing fineness can speed up the early stages of hydration, it has minimal impact on the total heat of hydration at very late ages. [16]

### 2.2.2 Water to Cement Ratio

Figure 2.5 depicts how modifying the water-to-cement ratio affects heat evolution for different concrete types. The water-cement ratio, which is also referred to as the water-to-cementitious materials ratio for blended systems, determines the available water for hydration in relation to the cementitious materials present in the mixture [3]. This proportion is a crucial factor in concrete strength development because it governs the degree of hydration achieved by the mix and the quantity of cementitious materials that will hydrate.

The maximum degree of hydration achievable in a concrete mix directly impacts the amount of heat generated during the hydration process. Therefore, it is crucial to consider this factor when developing models to predict the heat of hydration for

various concrete mixes [2]. As discussed in Section 2.5.1, the water-to-cement ratio significantly influences the degree of hydration attained and, thus, the quantity of heat generated during the process.

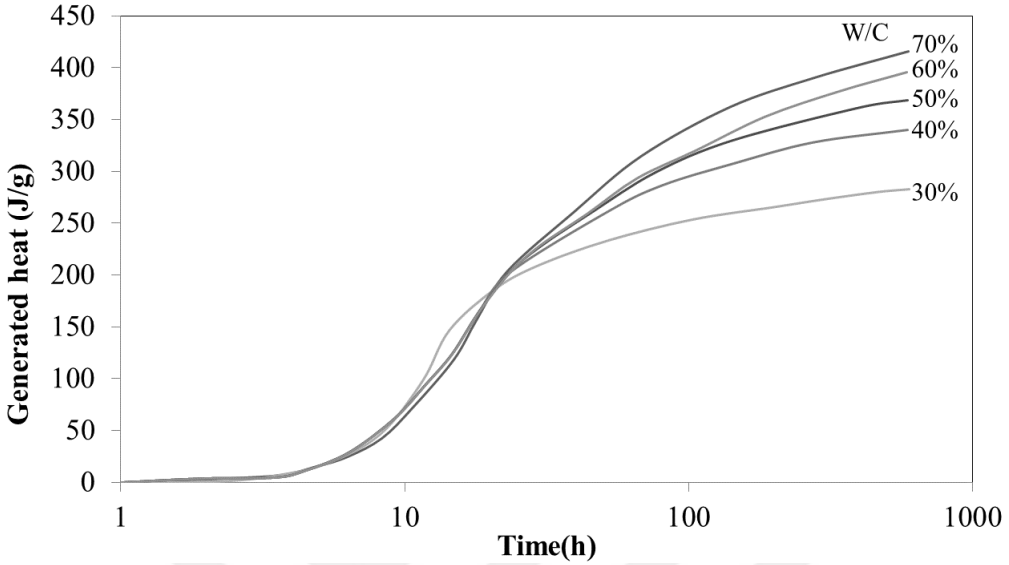


**Figure 2.5 :** Heat development for varying w/c ratios of concrete [2]

### 2.2.3 Use of Supplementary Cementing Materials

Ground granulated blast-furnace slag and Fly ash are generally used in concrete production to partially replace Portland cement. This is usually done to reduce production costs, as these materials are less expensive than Portland cement. Concrete made with these binary mixes has advantages over those made solely from Portland cement, such as increased resistance to chloride and sulfate attack. In addition to these benefits, the use of supplementary cementing materials (SCMs) can also help to manage the heat of hydration and improve certain mix design properties.

Douglas et al. (1990) conducted research that showed it is possible to use fly ash or slag to lessen the heat produced during hydration. Usually, the amount of replacement is linear with the reduction in heat, with a slightly greater reduction observed at higher replacement levels [18], also in the current study the same result was obtained. The decrease in heat development for various replacement levels of ground-granulated blast-furnace slag is shown in Figure 2.6, while the reduction as a result of the replacement of fly ash is shown in Figure 2.7. The reduction in total heat is mainly

brought about by the fact that SCMs generate less heat during reactions, especially at young ages. This drop in the total heat of hydration slows down the pace of Portland cement hydration. This effect is beneficial as it further enhances the properties of the concrete.

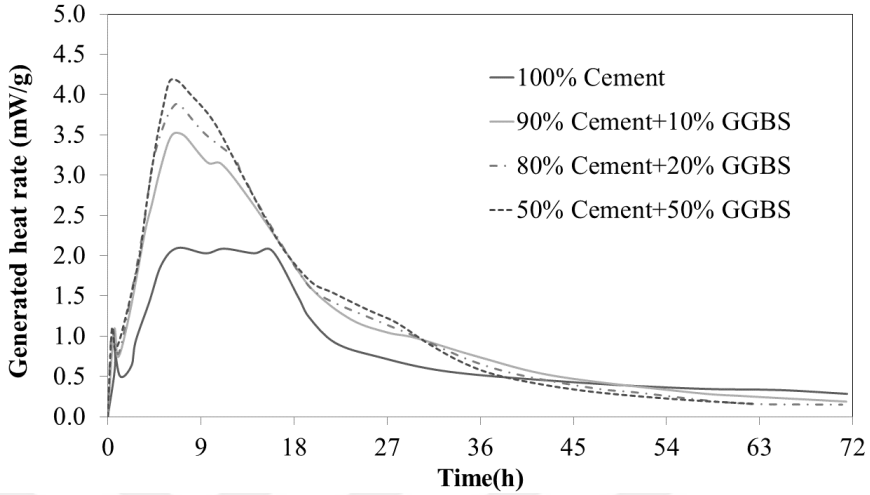


**Figure 2.6 :** Effect of various amounts of GGBS replacement on the heat development of cement (measured at 23°C)

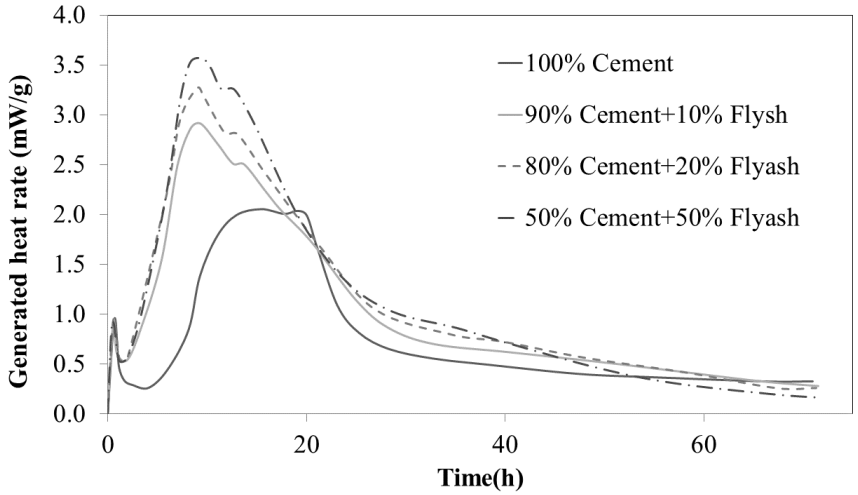


**Figure 2.7 :** Effect of various amounts of Fly ash replacement on the heat development of cement (measured at 23°C)

The research by Douglas et al. (1990) demonstrated that the addition of SCMs in concrete production can effectively reduce hydration heat. The use of SCMs not only lowers the amount of heat generated during hydration but also delays the time to reach maximum temperature rise. As a result, concrete containing SCMs experiences less severe but longer-lasting temperature rises compared to traditional Portland cement

mixtures [18], again the same result was obtained in the current study. The researchers found that fly ash is better than slag at reducing heat, but a %50 replacement of slag still provides a satisfactory balance between lowering the heat and retaining most of the compressive strength. If ultimate strength is not the primary concern, fly ash is more suitable for use [18].

### 2.3 Total Heat of Hydration

The heat of hydration, measured in joules per gram of material $(J/g)$, is the heat generated when a substance fully hydrates at a specific temperature. Both chemical processes and the water's adsorption in the calcium silicate hydrate $(C-S-H)$ matrix's gel layers contribute to this heat, with the latter contributing to around %25 of the total heat of hydration. According to Bogue (1955), the heat of hydration for normal Portland cement is created between one and three days in about %50 of cases, seven days in about %75, and six months in about %83-%91 of cases. This estimate is applicable to a wide variety of widely used cement types, however, the exact numbers depend on the chemical constituents of the cement. [19]

the total heat of cement hydration can be approximated by adding together the heat of hydration of its individual compounds, including $C3S$,$C2S$,$C4AF$, and $C3A$ when each is hydrated independently. As a result, the following equation may be used to fairly reliably determine cement's heat of hydration depending on its chemical composition. [3]:

$$H_{cem} = 136p_{C3S} + 62p_{C2S} + 200p_{C3A} + 30p_{c4AF} \tag{2.1}$$

$$H_{cem} = 570p_{C3S} + 260p_{C2S} + 840p_{C3A} + 12p_{c4AF} \tag{2.2}$$

The total heat of hydration of a cement may be estimated using the formulas in Equation 2.1 and 2.2 depending on the composition of the compound, result being measured in either calories per gram of material(equation 2.1) or joules per gram(equation 2.2). The mass proportion of each component is shown by the symbol

$p_i$. It should be emphasized that there is no relationship between the cementing abilities of each individual compound and the heat of hydration.

The method for determining the heat of hydration of cement has been published by many authors with modest differences in the numerical numbers signifying the specific heat of the various components. Nevertheless, as these variances are usually slight, the method may be used with any version and still get reliable results. This formula has been expanded upon by Schindler and Folliard (2005) to account for the existence of free lime, sulfur, and magnesium oxides. [20]

$$H_{cem} = 500p_{C3S} + 260p_{C2S} + 866p_{C3A} + 420p_{c4AF} + 624p_{so3} + 1186p_{FreeCaO} + 850p_{MgO} \tag{2.3}$$

Equation 2.4 computes the total heat of hydration for blended cement systems while taking into consideration the existence of SCMs in the mix design. According to Schindler and Folliard, Portland cement has been mixed with a cementitious material that produces lower heat, leading to a reduction in the overall heat of hydration. They provide an equation to support this finding. [20]

$$H_u = H_{cem} \cdot p_{cem} + H_{GGBS} \cdot p_{GGBS} + H_{FlyAsh} \cdot p_{FlyAsh} \tag{2.4}$$

The values of $H_{GGBS}$ and $H_{FlyAsh}$ vary from one material to another and depend on the composition and fineness of the material. The ideal technique to determine these values is by experimental determination, however, this is not always possible. In these situations, theoretical or presumptive values are used. Depending on the ash class, the literature offers a variety of values for certain materials, such as $H_{GGBS}$ ranging from 356 to 462 J/g and $H_{FlyAsh}$ ranging from 150 to 210 J/g. Using a $H_{GGBS}$ value of 461 J/g and a $H_{FlyAsh}$ value of $1800.p_{FACaO}$(J/g) is advised by Schindler and Folliard. [21]

Since Wet-chemical analysis techniques make it easier to determine the chemical composition of cement in terms of oxides than it does to estimate composition using microscopy or XRD, the calculation of compound or Bogue composition is often based on this information. The reported cement minerals are normally rounded to

the closest %1, therefore there may be some mistakes in these calculations because different procedures can produce different findings. The following equations, which meet ASTM C150-05 guidelines, can be used to determine the Bogue content.: [22]

$$C_3S = 4.071CaO - 7.600SiO_2 - 6.718Al_2O_3 - 1.430Fe_2O_3 - 2.852SO_3 - 5.188SO_2 \tag{2.5}$$

$$C_2S = 2.867SiO_2 - 0.754C_3S \tag{2.6}$$

$$C_3A = 650Al_2O_3 - 1.692Fe_2O_3 \tag{2.7}$$

$$C_4AF = 3.043Fe_2O_3 \tag{2.8}$$

The Bogue composition may only be determined using the provided formulae when using regular Portland cement. Therefore, it might not be acceptable to use these formulae to establish the Bogue content of blended cement.. There might be several approximations that produce the Bogue composition, though. For instance, while working with silica fume blended cement, one can deduct the silica fume replacement level (usually %90 $SiO_2$) from the total amount of silica content before determining the Bogue composition, The Bogue model is derived by defining the chemical composition of cement compounds as $C_3S$ for alite, $C_2S$ for belite, $C_3A$ for aluminate, and $C_4AF$ for ferrite.

### 2.3.1 Calorimetry Methods

Calorimetry methods are considered the most reliable way to determine cementitious materials' total heat of hydration and rate of hydration. In order to obtain accurate measurements of the total heat of hydration and the rate of hydration for cementitious materials, it is best to use calorimetry methods whenever possible. There are various forms of calorimetry that have been developed, including isothermal heat-conduction calorimetry, adiabatic methods, and semi-adiabatic methods. This discussion will mainly focus on semi-adiabatic calorimetry, which was the method used in this particular thesis project, but the other methods will also be discussed.

#### 2.3.1.1 Adiabatic calorimetry

Adiabatic calorimetry is a technique for analyzing recently cast samples in a sealed system to ensure adiabatic conditions by preventing heat energy exchanges with the environment. By using this technique, all heat generated by exothermic cement hydration reactions within the sample can be turned into a steady temperature increase. Concrete, mortar, and even cement paste can all be identified using adiabatic calorimetry. As the sample temperature rises during an adiabatic test, the generated heat must be converted in order to be measured as an output. The temperature field inside the adiabatic chamber can be found using equation 2.9. [7]

$$\dot{Q} = \rho c \frac{\delta T}{\delta t} \tag{2.9}$$

The equation shows that knowing the volumetric specific heat $\rho c$ of the sample is essential for calculating the heat rate generation. This is often seen as a disadvantage of adiabatic calorimetry since it requires either experimental determination or estimation of $\rho c$, which may lead to errors in the assessment of heat generation.

#### 2.3.1.2 Semi-adiabatic calorimetry

According to EN196-9, semi-adiabatic calorimetry entails putting a recently cast cementitious material sample into a container that permits a little amount of heat exchange with the surrounding environment. The EN 196-9 rule states that for a 20K temperature change, the calorimeter's coefficient of total heat loss should not be greater than $100 Jh^{-1}k^{-1}$. This approach can evaluate items up to 10 kg, including concrete samples. By adding the heat computed from the sample's temperature rise and the heat derived from the container's heat loss, the heat produced by the sample is determined. [23] The calculations required for this experiment can be found by looking at equation 2.10. But there are two prerequisites: By minimizing the calorimeter's overall heat loss, it is possible to ensure that: a) spatial temperature gradients within the sample are minimal; b) an additional term for heat losses, $P$, is introduced to the

equation. Thus, the equation produced to calculate $\dot{Q}$ is simple. [7] For the current study semi-adiabatic calorimetry is used.

$$\dot{Q} = \rho c \frac{\delta T}{\delta t} + \frac{\delta P}{\delta t} \tag{2.10}$$

#### 2.3.1.3 Isothermal calorimetry

Conduction calorimetry, another name for isothermal calorimetry, is a method for determining the heat output of the test sample. Using heat flux sensors, the heat output is monitored in this technique, which keeps the sample at a consistent temperature during the experiment. Nevertheless, as cement-based products must maintain isothermal conditions, only little samples of 45g cement paste (or mortar) are utilized, making it difficult to evaluate concrete in-situ. Yet, as cement paste is what generates the heat in concrete, it is possible to infer the anticipated heat generation from concrete from matching cement paste findings by understanding the volumetric amount of cement paste inside concrete. As long as the particles do not significantly alter the hydration kinetics of cement, which is normally the case for most concretes, this extrapolation is accurate. The buffering effects of the aggregates were cited by Morabito (1998) as causing difficulties in this extrapolation since concrete and cement paste have different kinetics. Despite this, the thesis work simplifies by neglecting this buffering effect because the acceptable temperature forecast coherences show that the aggregates have a minimal or insignificant impact. [24] [7]

## 2.4 Equivalent Age (Maturity)

Understanding the idea of maturity is essential before understanding the notion of determining the rate of hydration in concrete. The curing temperature has a significant impact on the strength development of young concrete. For instance, a concrete sample that has been cured at 40 °C for a day can be stronger than a similar sample that has been cured at 20 °C for the same time period. In regard to the development of concrete, particularly its mechanical characteristics and the energy released during hydration, maturity takes into consideration the combined effects of time and temperature. [2] [3]. Since the 1950s, this technique has been used to analyze the combined effects of

concrete temperature and age on the growth of concrete strength. The idea that the rate of concrete strength growth depends on temperature and time was originally advanced by McIntosh in 1949. [25] According to the "maturity rule" (Saul 1951), "Concrete of the same mix at the same maturity (reckoned in temperature time) has essentially the same strength, regardless of the combination of temperature and time that goes into making up that maturity." [26]

Nurse (1949) and Saul (1951) proposed the idea of "maturity" as the result of temperature and time. A datum temperature was also suggested by Saul (1951) for the determination of maturity. Carino (1984) provided an explanation of the Nurse-Saul maturity approach, which ASTM C 1074 accepted. [27]

$$M = \sum (T_r - T_0)\,\Delta t \tag{2.11}$$

In this equation, $M$ is the Nurse-Saul maturity factor at age $t$ (°C • hours), $T_r$ represents average concrete temperature during the $\Delta t$ (°C), $T_0$ indicates datum temperature (°C), and $\Delta t$ shows time interval (hours)

This thesis project will employ the equivalent age method and the Arrhenius formula to determine the maturity of cementitious systems, which is widely regarded as the most appropriate formula for this task [28]. The Arrhenius law is represented by the following equation:

$$K(T) = A.\exp\left(-\frac{E_a}{RT}\right) \tag{2.12}$$

The Arrhenius equation was suggested by Copeland et al. in 1962 as a way to calculate the non-linear cement hydration rate while accounting for the temperature influence. The Arrhenius maturity function was later established in 1977 by Freiesleben Hansen and Pedersen and included in ASTM C 1074. (Equation 2.12). This function has an advantage over Equation 2.11 in that it incorporates the activation energy (Ea). The energy threshold needed to start chemical reactions or physical processes is known as activation energy. It allows atoms or molecules to get to a condition where they can go through a chemical transformation or be transported physically. The mix is

characterized by the least energy necessary to start a specific reaction or activity. Due to the fact that the hydration of cement implies several concurrent and linked chemical processes, this activation energy is referred to as "apparent" in the case of concrete. [29] [30]

$$t_e = \sum_{i=1}^{n} \exp\left[\left(\frac{E_a}{R}\right)\left(\frac{1}{273+T_r} - \frac{1}{273+T_i}\right)\right]\Delta t_i \tag{2.13}$$

The formula consists of several variables: $t_e$ represents the equivalent age at the reference curing temperature (hours), $T_i$, is the average concrete temperature for the period of $\Delta t_i$ (°C), $T_r$, is the reference temperature (°C) which is generally assumed to be 73°F (23°C) in ASTM and 68°F (20°C) in European standards , $E_a$, denotes the apparent activation energy (J/mol), and $R$ represents the universal gas constant (8.3144 J/mol/K). This idea, which rates each curing period based on the typical concrete temperature in contrast to concrete cured at the reference temperature, is also referred to as an age conversion factor. Equation 2.14 can be used to express this conversion factor.

$$f(T_i) = \exp\left[\left(\frac{E_a}{R}\right)\left(\frac{1}{273+T_r} - \frac{1}{273+T_i}\right)\right] \tag{2.14}$$

### 2.4.1 Activation energy of concrete

The apparent activation energy must be ascertained in order to use the Arrhenius Equation to compute the equivalent age functions. According to the Glasstone (1941) Theory, the energy needed to start a molecule's reaction is known as activation energy. [31] The activation energy of concrete describes how responsive concrete qualities are to various curing temperatures [28]. The activation energy value is mix-design specific and is based on variables such as cement chemistry, particle size, and chemical admixtures that influence the pace at which concrete gains strength. Based on research in the literature [32], suggested activation energy values for regular TYPE I cement vary from 40 to 45 kJ/mol. Compressive strength tests or isothermal calorimetry experiments can be used to experimentally determine the activation energy value. Contradictory findings on the value of the apparent activation energy have been found,

however, as a result of several prediction models that have been put forth based on tests and theoretical study.

Schindler (2005) developed a regression model that takes the influence of various curing temperatures into account when predicting the activation energy for various cement kinds. The suggested equation estimates the activation energy while accounting for differences in the chemical composition of cement, its fineness, and its usage of additional cementitious ingredients. [21].

$$E_a = 22100 f_E . {p_{C3A}}^{0.3} . {p_{C4AF}}^{0.25} . Blaine^{0.35} \tag{2.15}$$

Where the activation energy modification factor for supplementary cementitious materials, denoted by $f_E$, $p_{C3A}$ represents the weight ratio of $C_3A$, and $p_{C4AF}$ represents the weight ratio of $C_4AF$.

$$f_E = 1 - 0.05 . p_{FA} \left(1 - \frac{p_{FACaO}}{0.4}\right) + 0.4 . p_{Slag} \tag{2.16}$$

## 2.5 Determining the Rate of Hydration

It is crucial to understand the cement's rate of hydration under real-world circumstances. Calorimetry methods are the quickest and most accurate approach to measure the rate of hydration, but they are time-consuming and expensive to set up. If testing the materials is not an option, the rate of reaction must be predicted using a numerical hydration model.

The method employed to determine the total heat of hydration cannot be used to ascertain the rate of hydration due to the varying reaction rates of each compound and their sensitivity to mix temperature. Figure 2.8 illustrates that the compounds $C_3A$ and $C_4AF$ achieve over %80 hydration within the first 24 hours of curing, while other factors such as cement fineness, the presence of supplementary cementing materials, gypsum content, and the proportion of $C_3A$ and $C_3S$ in the cement can also affect the rate of hydration, especially during the early stages of the process. [2]

A technique for assessing the degree of hydration of various types of cement as they cure is necessary to calculate the rate of hydration. It is essential to have such a

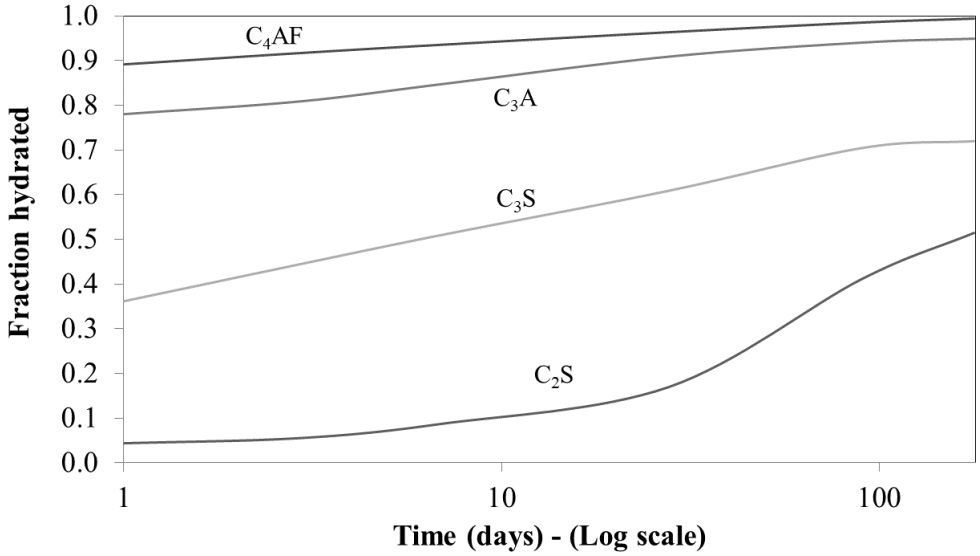


**Figure 2.8 :** Degree of hydration development for the various cement compounds [3]

procedure since, due to changes in the curing conditions, a comparison based merely on time is insufficient. The discussion of the equivalent age maturity technique, which is frequently used to account for variations in curing regimes, continues in this section.

### 2.5.1 Measurement of Hydration Level

The degree of hydration, $\alpha$, may be determined using the amount of hydration products and the initial amount of cementitious material contained in the mixture. As a function of time, this parameter changes from %0 at the beginning of hydration to %100 after all cementitious materials have reacted. It is crucial to consider this parameter in any heat of hydration model as emphasized by van Breugel, who stated that it is impossible to make a dependable prediction of temperatures without simultaneously calculating the progress of the hydration process [33]. The proportion of cement particles that have combined with water to create hydrated products, as compared to the total amount of cement in the mixture, determines the degree of hydration. Since it is hard to calculate, monitoring the cement's heat development can be used to infer the amount of hydrated cement present in the mixture. This approach is frequently employed and is mathematically represented as:

$$\alpha(t) = \frac{H(t)}{H_u} \tag{2.17}$$

where $\alpha(t)$ is the degree of hydration at time $t$, $H(t)$ is the cumulative heat released by the cement at a given time,t, and $H_u$ is the maximum heat that would be released if all the cement had reacted.

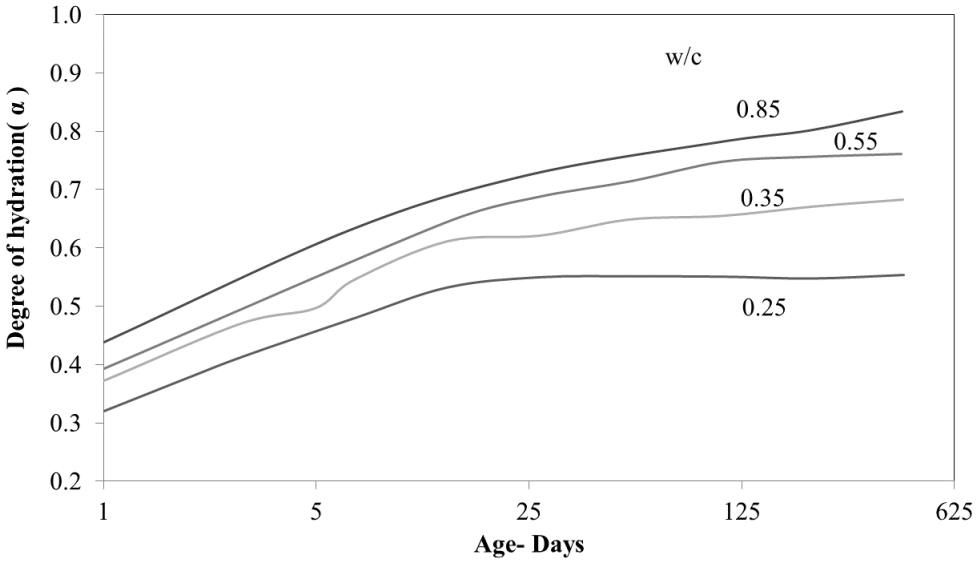


**Figure 2.9 :** Ratio of chemically bonded water to cement weight in relation to log curing time [4]

Several authors have observed that the degree of hydration of cement does not typically reach %100, and its ultimate degree is dependent on the water-cement ratio, as presented by Mills (1966) in Figure 2.9. Mills also proposed an equation, represented by Equation 2.18, to calculate the ultimate degree of hydration. The impact of SCMs on the ultimate degree of hydration was later included in the equation proposed by Schindler and Folliard (2005) as Equation 2.19. It is important to note that the curing temperature does not affect the ultimate degree of hydration.

$$\alpha_u = \frac{1.031.w/c}{0.194 + w/c} \tag{2.18}$$

$$\alpha_u = \frac{1.031.w/c}{0.194 + w/c} + 0.50.p_{FlyAsh} + 0.30.p_{GGBS} \leq 1.0 \tag{2.19}$$

s

Equation 2.20 provides an exponential formulation for predicting the level of hydration in combination with experimental data. It has been demonstrated that this S-shaped

function properly depicts how different Portland cement systems hydrate over time. [20] [34]. This formulation depends on the following two factors: a slope parameter for hydration, $\beta$, and a time parameter $\tau$.

$$\alpha(t_e) = \alpha_u . \exp\left(-\left(\frac{\tau}{t_e}\right)^{\beta}\right) \tag{2.20}$$

The hydration equation only considers one peak of hydration for a certain cementitious system, which is a crucial point to remember. This is true for regular Portland cement, but some researchers have suggested a more accurate method for estimating the degree of hydration in blended systems comprising fly ashes or GGBFS. They propose that the two peaks often seen in such systems can be represented by a superposition of two hydration functions. [35] [36].

$$\alpha(t_e) = \alpha_{u1} . \exp\left(-\left(\frac{\tau_1}{t_e}\right)^{\beta_1}\right) + \alpha_{u2} . \exp\left(-\left(\frac{\tau_2}{t_e}\right)^{\beta_2}\right) \tag{2.21}$$

The time which a hydration process reaches %38 is the value of the Schindler's model's hydration time parameter, $\tau$. This parameter's smaller value denotes a more faster hydration process. Changes in this parameter are seen in Figure 2.10, where a drop in $\tau$ causes a shift in the hydration curve to the left.

The hydration slope parameter, $\beta$, determines the steepness of the curve in the early stages of hydration. A larger value of $\beta$ indicates a faster initial rate of reaction and a steeper curve, while a smaller value of $\beta$ indicates a slower initial rate of reaction and a flatter curve. The value of $\beta$ also affects the time it takes for the degree of hydration to reach %100, illustrated in figure 2.11. Therefore, both parameters, $\tau$ and $\beta$, are important in predicting the degree of hydration and understanding the kinetics of the cement hydration process.

The degree of hydration curve can be scaled by using the ultimate degree of hydration term, $\alpha_u$, which is depicted in Figure 2.12. As the value of $\alpha_u$, increases, the degree of hydration curve also increases. While this term does not exactly replicate the impact of different water-cement ratios on the hydration process, according to Schindler (2002), it is still a useful tool for modeling the degree of hydration of cementitious systems.

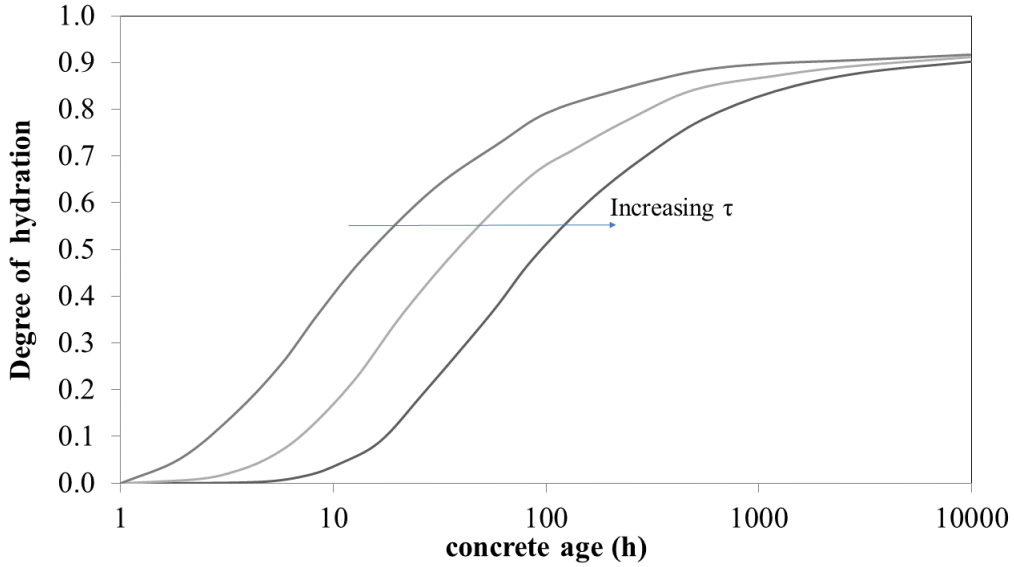


**Figure 2.10 :** Impact of hydration time parameter variation ($\tau$) on hydration development intensity [2]

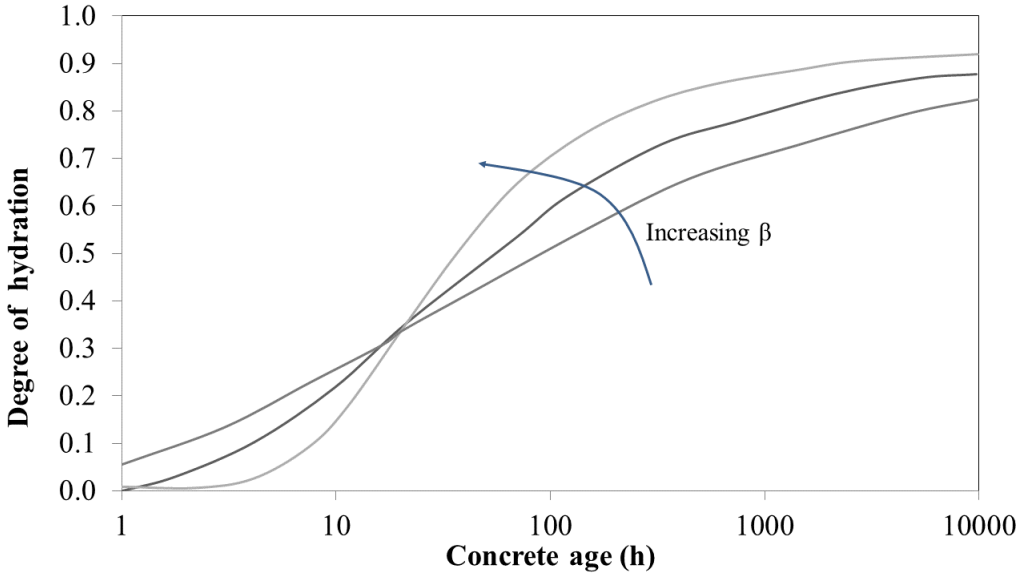


**Figure 2.11 :** Impact of hydration slope parameter variation ($\beta$) on hydration development intensity [2]

He suggests that the discrepancy between the two may be because the effect of the water-cement ratio only becomes apparent after ten to twenty hours of hydration. However, based on his research, he concludes that the use of this term is accurate enough for modeling the degree of hydration. [2]

The hydration parameter used in equation 2.19 can be determined in one of two methods. Using experimental equations is one approach. The values of the two

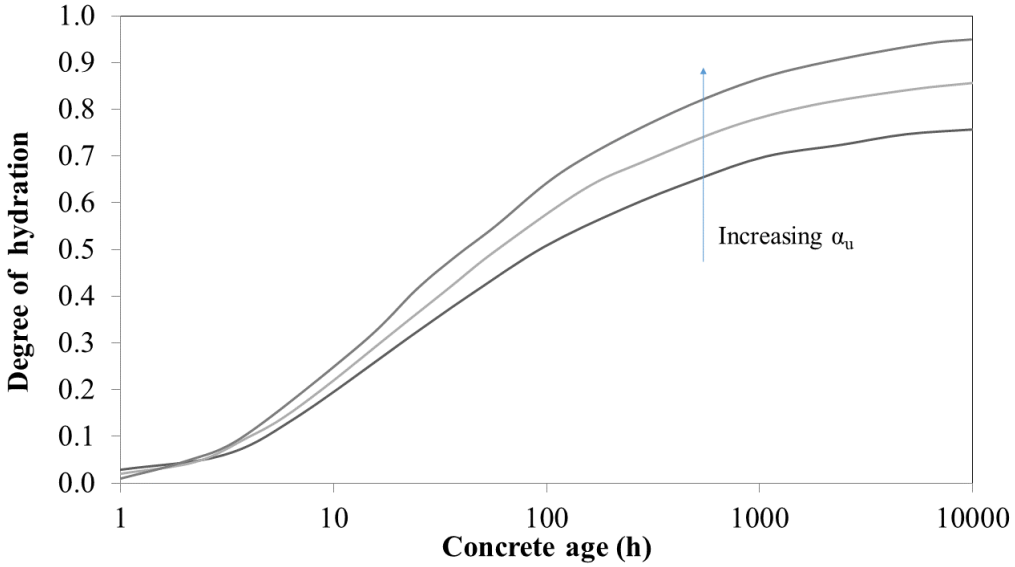


**Figure 2.12 :** Impact of a change in the final degree of hydration ($\alpha u$) on the growth of the degree of hydration [2]

hydration parameters may be calculated using the model Schindler has suggested. This model is based on their own semi-adiabatic tests as well as information from earlier studies carried out by independent researchers, such as a review of the 1948 Lerch and Ford hydration data set. [20]. The following two equations are the results of the non-linear multivariate regression analysis used in their model. The heat produced during cement hydration may also be measured using calorimetry tests, and the values of the Hydration parameter can be calculated using the fitting curve approach. The simulation section will include a detailed explanation of the latter strategy. The second approach, curve fitting, is applied in this thesis.

$$\tau = 66.78.{p_{C_3A}}^{-0.154}.{p_{C_3S}}^{-0.401}.Blaine^{-0.804}.{p_{SO_3}}^{-0.758}.\exp\left(2.187.p_{GGBS} + 9.50.p_{FlyAsh}.p_{FlyAshCaO}\right) \quad (2.22)$$

$$\beta = 181.4.{p_{C_3A}}^{0.146}.{p_{C_3S}}^{0.227}.Blaine^{-0.535}.{p_{SO_3}}^{0.558}.\exp\left(-0.647.p_{GGBS}\right) \quad (2.23)$$

## 2.6 Controlling mass concrete temperatures

Depending on the building techniques, several mass concrete temperature management strategies are used. Controlling temperatures to reduce cracking in mass concrete installations has been proven to be successful when combined with prescriptive requirements and easy procedures. These methods include restricting the maximum

cementitious content to 356 kilogram per cubic meter, incorporating between %25 and %30 fly ash, limiting the initial concrete temperatures to between 75 and 80 degrees Fahrenheit(24-27°C ), restricting the maximum concrete temperatures to 160°F (71°C) , and restricting temperature differentials to 35°C. It is vital to prequalify the concrete before placement and to keep an eye on the temperature while it is being placed in order to use these approaches. The American Concrete Institute (ACI) Committee 207 developed these regulations in 2005. [9]

The heat of hydration can be decreased, per ACI recommendations, by using TYPE II or TYPE IV cement or by substituting fly ash or ground granulated blast furnace slag (GGBFS) for cement. Reduced cement dose is also advised to lessen the heat of hydration in situations when the 57 or 90-day strength is suitable for service circumstances. Another technique suggested by ACI to give additional cooling throughout the summer is water-curing. According to ACI 207.1R, pre-cooling the component materials and post-cooling the element using cooling pipes can both be useful for controlling temperature. To reduce thermal cracking, a thermal management strategy should be created to limit the differential in temperature between the surface and the inside of the structure. When high maximum concrete temperatures are anticipated, adding reinforcing is advised to reduce crack width. For mass concrete applications, ACI 207.1R includes comprehensive information on component materials, concrete mixes, mechanical and thermal characteristics of in-place concrete, building techniques, and equipment requirements. The recommendation highlights that the key to reducing temperature rise inside the concrete is managing the kind and amount of cementitious material. [9] [37].

For mass concrete mixes, standard values for mechanical parameters like tensile strength and creep as well as thermal properties like specific heat, thermal diffusivity, thermal conductivity are specified in accordance with ACI 207.2R to foresee the possibility of cracking. In order to estimate the beginning concrete temperature, temperature growth, and final concrete temperature in mass concrete constructions, the guidelines offer several example problems that employ empirical data charts and

tables. The recommendations also include an explanation of the Schmidt Method, which calculates temperature rise and differences.

### 2.6.1 Allowable temperature difference

According to FitzGibbon M.E., the maximum permissible temperature differential in mass concrete standards is normally limited to 20°C. during the '70s. According to FitzGibbon's research, concrete reaches its breaking strain when the temperature differential approaches 20°C. The study found that there are two distinct processes that lead to heat cracking in mass concrete, as shown in Figure 2.13. First off, early formwork removal is a major contributor to external thermal cracking because thermal cracking develops as a result of rapid surface cooling. Second, thermal cracking can happen in the first one or two days following concrete laying when the temperature increases on the surface much more slowly than it does in the inner points of the concrete. [5]

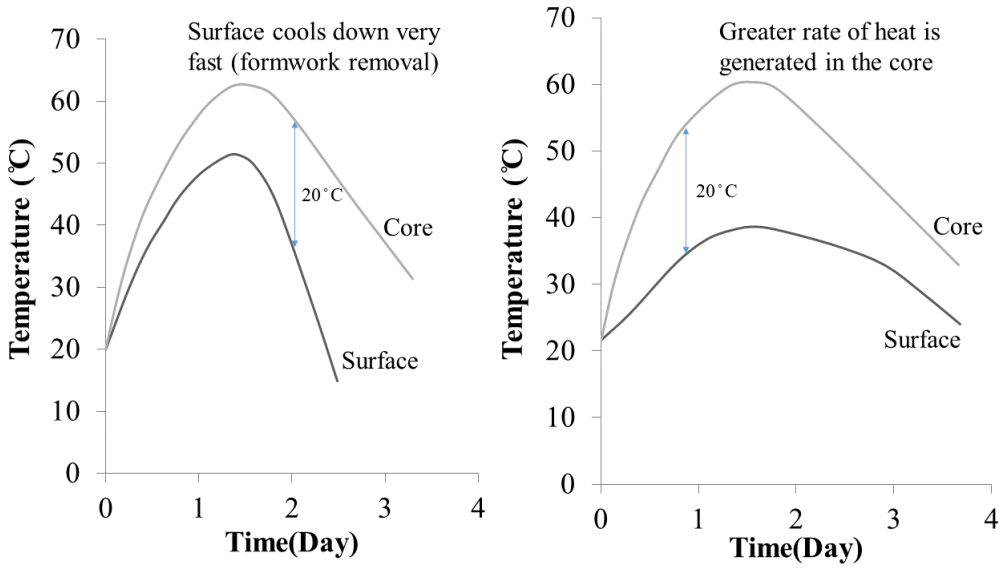


**Figure 2.13 :** Thermal cracking in constructions made of mass concrete [5]

The validity of the 20°C (35°F) maximum permitted temperature difference has come under scrutiny in recent talks among scholars. In some situations, even at bigger temperature differences, thermal cracking has not been seen, while in other reports, cracking has been noted at temperature differences as low as 20°C. [38]

According to Turkish standard TS 13515, a significant factor causing temperature differences and thermal cracking is the maximum temperature at a structure's core. For mass concrete structures, TS 13515 advises maintaining a fresh concrete temperature between 10°C and 30°C; for conventional structures, the limit can be raised to 35°C. Some techniques for regulating the temperature of fresh concrete include cooling the components of the concrete, adding mineral admixtures, and adjusting the production schedule. The parameters of the mixture design, such as low cement content, high mineral admixture content, and low-heat cement, are the main determinants of the heat produced during cement hydration. The maximum temperature allowed inside a structure is 65°C according to TS 13515. The size and volume of the concrete produced, along with meteorological conditions, ground characteristics, thermal characteristics, formwork insulation, and curing time, all affect temperature differentials and the likelihood of cracking. For reinforced concrete, TS 13515 states that the temperature differentials between the core and the concrete cover depth and between the concrete cover depth and the surface of the concrete shall both be less than 25°C. [39]

# 3. EXPERIMENTAL WORK

In this section, fourteen 1.5m cubes with varying levels of insulation using a combination of conventional Portland cement, crushed granulated blast furnace slag, and fly ash were created in the Busra Beton factorty.

the temperature of both internal and external nodes within the cubes were measured and discovered that the kind and amount of mineral admixture used in the concrete, as well as the starting temperature of the mixture, had a substantial influence on the maximum core temperature. It is discovered that employing a combination with a larger percentage of mineral admixtures resulted in lower temperatures within the concrete.

The study also emphasized the necessity of insulation in lowering temperature differences within the structure. Better insulated cubes had more constant temperatures throughout, showing that effective insulation can assist to maintain a more stable temperature profile in concrete structures. These findings are especially important for building projects in areas with harsh weather, where temperature changes can have a substantial influence on the structure's durability and lifetime.

## 3.1 Materials

### 3.1.1 Cement

Table 3.1 displays the properties of CEM I 42,5 R (Bursa Cement Factory Inc.), which was utilized in the current study.

**Table 3.1 :** Cement properties

| Phase No* | SiO2 (%) | Al2O3 (%) | Fe2O3 (%) | CaO (%) | MgO (%) | SO3 (%) | Na2O (%) | K2O (%) | Blaine (cm2/g) |
|---|---|---|---|---|---|---|---|---|---|
| 1 | 18.45 | 5.63 | 3.01 | 63.3 | 0.96 | 2.96 | 0.32 | 0.63 | 3420 |
| 2 | 18.78 | 5.51 | 3.16 | 63.28 | 0.79 | 2.63 | 0.28 | 0.52 | 3650 |
| 3 | 18.64 | 5.44 | 2.95 | 63.28 | 0.76 | 2.6 | 0.31 | 0.61 | 3820 |

### 3.1.2 Fly Ash

Fly ash was supplied from the Tunçbilek plant and its properties are given in Table 3.2.

**Table 3.2 :** Fly Ash properties

| SiO2 (%) | Al2O3 (%) | Fe2O3 (%) | CaO (%) | MgO (%) | SO3 (%) | Na2O (%) | K2O (%) | LOI (%) | Free CaO (%) |
|---|---|---|---|---|---|---|---|---|---|
| 55.97 | 19.44 | 10.49 | 3.54 | 4.15 | 0.38 | 0.14 | 1.7 | 1.52 | 0.06 |

### 3.1.3 Ground Granulated Blast Furnace Slag (GGBFS)

The properties of GGBFS is given in Table 3.3.

**Table 3.3 :** GGBFS properties

| SiO2 (%) | Al2O3 (%) | Fe2O3 (%) | CaO (%) | MgO (%) | SO3 (%) | Na2O (%) | K2O (%) | LOI (%) | d (g/cm3) | Blaine (cm2/g) |
|---|---|---|---|---|---|---|---|---|---|---|
| 41.91 | 10.96 | 0.59 | 36.91 | 4.95 | 0.29 | 0.48 | 1.21 | 0 | 2.89 | 5090 |

### 3.1.4 Aggregates

Properties of the limestone used in the concrete production is given in Table 3.4.

### 3.1.5 Chemical admixture

In the production of concrete, a superplasticizer admixture based on phosphonate polycarboxylate and compliant with TS EN 934-2 standards was utilized.

## 3.2 Mixture designs

In all of the mixtures, the binder phase comprised 400 $kg/m^3$ of cementitious material. The volume proportions of the aggregates were %60 sand, %17 No. I (5/12), and %23 No. II (12/22). The water-to-binder ratio was calculated using an activity index of 0.4 for fly ash and 0.8 for GGBFS. The specific mixture proportions are outlined in Table 3.5.

To ensure the durability of mass concrete is sufficient, it is generally recommended to have a high cementitious content and a low water-to-binder ratio. In this case, a cementitious content of 400 kg/m3 was chosen based on considerations for workability,

**Table 3.4 :** Properties of aggregates

| Property | Crushed sand (0/5) | I No. (5/12) | II No. (12/22) |
|---|---|---|---|
| Density (g/cm3) | 2,64 | 2,68 | 2,70 |
| Water absorption (%) | 1,9 | 0,8 | 0,5 |
| Fineness Modulus | 3,55 | - | - |
| Methylene blue (g/kg) | 0.6 | - | - |
| Sieve size (mm) | Passing (%) | | |
| 31,5 | 100 | 100 | 100 |
| 22,4 | 100 | 100 | 96 |
| 16 | 100 | 100 | 42 |
| 11,2 | 100 | 94 | 5 |
| 8 | 100 | 55 | - |
| 5,6 | 100 | 18 | - |
| 4 | 89 | 3 | - |
| 2 | 59 | 1 | - |
| 1 | 39 | - | - |
| 0,5 | 27 | - | - |
| 0,25 | 19 | - | - |
| 0,150 | 13 | - | - |
| 0,063 | 7 | - | - |

strength, and durability requirements. The maximum water-to-binder ratios according to TS EN 206 and TS 13515 were %40-%45. The resultant concrete had a high viscosity due to the fly ash's low activity index, thus a water-to-binder ratio of %50 was used.

### 3.3 Generated heat result

As mentioned in the section 2.3.1.2, in this study Semi-adiabatic test is conducted. The heat of hydration produced by cementitious materials is frequently measured using semi-adiabatic testing. In order to conduct the test, a sample of cementitious material is placed in a temperature-controlled space, and the rate at which the temperature rises when the material interacts with water is observed.

For accurate results, it's crucial to calibrate the semi-adiabatic device. Water samples are frequently used in calibration since they have a known specific heat capacity and thermal conductivity. The water inside the apparatus is added, and the temperature

**Table 3.5 :** Mixture proportions (kg/m3)

| Code | Cement | Fly Ash | GGBFS | Water | W/B | Sand | 5/12 | 12/22 |
|---|---|---|---|---|---|---|---|---|
| C100-GBFS300-0.40 | 100 | 0 | 300 | 136 | 0,40 | 1135 | 324 | 440 |
| C100-GBFS300-0.45 | 100 | 0 | 300 | 153 | 0,45 | 1100 | 316 | 428 |
| C150-GBFS250-0.40 | 150 | 0 | 250 | 140 | 0,40 | 1131 | 323 | 438 |
| C150-GBFS250-0.45 | 150 | 0 | 250 | 158 | 0,45 | 1101 | 314 | 427 |
| C300-FA100-0.45 | 300 | 100 | 0 | 153 | 0,45 | 1089 | 312 | 424 |
| C200-FA200-0.50 | 200 | 200 | 0 | 140 | 0,50 | 1081 | 306 | 414 |
| C150-FA250-0.50 | 150 | 250 | 0 | 125 | 0,50 | 1087 | 312 | 423 |

**Table 3.6 :** Adiabatic Heat result of mixtures

| Mix Code | Mix ID Cement+... | W/C | Slump [cm] | Density [kg/m3] | Adiabatic Heat [kj/kg] 24 | 48 | 168 | 336 |
|---|---|---|---|---|---|---|---|---|
| Code 1 | 100+300 GGBS | 0.40 | 19 | 2457 | 59 | 92 | 159 | 179 |
| Code 2 | 100+300 GGBS | 0.45 | 20 | 2423 | 54 | 93 | 176 | 209 |
| Code 3 | 150+250 GGBS | 0.40 | 20 | 2485 | 69 | 134 | 233 | 272 |
| Code 4 | 150+250 GGBS | 0.45 | 21 | 2436 | 72 | 122 | 209 | 247 |
| Code 5 | 300+100 FlyAsh | 0.40 | 23 | 2381 | 141 | 227 | 306 | 330 |
| Code 6 | 150+250 FlyAsh | 0.50 | 24 | 2341 | 102 | 154 | 226 | 245 |

is then allowed to stabilize. The temperature of the water sample is then measured after the thermocouple has been inserted. The instrument receives heat from a heater inside the chamber, and the rate of temperature rise is tracked and recorded. The relationship between heat flow and temperature rise (equation 2.10) in the water sample is established, which is used to find the second part of equation 2.10, and then we used that wasted heat in semi-adiabatic test device to calculate the adiabatic heat flow produced by the cementitious material.

It is essential to obtain the results of the semi-adiabatic test at various ages of the cementitious material in order to use this information for our model. The maturity concept, which is based on the idea that concrete's rate of strength development is a function of temperature and time, can be used to achieve this. The maturity concept involves monitoring the concrete's temperature over time and using this data to determine the concrete's equivalent age at a particular temperature. The results of the semi-adiabatic tests for mixtures Code1 and Code 2 are shown in Figure 3.1 :

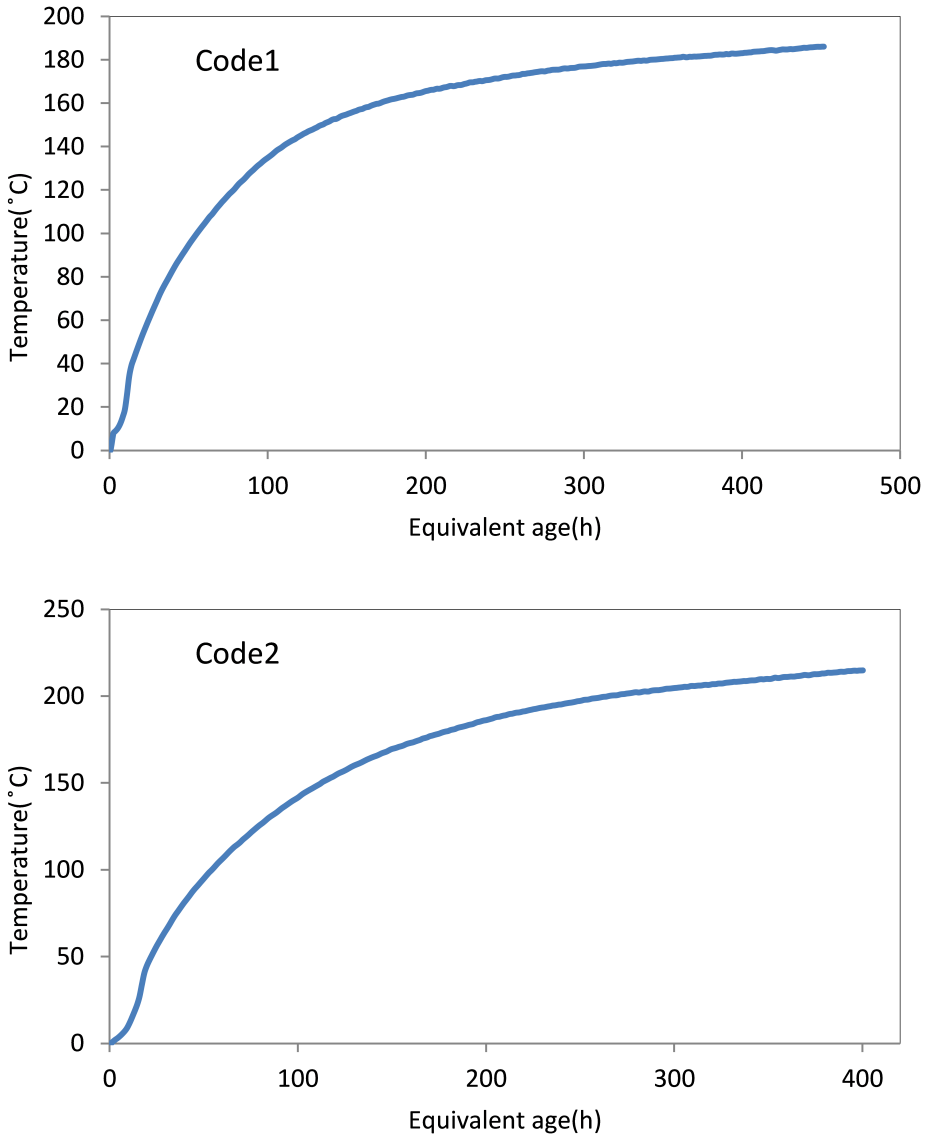


**Figure 3.1 :** Code1, Code 2 Mix generated heat

### 3.4 Production

The mixing and casting of materials occurred at the Görükle Plant, which is the Central Laboratory Site of Bursa Beton A.Ş. To maximize the use of space, data recorders, and formwork, three phases were used to carry out the experimental study. During each stage, cubic structures measuring 1.5x1.5x1.5 m were cast with varying degrees of insulation. The first, second, and third phases involved the casting of 4, 5, and 5 cubic structures, respectively.

In the simulation section, three cases were considered (case 1, case 7, and case 11). The mixture information for code 1 and code 2 will be presented, while the heat graphs for the other codes will be included in the appendix section.

### 3.4.1 Phase1

The diagram shows the insulation properties of the formwork for concrete Castings No. 1, 2, 3, and 4, with the corresponding mixture codes. The formwork was insulated with 10 cm thick and 32 kg/m3 density EPS board on all sides. The objective of this phase is to assess how the heat developing within concrete is affected by the w/c ratio and binder content. Additionally, the study will examine the temperature differences in various areas of the insulated structure.

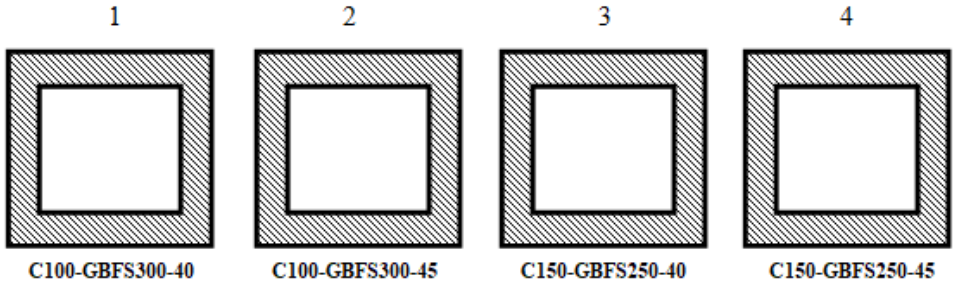


**Figure 3.2 :** Phase1 samples

### 3.4.2 Phase2

The Figure 3.3 below presents side views of the different casting conditions, with no insulation used for Casting No. 5. For Castings No. 6, 8, and 9, only the sides were insulated with 3 cm thick and 32 kg/m3 density XPS board, while no top or bottom insulation was applied. Casting No. 7 had no top or bottom insulation, but the sides were insulated with 10 cm thick and 32 kg/m3 density EPS board. This phase of the study aims to investigate the impact of various insulation conditions on a specific concrete mixture design. Additionally, the study will examine the effects of fly ash on the temperature development of mass concrete and compare it to slag concrete. To replicate typical site conditions, the concrete cubic blocks will not be insulated from the top or bottom.

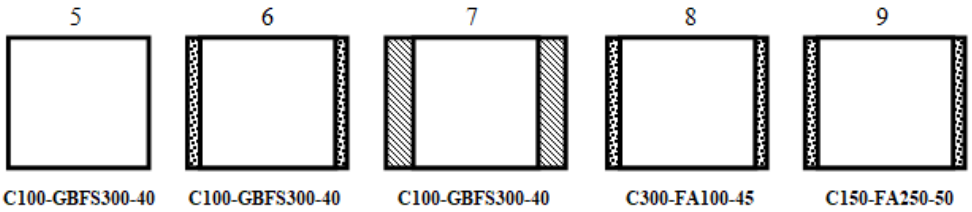


**Figure 3.3 :** Phase2 samples

### 3.4.3 Phase3

The Figure 3.4 shows side views of various casting conditions, with Casting No. 10 having no bottom or top insulation, but with 10 cm thick and 32 kg/m3 density EPS board insulation on the sides. Castings No. 11 and 12 were fully insulated on all sides with 10 cm thick and 32 kg/m3 density EPS board, while Castings No. 13 and 14 had no bottom insulation, but were insulated on all other five sides with 3 cm thick and 32 kg/m3 density XPS board inside the formwork.

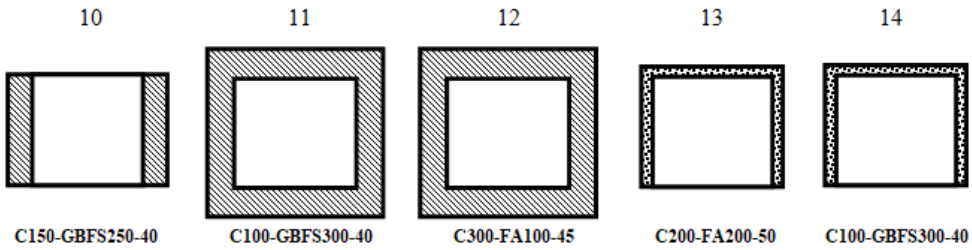


**Figure 3.4 :** Phase3 samples

In this phase of the study, Mixture No.3 from the first phase is analyzed under various insulation conditions. The study also investigates the impact of fresh concrete temperature by comparing it to the first phase, with a temperature difference of $10°C$ observed between the two phases. The study also observes the temperature variations in concrete with the highest cement content under full insulation. The effect of increased cement content on temperature differentials is also examined, as higher cement content can increase water content and reduce the viscosity and pumping difficulty of Mixture No.9. Finally, the effect of insulation on only the sides and top with 3 cm thick XPS board is investigated, as this type of insulation is applicable to typical site conditions.

To prevent evaporation, plastic covers were used to cover Casting No. 5, 6, 7, 8, 9, and 10.Each stage used 11 dataloggers with 4 channels and many meters of thermocouples to detect temperature. The Figure 3.5 shows the positions of the temperature readings within the cubic construction at 5, 40, and 75 cm (core) from the edges. 3.5.

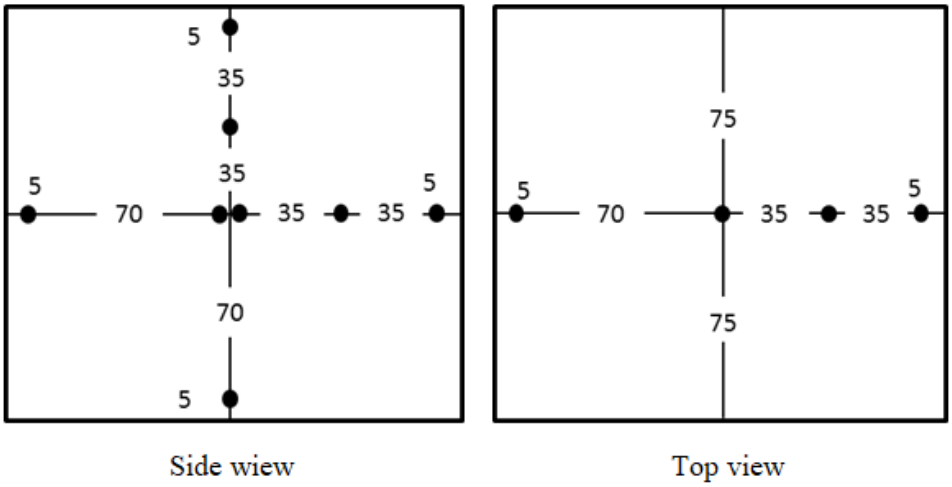


**Figure 3.5 :** Setting thermocouples and casting concrete

Due to mobilization issues and temperature monitoring periods, each stage was initiated 2 weeks after the one before. The aggregates were taken from the same stock and stored under cover until the castings were finished, while fly ash and GGBFS were stored in separate silos at the plant. The cubic constructions were cast using the same cement that was utilized in regular manufacture. Although samples from fresh cement shipments were gathered before each production (as shown in Table 3.1), it was impossible to tell the difference between the fresh shipment and the cement already in the silo. To ensure that regular production activities could go on as usual on other working days, all castings took place on Sundays. The plant was set aside for testing throughout the day, and before each production stage, all bunkers were empty, cleaned, and loaded with aggregates obtained from a special supply.

The concrete mixing process lasted for 40 seconds, and two batches of 2.5 cubic meters were produced to obtain a total volume of 5 cubic meters. The concrete was then pumped into the formwork and poured in five levels, with each 30-centimeter pour being vibrated. To simulate transportation time, the concrete was left in the trans-mixer for 30 minutes at a low rotation speed before pumping. Casting was

**Figure 3.6 :** Phase3 samples

completed approximately one hour after production, during which the fresh concrete's slump, air content, unit weight, and temperature were recorded. The development of compressive and tensile strength, as well as the heat generated during the hardening of the concrete, were also measured.

## 3.5 Experimental Results

### 3.5.1 Fresh concrete properties

Table 3.7 presents the results of the experiments, where the slump value was maintained at a minimum of 20 ± 1 cm. When the flow value reached $40cm$ or above, it was measured and reported. The air and concrete temperatures, unit weight, and air measurements were taken after pumping at $t = 60min$. At the plant ($t = 0min$), before pumping ($t = 30min$), and after pumping ($t = 60min$), the slump was measured.

The slump requirements were fulfilled before pumping. The lower slump values measured during the 3rd phase could be due to the cement properties described in Table 3.1. The increase in concrete workability over time could be attributed to the

**Table 3.7 :** Fresh concrete properties

| Phase No | Casting No | Code | Air (°C) | Conc. (°C) | Slump/Flow (cm/cm) t=0 min | t=30 min | t= 60 min | Unit weight (kg/m$^3$) |
|---|---|---|---|---|---|---|---|---|
| 1 | 1 | C100-GBFS300-0.40 | 27 | 31 | 22/40 | 22/40 | 24/45 | 2394 |
| | 2 | C100-GBFS300-0.45 | 30 | 32 | 22/- | 23/40 | 23/40 | 2365 |
| | 3 | C150-GBFS250-0.40 | 33 | 32 | 24/45 | 24/45 | 25/60 | 2395 |
| | 4 | C150-GBFS250-0.45 | 30 | 33 | 22/- | 22/- | 25/50 | 2389 |
| 2 | 5 | C100-GBFS300-0.40 | 18 | 23 | 20/- | 23/40 | 24/45 | 2412 |
| | 6 | C100-GBFS300-0.40 | 17 | 23 | 15/- | 22/- | 23/45 | 2407 |
| | 7 | C100-GBFS300-0.40 | 16 | 23 | 19/- | 24/45 | 25/50 | 2396 |
| | 8 | C300-FA100-0.45 | 16 | 25 | 23/- | 23/- | 25/45 | 2340 |
| | 9 | C150-FA250-0.50 | 16 | 24 | 24/45 | 25/60 | 25/65 | 2406 |
| 3 | 10 | C150-GBFS250-0.40 | 13 | 20 | 16/- | 20/- | 22/- | 2400 |
| | 11 | C100-GBFS300-0.40 | 13 | 21 | 10/- | 19/- | 22/- | 2384 |
| | 12 | C300-FA100-0.45 | 13 | 21 | 14/- | 22/- | 23/- | 2332 |
| | 13 | C200-FA200-0.50 | 13 | 22 | 19/- | 23/40 | 25/50 | 2350 |
| | 14 | C100-GBFS300-0.40 | 13 | 21 | 10/- | 20/- | 22/40 | 2395 |

properties of the superplasticizer. The measured air content of %2-%3 was reasonable.

Mixtures containing fly ash showed high viscosity and pumping difficulties.

**Table 3.8 :** General temperature measurement results

| Mixture No | Design Code | Insulation Properties | | | | | Fresh Conc. Temp. | Max. Temp At Core |
|---|---|---|---|---|---|---|---|---|
| | | Top | Bottom | Sides | Thickness (cm) | Type | °C | °C |
| 1 | C100-GBFS300-0.40 | *Yes* | *Yes* | *Yes* | 10 | EPS | 31 | 57.2 |
| 2 | C100-GBFS300-0.45 | *Yes* | *Yes* | *Yes* | 10 | EPS | 32 | 57.3 |
| 3 | C150-GBFS250-0.40 | *Yes* | *Yes* | *Yes* | 10 | EPS | 32 | 65.4 |
| 4 | C150-GBFS250-0.45 | *Yes* | *Yes* | *Yes* | 10 | EPS | 33 | 67.1 |
| 5 | C100-GBFS300-0.40 | No | No | No | - | - | 23 | 37.2 |
| 6 | C100-GBFS300-0.40 | No | No | *Yes* | 3 | XPS | 23 | 40.5 |
| 7 | C100-GBFS300-0.40 | No | No | *Yes* | 10 | EPS | 23 | 41.8 |
| 8 | C300-FA100-0.45 | No | No | *Yes* | 3 | XPS | 25 | 59.2 |
| 9 | C150-FA250-0.50 | No | No | *Yes* | 3 | XPS | 24 | 46.3 |
| 10 | C150-GBFS250-0.40 | No | No | *Yes* | 10 | EPS | 20 | 46.2 |
| 11 | C100-GBFS300-0.40 | *Yes* | *Yes* | *Yes* | 10 | EPS | 21 | 46.7 |
| 12 | C300-FA100-0.45 | *Yes* | *Yes* | *Yes* | 10 | EPS | 21 | 66.3 |
| 13 | C200-FA200-0.50 | No | *Yes* | *Yes* | 3 | XPS | 22 | 53.3 |
| 14 | C100-GBFS300-0.40 | No | *Yes* | *Yes* | 3 | XPS | 21 | 43.4 |

### 3.5.2 Temperature development measurements

The temperature increase brought on by the heat of hydration in the concrete blocks was monitored every six hours using thermocouples. The thermocouples' side view plan is depicted in Figure 3.7 together with the relevant codes. The analysis also made use of the average air temperature, which was obtained at four distinct places.

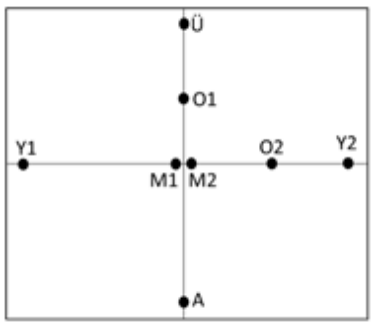


U : Top surface
A : Bottom surface
Y1 : Side surface 1
Y2 : Side surface 2
O1 : Intermediate 1
O2 : Intermediate 2
M1 : Core 1
M2 : Core 2

**Figure 3.7 :** Thermocouple plan

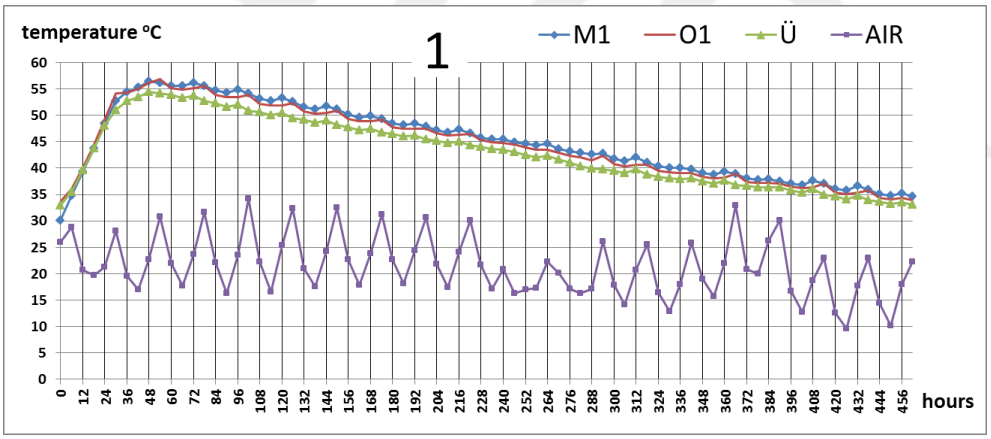


**Figure 3.8 :** Case1 Temperature-Time

Measurements were made to ascertain how the heat produced during the hydration of the concrete blocks affected the temperature development at the surfaces (bottom,top, and sides), at a middle region, and at the core. Graphs were created to analyze selected locations with varying thermal insulation, as there was a high correlation among similar measurement points. The main findings of the analysis are presented in Table 3.8.

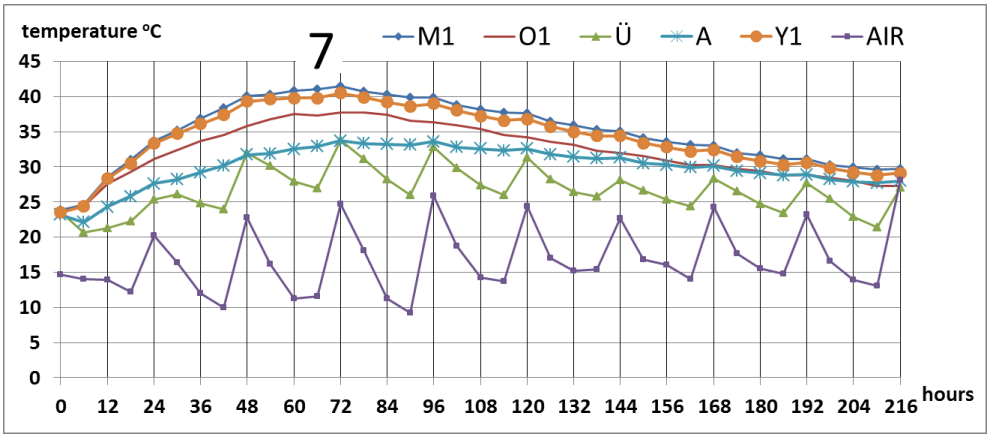


**Figure 3.9 :** Case7 Temperature-Time

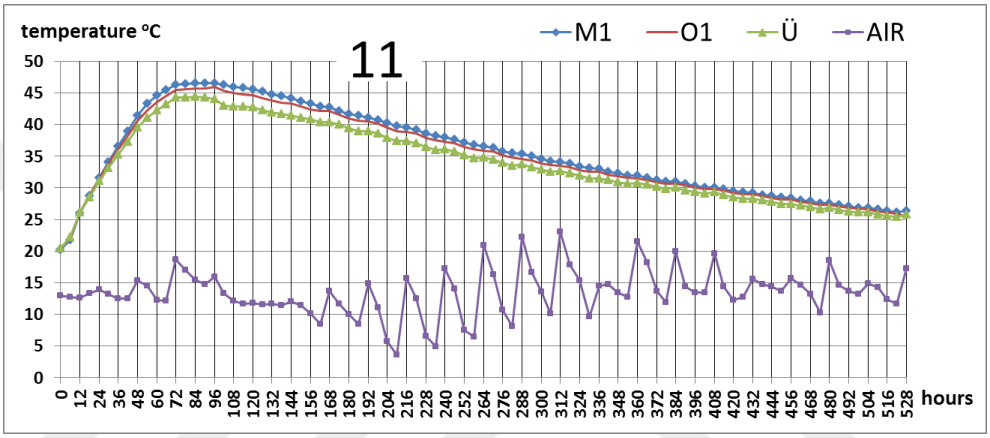


**Figure 3.10 :** Case11 Temperature-Time

### 3.5.3 Micro-climate effect

Unique behavior was seen in the recorded data from the right and left thermocouples in cases where insulation was absent which is shown in Figures 3.12 and 3.13. The difference can be attributed to how the microclimate affects the concrete hydrates. The two main causes of this phenomenon are shading and solar radiation exposure. The concrete's right and left sides may experience different temperatures as a result of uneven solar exposure. Another significant factor is also introduced by the concrete sample's placement because the geometry of the area and the proximity of nearby structures can change wind speed, which can change the convection coefficients. This topic can be investigated more in detail in the future.

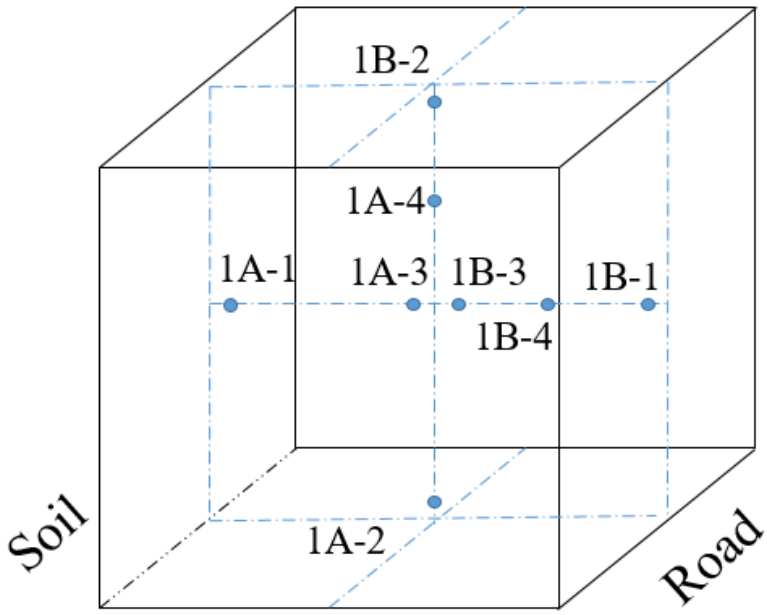


**Figure 3.11 :** The location of thermocouples

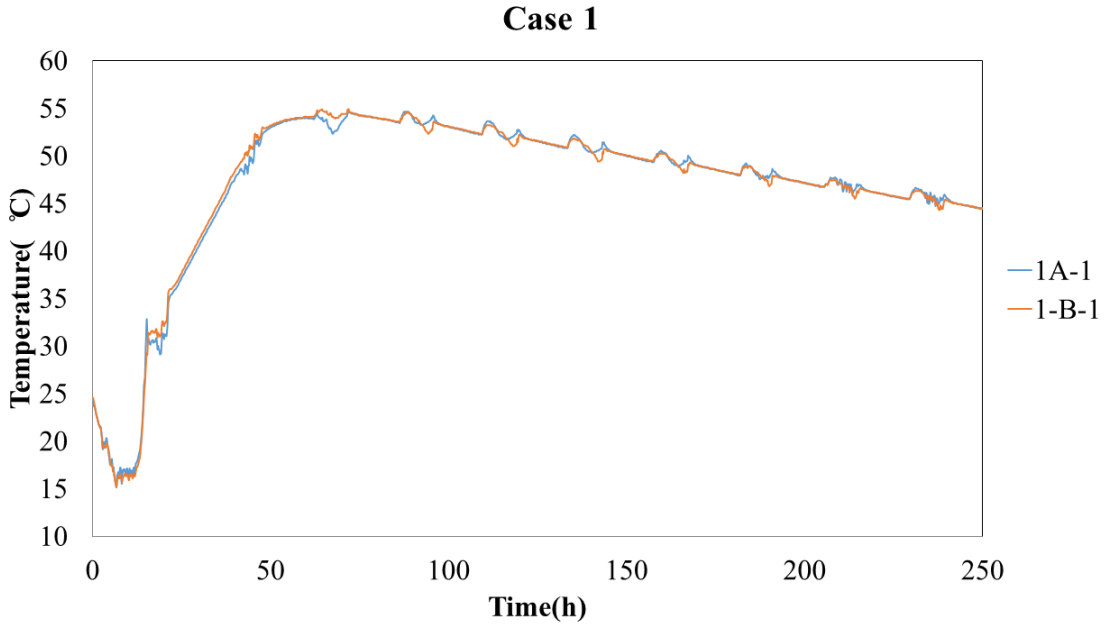


**Figure 3.12 :** The effect of microclimate on right side and left side of the concrete element in Case1

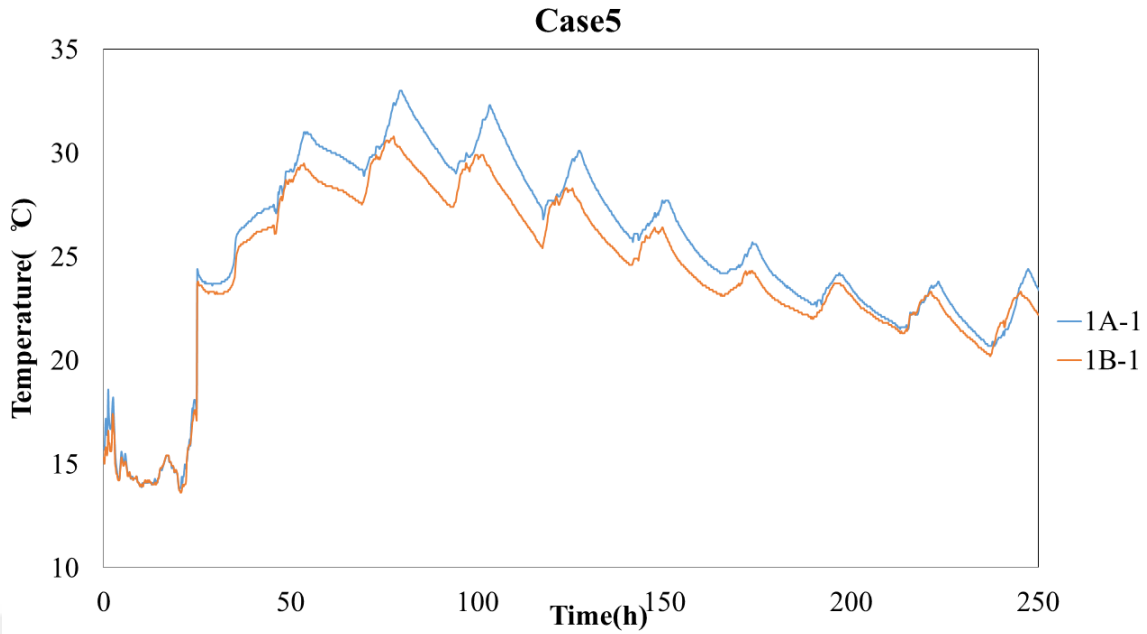


**Figure 3.13 :** The effect of microclimate on right side and left side of the concrete element in Case5

The appendix section (Appendix 1) contains graphical representations of the results obtained for all 14 cases, depicting the temperature evolution of different nodes over time, along with the corresponding ambient temperature. However, in this particular chapter, only case 1, case 7, and case 11 have been depicted as they will be used for validating the current model, with one case chosen from each phase.

### 3.6 Analysis of the results

In conclusion, it is customary to insulate the sides of mass foundation concretes but not their top surface and curing sheets used to stop evaporation are ineffective at insulating heat. Additionally, many projects only limit the maximum temperature and don't take any steps to minimize temperature gradient, specific to the side surfaces. The value of heat insulation in reducing temperature disparities is demonstrated by this experiment.

1- The maximum temperatures for mass concrete are generally reached within 48 hours, depending on various factors.

2- Rather than insulating qualities, cement quantity and the temperature of freshly laid concrete impact the maximum temperature.

3- Insulation on all surfaces of the structure can significantly lower temperature differences and provide a longer cooling period.

4- Ground temperature should also be considered when analyzing temperature differences in concrete.

5- XPS, EPS, or other materials with low heat conductivity can be used to insulate the top surface of the structure efficiently.

5- The microclimate has a significant effect on the temperature profile within concrete elements. In contrast to prior models that usually assumed symmetry, consideration of the microclimate introduces the idea that a concrete element might experience varying environmental conditions on different sides.

# 4. SIMULATION

The construction of a thermal simulation that is intended to estimate the increase in internal temperature in concrete elements during the initial stages of hydration will be discussed in this chapter. The simulation was created using the finite volume approach, and the assumptions that were adopted to make the problem simpler are described. Additionally, the simulation's boundary conditions are shown. The chapter will conclude with a summary of the steps and justification for the Python-based numerical simulation.

## 4.1 Problem Outline

The purpose of the thermal simulation is to compute the heat flow equations to figure out how the interior temperature of concrete elements develops throughout the early stages of their life. The two most important parameters that influence temperature development are the pace at which cementitious materials hydrate and the level at which the heat is exchanged with the surrounding environment. Figure 4.1 demonstrates how these factors are combined to develop the thermal simulation. The rate of hydration can be determined either by calorimetry data or a hydration model, as discussed in Chapter 2. Isothermal heat-conduction calorimetry is the preferred method, but it may not be possible due to budgetary or scheduling constraints. The second part required for this simulation is understanding the environmental influences, including the environmental temperature, wind velocity, and solar radiation. The boundary conditions for simulating the element are determined by these variables, and their prediction is determined by previous models, as explained in Section 4.4.4.

Figure 3-1:

Once a sufficient understanding of the rate of hydration and environmental influences has been obtained, the heat flow equation (Equations 4.2 and 4.2) can be utilized to calculate the heat flow between the concrete element and its surrounding environment,

and ultimately determine the resulting temperature rise. It is important to note that there are multiple approaches to solving the problem at hand, given the information presented above. One such approach is to use a general-purpose software application such as ANSYS, which is capable of performing linear and non-linear heat conduction problems in addition to finite-element structural analysis, maturity concept can be added to this simulation by APDL. However, this method requires a thorough understanding of the solution techniques and the various thermal inputs, also it has a drawing phase in the software which is a time-consuming process.

Using specialized computer simulation software made for the hydration of cementitious systems is a second way to overcome the problem of temperature modeling. Comparing this strategy to employing a general-purpose application has a number of advantages. First off, it makes the program's use simpler by allowing the designer to choose between different issue divisions and numerical solution techniques. This method also enables the creation of a specific input dataset based on experimental material testing, which is superior to depending solely on calorimetry method data. Additionally, it is quite quick, making it the ideal option for preliminary modeling. Later, for extensive modeling, it may be combined with finite element modeling in ANSYS and ABAQUS. Because of these benefits, the specific-purpose program will be used for this thesis project, and the thermal simulator program will be developed accordingly.

### 4.1.1 Design Goals

A solid understanding of the numerical methods used in heat transfer analysis is necessary when creating a computer program to do one. It's also important to make an effort to meet the software's capabilities with the demands of the end user. These features include the program's flexibility, reliability, portability, and usability among other things. This is the main reason for choosing Python as the simulation software since it gives the capability for developing further.

As previously mentioned in Chapter 1, the development of the thermal simulation involved establishing a set of design goals to guide the development process and determine its success. These design goals include: (1) providing estimates of the

maximum internal concrete temperature to determine the need for a more complete thermal analysis, (2) utilizing a simplified set of inputs based on known material properties , and (3) allowing the user to override any input data supplied by the program for situations where better input data is available.

The development of this program will also be influenced by the identification of the target end-users. Consulting engineers and technical service professionals from ready-mixed concrete and cement businesses were among the two groups of end-users that were defined. The application would be used by consulting engineers to conduct an initial assessment of the appropriateness of a certain mix design in relation to thermal cracking difficulties for a given element. Technical service personnel, on the other side, would utilize the simulation to show how mixes with additional cementing ingredients may successfully reduce thermal cracking problems.

Due to the broad nature of the two identified end-user categories, there may be varying demands for different inputs and outputs of the simulation program. For instance, technical service personnel may depend on their own knowledge of cement chemistry whereas consulting engineers might choose to employ inputs derived from isothermal calorimetry. and the power of this simulation is that both of these inputs can be used.

### 4.2 Different simulation methods

In simulating the heat development of concrete, there are different numerical methods available such as the finite difference method, finite element method, and finite volume method. The finite difference method approximates the solution by discretizing the domain into a grid of nodes and solving the heat equation at each node using the temperature values at neighboring nodes. The finite element method subdivides the domain into smaller subdomains called elements and uses a system of equations to solve for the temperature distribution. The finite volume method, on the other hand, divides the domain into small control volumes and applies the conservation laws to the control volumes, resulting in a set of algebraic equations that can be solved to obtain the temperature distribution.

### 4.2.1 Finite-Difference Methods

Anderson et al. (1984) explained that the finite difference method involves discretizing the continuous problem into a grid of defined points where the dependent variables are considered. To obtain the discretized equations, a Taylor series expansion of Fourier Law (Equation 4.1) is performed using a central difference approximation around each grid point. The outcome is an algebraic representation of the partial differential equation (PDE). The finite difference method is one of the most straightforward numerical methods for solving partial differential equations, but it may not be suitable for complex geometries or irregularly shaped domains.

### 4.2.2 Finite-Element Method

The finite-element method is often used for more complex thermal analyses as it provides a better ability to model complex shapes, changes in material, and irregular boundary conditions. It can also simultaneously perform thermal analysis and stress-strain analysis but requires an advanced discretization procedure, particularly for 3D analyses. However, for the purpose of the thermal simulation program being developed the main benefit of the finite element method is for modeling the irregular shape element.

### 4.2.3 Finite-Volume Method

The finite volume method is a numerical technique used to solve partial differential equations, which is commonly used in simulating heat development in concrete. This method discretizes the problem domain into a set of small control volumes, where the conservation laws are applied to each control volume. The method calculates the flow of heat or mass across the boundaries of each control volume and then integrates these fluxes over the volume to calculate the change in temperature or concentration within each control volume over time. It has a conservative nature, which means that it accurately conserves mass, energy, and other properties within each control volume. In this thesis, the finite volume method is used to simulate heat development

in concrete, as it provides a reliable and efficient way to solve the governing equations while accurately capturing the behavior of the concrete material.

## 4.3 Assumptions and Limitations

The thermal simulation program was developed with several assumptions to make the program less complex. These assumptions will be discussed in the following sections, and their limitations will be explained.

### 4.3.1 Geometry

In the current simulation program, we assume that the concrete elements have a rectangular shape. This is a simplification that allows us to more easily divide the element into a regular grid and apply the finite volume method. However, this assumption limits the program's ability to simulate thermal development in elements with irregular shapes. The simulation program can only handle rectangular elements with a consistent cross-section.

Despite this limitation, the rectangular shape assumption is reasonable for many structural elements such as walls, beams, and slabs. These elements are often designed with a rectangular cross-section, and therefore, the simulation program can be used effectively for many applications. However, for more complex shapes, finite element methods software such as ANSYS and ABAQUS may be more appropriate. These software programs can handle irregular shapes and more complex boundary conditions, providing more accurate simulations for specific applications. Therefore, while the current simulation program has its limitations, it is still a useful tool for simulating heat development in many rectangular concrete elements.

### 4.3.2 Boundary Conditions

Various external factors can influence the heat flow between a block of concrete and its surroundings, which are known as boundary conditions. These factors include the conduction of heat to the supporting layers, formwork, and surface coatings; convection from the concrete surface and formwork; absorption of solar radiation; heat loss due to evaporation of water on the surface caused by bleeding or curing water;

and radiation from the concrete surface [40]. These factors can significantly affect the thermal behavior of concrete elements, and their inclusion in thermal simulations is essential for accurate predictions of temperature development, however, all of them do not have the same effect and some of them can be neglected for faster and simpler simulation.

The thermal simulator used in this study will only consider conduction, convection, and radiation boundary conditions, ignoring the other external influences. The reason behind this decision is that conduction and convection are typically the most significant boundary conditions that affect concrete elements under field conditions. To improve the accuracy of the simulation, equivalent convection coefficients will be used to account for the effects of formwork [7]. However, the effects of evaporation from the concrete surface will be neglected in the simulation, assuming that the concrete's surface is properly protected by surface coverings.

It is worth noting that the exclusion of certain boundary conditions may limit the accuracy of the thermal simulation. Therefore, for more complex simulations, including all external influences would be necessary. For instance, in situations where evaporation plays a crucial role, its effect must be considered, and appropriate measures should be taken to protect the concrete's surface from excessive water loss. Similarly, in cases where solar absorption or radiation from the concrete surface is significant, incorporating these boundary conditions into the simulation would be essential to obtain accurate results. Since this simulation is on python adding these features, if it is needed for a project, is easy. Exploring the integration of mechanisms that are currently not incorporated as a potential avenue for future research could be one way to improve the precision of modeling in this area.

## 4.4 2-D Mathematical Modeling

### 4.4.1 Heat Model

The Fourier equation is used to study heat flow in a rectangular concrete element. for a 2-D modeling corresponding form given as Equation 4.1

$$\rho \times C_p \times \frac{\delta T}{\delta t} = k\left(\frac{\delta^2 T}{\delta x^2} + \frac{\delta^2 T}{\delta y^2}\right) + Q' \tag{4.1}$$

where $T$, $t$, $k$, $\rho$, $C_p$, and $Q'$ are temperature, time, thermal conductivity, density, specific heat capacity and heat flux, respectively.

The equation governing heat transfer in a 3-D solid is presented in Equation4.2, with variables including temperature ($T$), time ($t$), thermal conductivity ($k$), density ( $\rho$), specific heat ( $C_p$), and heat flux ($Q'$). Throughout this chapter, a comprehensive discussion is provided regarding all parameters related to early age concrete. :

$$\rho \times C_p \times \frac{\delta T}{\delta t} = k\left(\frac{\delta^2 T}{\delta x^2} + \frac{\delta^2 T}{\delta y^2} + \frac{\delta^2 T}{\delta z^2}\right) + Q' \tag{4.2}$$

This thesis will continue with both 2-D and 3-D modelings.

### 4.4.2 Developing The Finite Volume Model

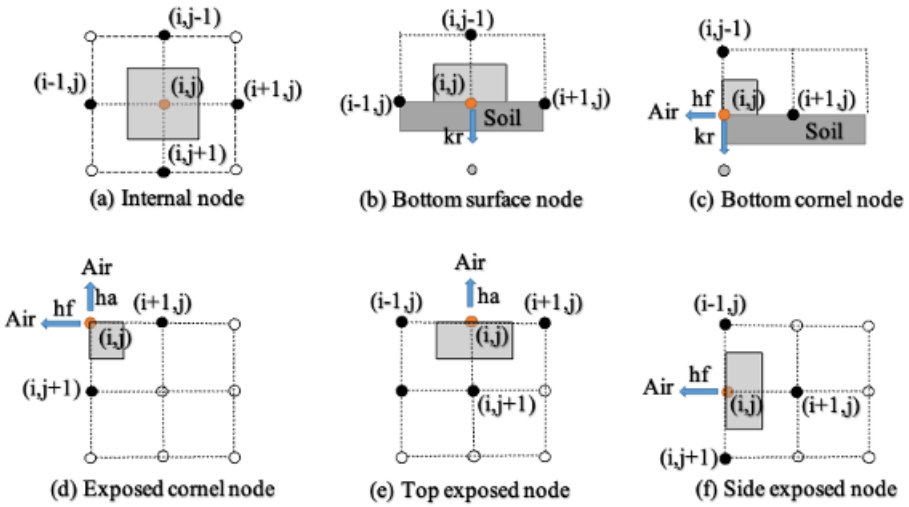


**Figure 4.1 :** Constituent points of an element.

Figure 4.1 depicts the constituent points of an element along with various heat transfer mechanisms between the concrete and its surroundings at a particular node. The control region associated with each node is represented by a gray rectangular area, and the equilibrium equations are presented below:

The equilibrium equation for an internal node Figure 4.1 (a) is.

$$k\Delta\left[\frac{T_{i+1,j}+T_{i-1,j}+T_{i,j-1}+T_{i,j+1}-4T_{i,j}}{\Delta}\right]+Q'\Delta^2 = C_p\rho\frac{\delta T}{\delta t}\Delta^2 \tag{4.3}$$

$$\delta t \leq \frac{C_p\rho\Delta^2}{4k} \tag{4.4}$$

For the bottom surface node Figure 4.1 (b) Considering a fictitious node at a distance from the point in soil with thermal conductivity of $K_r$. Because the impact of solar radiation is not taken into account in this research, the temperature of the soil($T_r$) won't change quickly in response to the ambient temperature; therefore, it can be regarded as the previous day's minimum temperature [6]. the governing equation is then of the form:

$$k\frac{\Delta}{2}\left[\frac{T_{i+1,j}+T_{i-1,j}+T_{i,j-1}-4T_{i,j}}{\Delta}\right]+k_r\frac{\Delta}{2}\left(2T_r-2T_{i,j}\right) +Q'\frac{\Delta^2}{4} = C_p\rho\frac{\delta T}{\delta t}\frac{\Delta^2}{4} \tag{4.5}$$

$$\delta t \leq \frac{C_p\rho\Delta^2}{k\left(4+2\frac{k_r}{k}\right)} \tag{4.6}$$

In the exposed corner node Figure 4.1 (c), Convection is given two different coefficients. $h_a$ is the convection between the concrete's surface and the air; $h_f$ is the equivalent convection coefficient when the formwork is taken into account[4] (described in detail in section 4.4.7.7), after removing the formwork hf will be equal to ha.

$$k\frac{\Delta}{2}\left[\frac{T_{i+1,j}+T_{i,j+1}-2T_{i,j}}{\Delta}\right]+h_f\frac{\Delta}{2}\left(T_a-T_{i,j}\right)+ h_a\frac{\Delta}{2}\left(T_a-T_{i,j}\right)+Q'\frac{\Delta^2}{4} = C_p\rho\frac{\delta T}{\delta t}\frac{\Delta^2}{4} \tag{4.7}$$

$$\delta t \leq \frac{C_p \rho \Delta^2}{4k\left(1+\frac{(hf+ha)\Delta}{2k}\right)} \tag{4.8}$$

The transferred heat on the bottom corner nodes Figure 4.1 (d), where concrete contacts the soil, is the combination of conduction between concrete and soil, and convection with the environment, so the equilibrium equation for this node is

$$\begin{aligned} &k\frac{\Delta}{2}\left[\frac{T_{i+1,j}+T_{i,j-1}-2T_{i,j}}{\Delta}\right]+h_f\frac{\Delta}{2}\left(T_a-T_{i,j}\right)+ \\ &k_r\frac{\Delta}{2}\left(T_r-T_{i,j}\right)+Q'\frac{\Delta^2}{4}=C_p\rho\frac{\delta T}{\delta t}\frac{\Delta^2}{4} \end{aligned} \tag{4.9}$$

$$\delta t \leq \frac{C_p \rho \Delta^2}{2\left(2k+k_r+h_f\Delta\right)} \tag{4.10}$$

Side exposed node Figure 4.1 (e) equilibrium equation is

$$\begin{aligned} &k\frac{\Delta}{2}\left[\frac{2T_{i+1,j}+T_{i,j+1}+T_{i,j-1}-4T_{i,j}}{\Delta}\right]+h_f\frac{\Delta}{2}\left(T_a-T_{i,j}\right)+ \\ &+Q'\frac{\Delta^2}{4}=C_p\rho\frac{\delta T}{\delta t}\frac{\Delta^2}{2} \end{aligned} \tag{4.11}$$

$$\delta t \leq \frac{C_p \rho \Delta^2}{4k+2hf\Delta} \tag{4.12}$$

The equilibrium equation for top exposed node Figure 4.1 (f) is

$$\begin{aligned} &k\frac{\Delta}{2}\left[\frac{T_{i+1,j}+2T_{i,j+1}+T_{i-1,j}-4T_{i,j}}{\Delta}\right]+h_f\Delta\left(T_a-T_{i,j}\right)+ \\ &Q'\frac{\Delta^2}{2}=C_p\rho\frac{\delta T}{\delta t}\frac{\Delta^2}{2} \end{aligned} \tag{4.13}$$

$$\delta t \leq \frac{C_p \rho \Delta^2}{4k+2ha\Delta} \tag{4.14}$$

While selecting time steps ($\delta t$) limited consideration should apply according to the second law of thermodynamics.

### 4.4.3 Modelling Of Internal Heat Generation Rate

To develop accurate mathematical models for temperature development in cement-based systems, adiabatic tests are conducted on samples to determine the liberated heat during hydration and the associated generated heat rate. The maturity approach is used to consider the effects of time and temperature concurrently. Instead of a time rate, the heat evolved during the adiabatic test must be expressed as a function of cumulative maturity, in terms of the "maturity heat rate."

$$Q'_M = \frac{dQ}{dM} \tag{4.15}$$

The adiabatic test provides a heat rate as shown in Figure 4.2, which accounts for the effects of both time and temperature. The x-axis represents equivalent age, taking into consideration the impact of both time and temperature. these data are taken from Ballim's research[3]

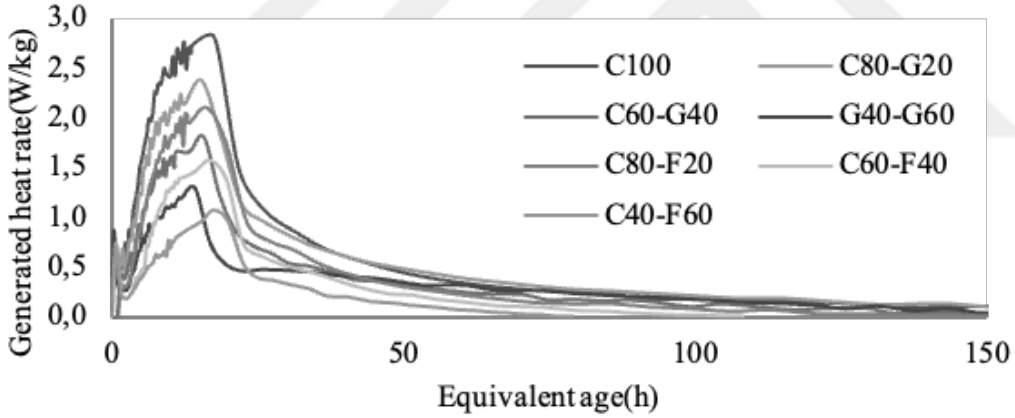


**Figure 4.2 :** The results of the heat of hydration test, the adiabatic analysis of the GGBF slag, and the class F fly ash [6]

Equation 4.1 requires the temporal heat rate, which can be obtained using the chain rule to calculate the "time-based heat rate". in this method $Q'_M$ obtained from adiabatic or semi-adiabatic test, then $\frac{dM}{dt}$ is found by equation 4.18.

$$Q'_t = Q'_M \frac{dM}{dt} \tag{4.16}$$

Rastrup [41] proposed a linear function for maturity in 1954, represented by equation 4.17 where $\tau_{ns}$,$T_r$ are equivalent age and reference temperature respectively. Here, $T$ represents the average temperature of concrete within time interval $t$, and $T_0$ is the datum temperature which is typically considered as 10°C. The affinity ratio is represented by $\gamma(T)$. However, it was later found that the linear maturity approximation is not suitable for a wide range of temperatures. Therefore, a new expression for maturity was introduced using the Arrhenius equation 4.18, which takes into account the non-linear effect of temperature on the hydration of concrete [5].

$$\tau_{ns} = \int_0^t \frac{T - T_0}{T_r - T_0} dt = \int_0^t \gamma(T)\, dt \tag{4.17}$$

$$M = \sum_{i=1}^{n} \exp\left[\left(\frac{E_a}{R}\right)\left(\frac{1}{273 + T_r} - \frac{1}{273 + T_i}\right)\right]\Delta t_i \tag{4.18}$$

Where $M$ is the time needed to reach an equivalent maturity while curing at 20°C; $T_i$ is the concrete average temperature ($^\circ C$) in the time interval $\Delta t_i$; $T_r$ is the reference temperature (taken as 20°C); $R$ is the universal gas constant $(8.31 J/molK)$ and $E_a$ is the apparent activation energy.

Another technique involves using the degree of hydration function to determine the generated heat rate during hydration. As explained in the section4.4.7.6, this approach requires finding the hydration parameters and fitting the corresponding curve to the heat curve obtained from the semi-adiabatic test. By doing so, three parameters, $\alpha_u$, $\tau$, and $\beta$ - can be obtained. These parameters can then be utilized with equation 4.19 and 4.20 to estimate the generated heat rate during the hydration process.

$$Q(t_e) = Q_u.[\alpha(t_e)] \tag{4.19}$$

$$q(t_e) = Q_u.\alpha(t_e).\left(\frac{\tau}{t_e}\right)^{\beta}.\left(\frac{\beta}{t_e}\right) \tag{4.20}$$

Equation 4.20 describes the rate of heat generation during cement hydration as a function of equivalent age. However, when simulating the hydration process, it is

necessary to use equation 4.16 and obtain equation 4.21 since it is based on real-time rather than equivalent age.

$$q(t) = Q_u.\alpha(t_e).\left(\frac{\tau}{t_e}\right)^{\beta}.\left(\frac{\beta}{t_e}\right).\exp\left[\left(\frac{E_a}{R}\right)\left(\frac{1}{273+T_r}-\frac{1}{273+T_i}\right)\right] \quad (4.21)$$

In this thesis, for 2-D simulation, we used the first approach, but for 3-D simulation equation 4.21 is used.

### 4.4.4 Boundary Conditions

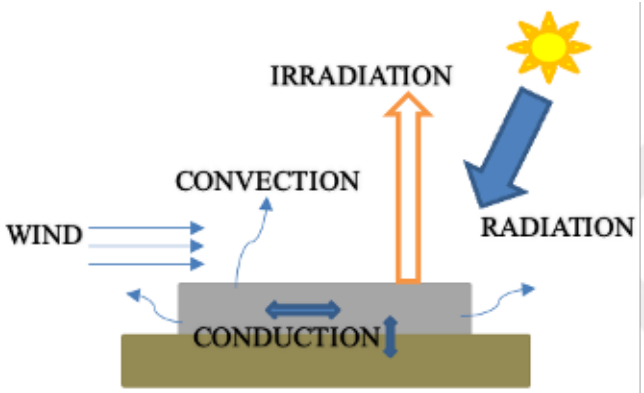


**Figure 4.3 :** Heat transfer between concrete and its surroundings

External heat exchange between concrete structures and their environment is a critical factor that affects the temperature development in concrete. Concrete structures can lose heat to their surroundings through four main mechanisms: radiation, conduction, convection, and irradiation. These mechanisms are illustrated in Figure 4.3. The extent to which each of these mechanisms occurs depends on several factors, such as the type of concrete, ambient temperature, and wind speed. Accurately understanding and modeling the heat exchange between concrete structures and their environment is essential for designing and maintaining durable and safe concrete structures.

#### 4.4.4.1 Thermal conductivity

Thermal conductivity refers to the measure of how quickly heat is transferred across a unit cross-sectional area by conduction when there is a temperature gradient perpendicular to the area. In other words, it describes how efficiently a material conducts heat. The thermal conductivity of a material depends on several factors,

**Table 4.1 :** Thermal conductivity of the concrete with different types of aggregates.

| Aggregate type | Thermal conductivity [$Wm^{-1}K^{-1}$] |
|---|---|
| Quartzite | 3.5 |
| Dolomite | 3.2 |
| Limestone | 2.6 - 3.3 |
| Rhyolite | 2.2 |
| Basalt | 1.9 - 2.2 |
| Granite | 2.6 - 2.7 |

including its composition, density, and temperature. Materials with higher thermal conductivity transfer heat more quickly than materials with lower thermal conductivity, As the heat conductivity of a concrete element increases, the thermal gradient within the concrete decreases.

$$q = \frac{k\Delta T}{d} \tag{4.22}$$

Where $q$ is the conduction heat flux per unit area, $k$ is the conduction coefficient, $\Delta T$ is the temperature difference between two points, and d is the distance between two points.

Since almost 80% of the concrete is aggregate, the main influencing factor in the conduction coefficient is the $k$ value of the aggregates (Table. 4.1).

Studies have shown that various factors can affect the thermal conductivity of concrete, such as the saturation water-to-cement ratio ($w/c$), age, admixture types, aggregate volume fraction, temperature, and free water content [42]. The recommended range of thermal conductivity for cured concrete at $20°C$ is between 1.2 and 3.5 $Wm^{-1}K^{-1}$ [33].

Another important aspect to consider is the change in the thermal conductivity of concrete over time as it hydrates. The conductivity is influenced by the amount of free moisture content in the concrete, which changes as the cement hydration reactions continue. Therefore, it is reasonable to expect changes in concrete thermal conductivity at early ages [42], in the section 6.2 sensitive analysis is conducted on this topic.

Researchers [43] have observed that the thermal conductivity of concrete drops linearly with respect to its initial value as a function of the degree of hydration. They concluded that the initial value is %110 of its final value. Understanding the temporal evolution

of thermal conductivity in concrete is crucial for accurate prediction of the temperature profile in concrete structures.

$$k(\alpha) = k(1.10 - 0.10\alpha) \tag{4.23}$$

However, contradictory results are reported in other studies on this topic, for instance, [44], considered the initial $k$ as being %133 of its final value.

$$k(\alpha) = k(1.33 - 0.33\alpha) \tag{4.24}$$

#### 4.4.4.2 Specific Heat Capacity

The specific heat capacity is the amount of heat energy per kilogram required to raise the temperature of a substance by one degree Celsius. In hardened concrete, this value has been reported to range from 840-1170 $JKg^{-1}\mathrm{K}^{-1}$ [3]. A substance with a higher specific heat capacity requires less temperature rise for a given energy input.

Numerous studies have investigated changes in concrete's specific heat capacity over time, and most agree that the value of $C_p$ is slightly higher at the beginning of hydration compared to the end. This is because concrete contains a significant amount of free water at the beginning, but less as hydration progresses. However, there are varying opinions among researchers regarding the magnitude of this decrease in specific heat capacity [45].

One study suggested that the specific heat of concrete decreases linearly as a function of the degree of hydration, with the initial value being %115 higher than the final value [43]. This relationship can be expressed using the equation:

$$C_p(\alpha) = C_p(1.15 - 0.15\alpha) \tag{4.25}$$

where $\alpha$ represents the degree of hydration.

Another study reported the highest specific heat drop during hydration in cement pastes, which was about %27 [46]. This relationship can be expressed using the equation:

$$C_p(\alpha) = C_p(1.27 - 0.27\alpha). \tag{4.26}$$

The specific heat capacity of concrete is an important factor in the thermal analysis and design of concrete structures, as it influences the material's ability to absorb and release heat. Understanding how specific heat changes during hydration is crucial for accurately predicting the thermal behavior of concrete over time.

#### 4.4.4.3 Thermal Convection

Convection is the process of heat transfer between a concrete outer layer and a moving fluid around it. Convection is of two types, namely natural and forced. Natural convection happens when temperature differences cause the fluid to flow, but forced convection happens when the fluid is forcibly made to move. The convective heat transfer equation (equation 4.27), which says that the rate of heat transfer is proportional to the temperature differential between the fluid and the surface of the concrete, may be expressed using Newton's cooling equation. The convective heat transfer coefficient, which is often referred to as the proportionality constant, is influenced by a number of variables including fluid velocity, fluid characteristics, and surface shape.

$$q_a = h_a(T_a - T_c) \tag{4.27}$$

Where $q$ is the convective heat flow per unit area, $h_a$ is the convection coefficient. $T_a$ and $T_c$ are the ambient temperature and the surface temperatures of the concrete, respectively. Convection coefficient $(h_a)$ is primarily affected by wind velocity, which can be calculated using the formula [47]

$$h_a = \begin{cases} 5.6 + 3.95v & v \leq 5ms^{-1} \\ 7.6v^{0.78} & v > 5ms^{-1} \end{cases} \tag{4.28}$$

#### 4.4.4.4 Formwork modeling

When modeling the heat transfer in concrete structures, it is not necessary to replicate the exact formwork geometry. This is because most of the heat flows through concrete surfaces are perpendicular to them, and formwork is usually thin. Therefore, the impact

of heat conduction through the formwork can be combined with the surface boundary coefficient using an electrical analogy, as shown in Figure 4.4. This approach leads to equation 4.29 which simplifies the modeling process and reduces the computational resources required. It is important to note that the accuracy of the simulation depends on the assumptions made in the model, such as the formwork thickness and material properties. Inaccurate modeling of formwork can lead to errors in predicting the temperature and thermal stresses in the concrete, which can affect the long-term durability and performance of the structure. Therefore, careful consideration of the formwork's impact on heat transfer is necessary for the modeling process. .

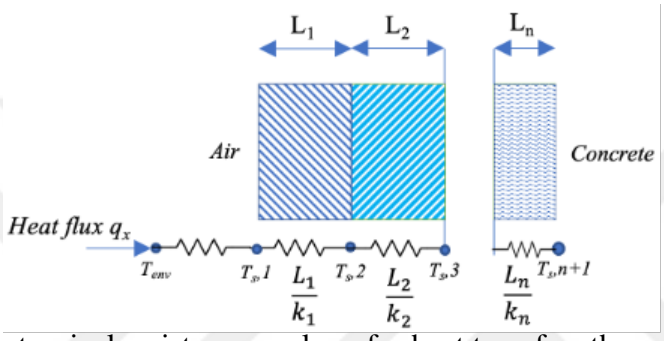


**Figure 4.4 :** Electronical resistance analogy for heat transfers through formwork [7]

$$h_f = \left( \frac{1}{h_a} + \sum_{i=1}^{n} \frac{L_i}{k_i} \right)^{-1} \tag{4.29}$$

#### 4.4.4.5 Radiation

A material medium, such as air or a solid, is not required for the energy transfer that takes place during radiation. It can be conveyed most effectively in a vacuum, where photons move at the speed of light without being absorbed or dispersed. Thermally activated molecules in a body create electromagnetic waves, mostly in the infrared spectrum, which convey energy out of the body. All items that people are aware of produce electromagnetic waves and interact with one another by radiation heat transfer since all of them have a temperature higher than $0K$.

Branco et al. (1992) proposed a method that uses an equation like the boundary equation for convection to determine longwave radiation. The formula involves an energy balance and the use of a radiation exchange coefficient $h_r$:

$$q_{h,r} = h_r.(T_c - T_a) \tag{4.30}$$

$$h_r = \varepsilon\,[4.8 + 0.075.(T_a - 278.15)] \tag{4.31}$$

The emissivity parameter $\varepsilon$ is used to describe the ability of an object to emit radiation, with values ranging from 0 to 1. A perfect emitter is referred to as a black body and has an emissivity of 1, while objects with emissivity values less than 1 are called grey bodies. according to azenha [7], $\varepsilon$=0.88 considered for a concrete material.

The convective heat flux and long-wave radiation heat flux are described by equations 4.27 and 4.30 respectively, and there is a similarity between these equations. As a result, it is possible to simplify the analysis by assuming a single heat transfer coefficient that takes into account both convection and radiation effects. This combined coefficient is denoted as $h_{cr}$ and can be calculated by adding the individual coefficients $h_a$ and $h_r$. In other words, this approach considers the effects of both convection and radiation together to arrive at a single value for the heat transfer coefficient. This simplification can make the analysis of heat transfer easier and more efficient.

$$q_h = q_a + q_{h,r} = h_{cr}.\left(T_{surf} - T_{env}\right) \tag{4.32}$$

With considering radiation and convection together, equation 4.33 will be as follow:

$$h_{eq} = \left(\frac{1}{h_{cr}} + \sum_{i=1}^{n} \frac{L_i}{k_i}\right)^{-1} \tag{4.33}$$

Where $L_i$ and $k_i$ are, respectively, the thickness and thermal conductivity of the $i_{th}$ layer of material in the middle of concrete and the environment, and $h_{cr}$ is the conductivity coefficient of concrete surface and environment with considering radiation and convection together.

#### 4.4.4.6 Environmental Temperature Model

The thermal simulator will also make some assumptions about the environmental conditions to simplify the modeling of boundary conditions. The ambient temperature, T (°C), will be assumed to follow a sinusoidal distribution, given by the following equation [6]:

$$T_A = -\sin\left(\frac{2\pi\,(t_d + t_w)}{24}\right)\left(\frac{T_{max} - T_{min}}{2}\right) + \left(\frac{T_{max} + T_{min}}{2}\right) \tag{4.34}$$

$t_d$ is the clock time of day (0–24 h); $T_{max}$ and $T_{min}$ are the highest and minimum temperatures for the day being considered, respectively; and $t_w$ is the time when the minimum temperature occurs within a day(usually immediately before sunrise). Despite the fact that the ambient temperature mentioned earlier does not account for many variables, such as cloudy weather and direct sun exposure, it can be relied upon as an acceptable model in this study.

In order to improve the accuracy of our thermal simulation and address the limitation of assuming a sinusoidal distribution for ambient temperature, the feature that allows users to input real ambient temperature history data has been added to the model. This means that instead of relying on a simplified model of ambient temperature, the simulation can now use actual recorded temperatures at the site of the concrete element. This feature greatly enhances the accuracy of the simulation by taking into account the actual environmental conditions that the concrete element is exposed to. By allowing users to input real ambient temperature history data, this simulation provides a more precise prediction of heat development and allows engineers to make more informed decisions regarding concrete element design and performance.

As with any simulation program, there is always a degree of uncertainty associated with predicting future temperatures, especially for projects that are not yet underway. While the real ambient temperature history can be introduced into the model, there is always the possibility that this data may not accurately reflect the future conditions

**Table 4.2 :** Thermal conductivity of the concrete with different types of aggregates.

| Input | Value |
|---|---|
| size | 1.5mx1.5m |
| Initial temperature | 23°C |
| Max ambient temperature | 30°C |
| Min ambient temperature | 19°C |
| Formwork removal time | 20h |
| Specific heat capacity | $1097 Jkg^{-1}K^{-1}$ |
| Concrete heat conductivity | $3.5\ Wm^{-1}K^{-1}(Quartzite)$ |
| Formwork material | Wood |
| Soil conductivity | $1.2\ Wm^{-1}K^{-1}$ |
| Air and concrete convection coefficient | $20\ Wm^{-2}K^{-1}$ |
| Formwork equivalent heat convection coefficient | $5\ Wm^{-2}K^{-1}$ |

of the site. Additionally, unforeseen events such as weather extremes or construction delays can also impact the accuracy of temperature predictions.

### 4.4.5 2-D modeling inputs

The simulation requires inputs which are listed in the Table4.2. These inputs are sufficient for the simulation and have been simplified to make it more user-friendly. The simulation is designed to be compared with a previous study conducted by Ballim [6], and therefore, the same inputs have been used to enable a fair comparison.

for the mix design (Table4.3) and heat rate inputs also taken from ballim's research (Figure4.2). [6]

Radiation has not been considered in the current 2-D simulation because it was not a part of Ballim's original model. Radiation will be included in the simulation when this model is developed into a 3-D simulation and tested against actual tests. Moreover, because the reference study did not incorporate variations in thermal conductivity

and specific heat capacity into their research, they are not taken into account in this simulation.

**Table 4.3 :** Mix Design [Kg/m$^3$]

| Component | C100 | C80-G20 | C60-G40 | C40-G60 | C80-F20 | C60-F40 | C40-F60 |
|---|---|---|---|---|---|---|---|
| CEM I 42,5R | 400 | 320 | 240 | 160 | 320 | 240 | 160 |
| Class F Fly ash | - | - | - | - | 80 | 160 | 240 |
| GGBF Slag | - | 80 | 160 | 240 | - | - | - |
| Water | 140 | 140 | 140 | 140 | 140 | 140 | 140 |
| Aggregate 5-22 mm | 1100 | 1100 | 1100 | 1100 | 1100 | 1100 | 1100 |
| Sand 0-4mm | 850 | 850 | 850 | 850 | 850 | 850 | 850 |
| Total | 2490 | 2490 | 2490 | 2490 | 2490 | 2490 | 2490 |

### 4.4.6 2-D modeling result

First result is for CEM100, with the aforementioned inputs (Table4.2)

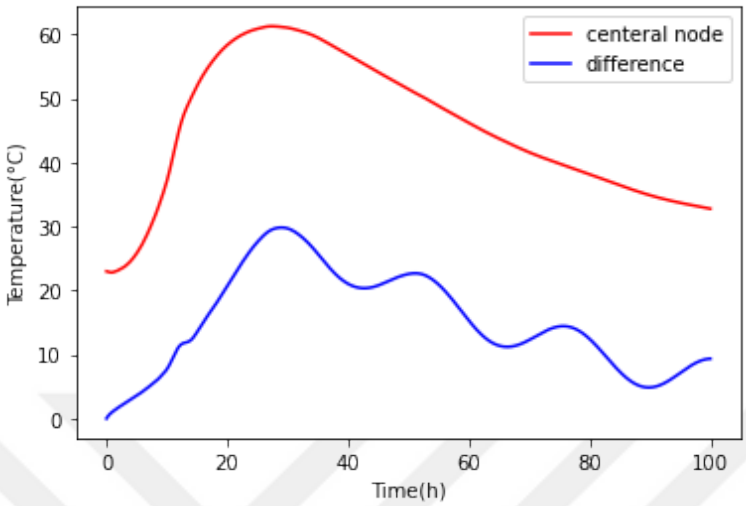


**Figure 4.5 :** 2-D modeling result(C100)

In this test 1.5m x 1.5m cubic concrete element is simulated, as shown in Figure4.5 the maximum temperature that the central node reaches is 61.28°C, and the maximum temperature difference between the central node and the side node is 29.84°C

Secondly, Figure4.6 depicts the result for C40-G60, with the same inputs (table 4.2).

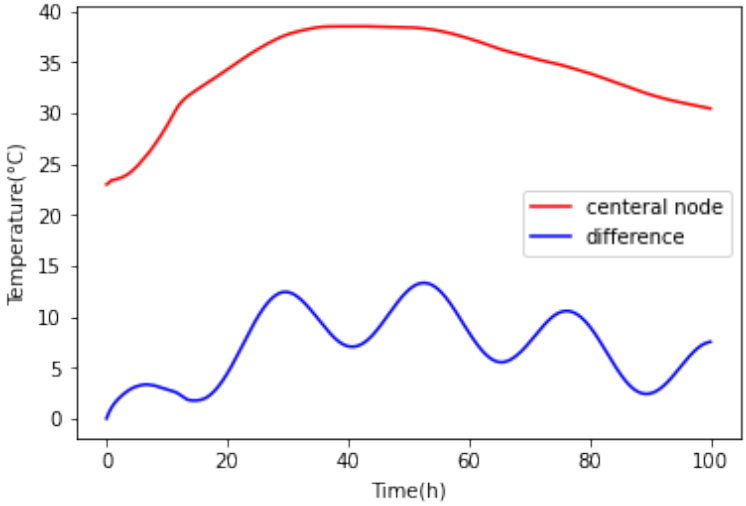


**Figure 4.6 :** 2-D modeling result(C40-G60)

As it is noticeable in the figure4.6 using %60 slag can decrease the max temperature from 61.28°C to 38.55°C, also the difference between the center of the concrete elements and side node is decreased from 29.84°C to 13.33°C by replacing cement with Ground Granulated Blast-furnace Slag.

Finally, the same input is used just this time instead of %60 slag, the same percentage of FlyAsh is used. the result is illustrated in Figure4.7.

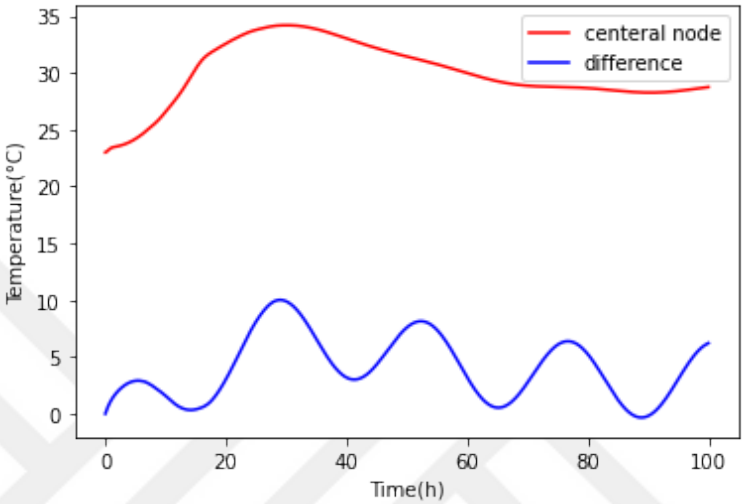


**Figure 4.7 :** 2-D modeling result(C40-F60)

As shown in figure 4.7, using %60 FlyAsh reduces the maximum temperature from 61.28°C to 34.18°C. Also, substituting cement with FlyAsh reduces the temperature differential between the center of the concrete components and the side node from 29.84°C to 10.01°C.

### 4.4.7 3-D modeling inputs and boundary conditions

This work developed a 3D numerical analytical approach that used the finite volume method (FVM) to address fluctuating heat conductivity and capacity throughout early ages. Python was used to build a finite volume numerical model in order to solve the governing equation for transferring heat. This model was created to improve the thermal analysis capabilities of current tools, such as Ballim's spreadsheet application (2003). The findings of the study were compared to temperature-time histories obtained from 1.5m cube castings concrete samples in Bursa Beton factory.

The finite volume approach was used in this work to solve Equation 4.2 and simulate the thermal behavior of concrete element at early ages. To do this, the thermal characteristics of concrete were evaluated using existing models from the literature.

Initially, cement and its composition were used as inputs for this simulation. The subsequent sections of this chapter (section 4.4.7.6) indicate how these properties were incorporated into the model. The following is a summary of the inputs that were available and utilized for the modeling process.

#### 4.4.7.1 Density

Concrete density may be computed easily by summing the component unit weights and determining the total weight of concrete per unit volume.

$P = Binder + Sand + Stone + Water + Admixture\ (kg/m^3)$

#### 4.4.7.2 Thermal conductivity

As stated in section 4.4.4.1, the thermal conductivity of concrete is significantly influenced by the type of aggregate utilized in the mixture. To determine this thermal property accurately, Table 4.1 can be utilized as a useful tool for calculating thermal conductivity, in this experiment as mentioned in section 3.4 limestone is used so the thermal conductivity will be considered as 3.3 $Wm^{-1}K^{-1}$.

#### 4.4.7.3 Cement components

In this investigation, three distinct variations of cement were employed as outlined in Table 3.1, each containing divergent proportions of their constituent elements. These details are crucial in determining the potential amount of heat generated by applying Equations 2.3 - 2.8.

#### 4.4.7.4 Ultimate Degree of hydration

To construct a reliable model, the ultimate degree of hydration must be determined, for which Equation 4.35 will be employed. The requisite water-to-cement ratio can be

obtained from Table 3.5. The ultimate degree of hydration for each case examined in this study is presented below.

$$\alpha_u = \frac{(1.031).(0.34)}{0.194+0.34} + (0.30).(0.75) = 0.88 \leq 1.0 \tag{4.35}$$

#### 4.4.7.5 Ambient temperature

In order to verify the reliability of our model, experimental data was used to input the ambient temperature information. To obtain this information, data collected from Excel was utilized, and interpolation functions in Python were applied to determine the ambient temperature for each loop. The resulting ambient temperature graph was then utilized in our calculations to ensure accurate modeling. The ambient temperature for each cases are depicted in Figures 4.8, 4.9, and 4.10.

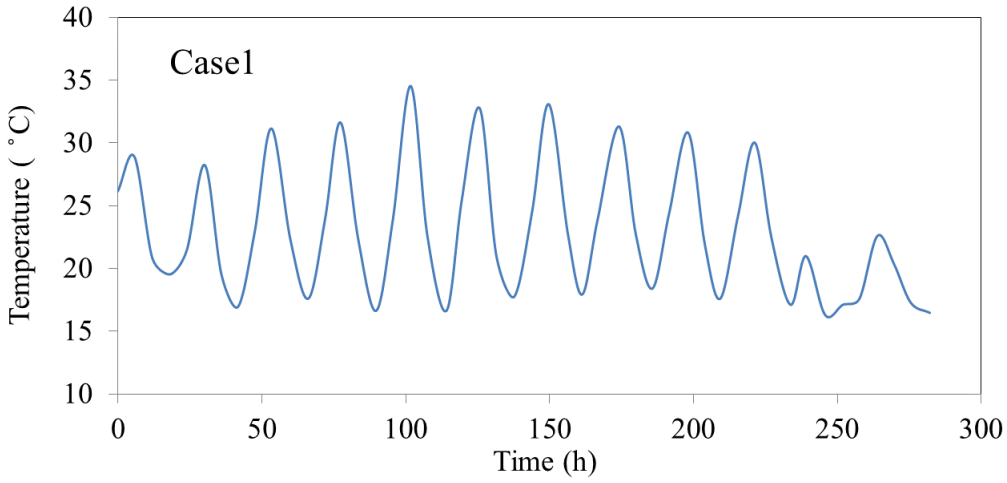


**Figure 4.8 :** Case1 ambient temperature

#### 4.4.7.6 Generated heat rate

To determine the generated heat rate during hydration, two distinct approaches are employed. The fitting curve method is utilized for 3-D simulation. To accomplish this, the generated heat data obtained from semi-adiabatic experiments is transformed into an adiabatic test, and the resulting curve is presented in Figure. 4.11

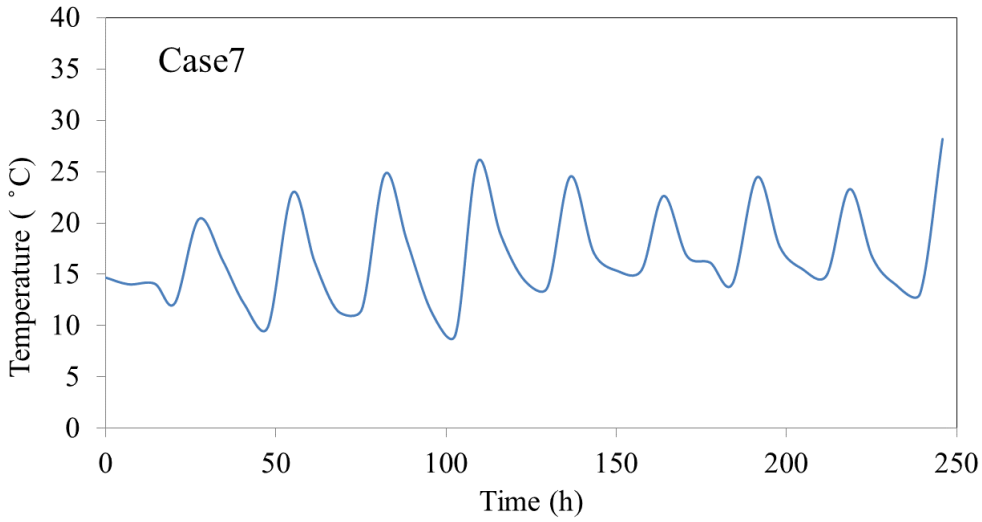


**Figure 4.9 :** Case7 ambient temperature

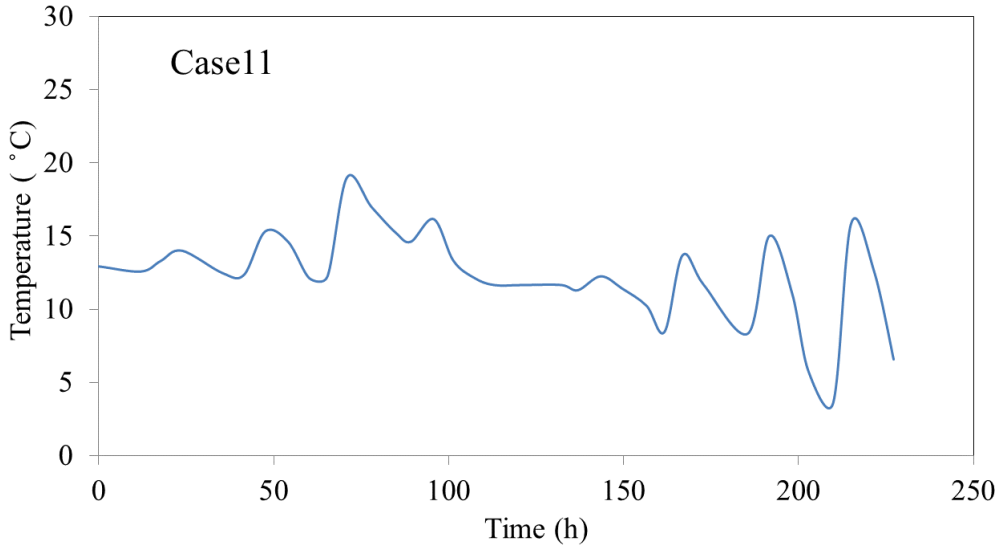


**Figure 4.10 :** Case11 ambient temperature

The thermal parameters for the fitting curve method (Equation 4.36) are provided in Table 4.4, while Figure 4.12 displays the fitting curve itself. Due to the fact that this study uses blended concrete and grand grounded blend slag, two sets of thermal parameters are employed to catch the curve in a better way, this is one of the weaknesses of previous studies [12] where for blended cement they just consider one set of parameters and use equation 2.20, as it is shown in Figure 4.12 by using this equation it is not possible to catch all points from generated heat curve which is

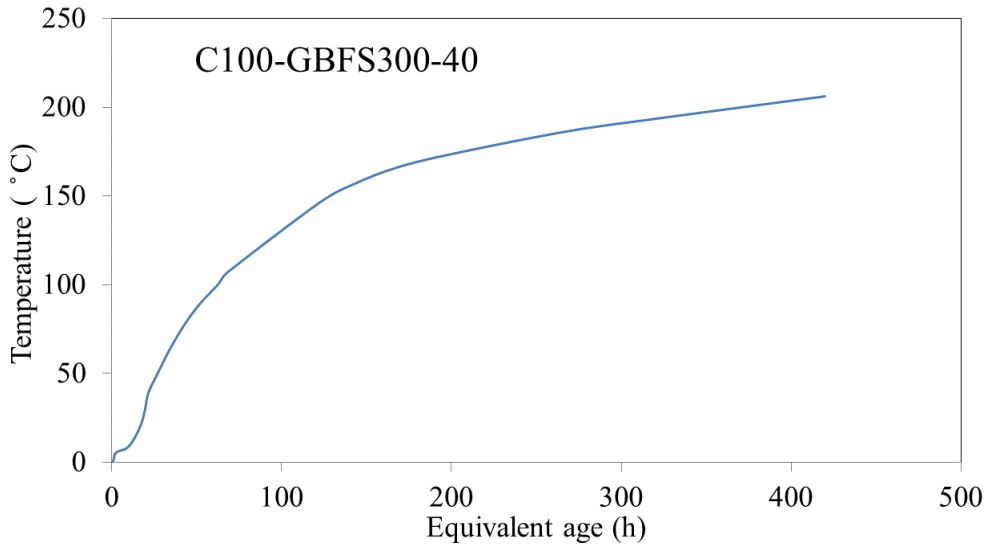


**Figure 4.11 :** C100-GBFS300-0.40 generated heat curve

obtained from the calorimetry test .however, in this study equation 4.36 is used and all points from the calorimetry test data are caught by utilizing this equation in our model:

$$Q(t_e) = Q_u . \left[ \alpha_{u1} . \exp\left( -\left( \frac{\tau_1}{t_e} \right)^{\beta_1} \right) + \alpha_{u2} . \exp\left( -\left( \frac{\tau_2}{t_e} \right)^{\beta_2} \right) \right] \tag{4.36}$$

And it is known that:

$$\alpha_{u1} + \alpha_{u2} = \alpha_u \tag{4.37}$$

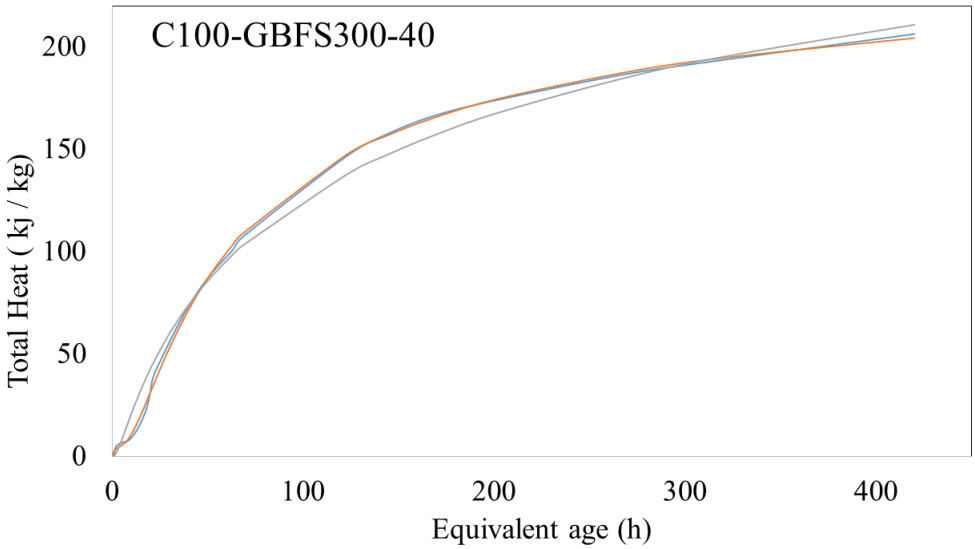


**Figure 4.12 :** C100-GBFS300-0.40 fitting curve

**Table 4.4 :** Thermal parameters

| Parameter | Value |
|---|---|
| $\tau_1$ | 2402.099 |
| $\beta_1$ | 0.149782 |
| $\alpha_{u1}$ | 0.1349 |
| $\tau_2$ | 55.77154 |
| $\beta_2$ | 0.807569 |
| $\alpha_{u2}$ | 0.4854 |

Once the thermal parameters have been obtained, calculating the generated heat rate based on equivalent age is a straightforward process using Equation 4.38.

$$q(t_e) = Q_u \left[ \alpha u_1 \beta_1 \left( \frac{\tau_1}{t_e} \right)^{\beta_1} \exp\left( - \left( \frac{\tau_1}{t_e} \right)^{\beta_1} \right) + \alpha u_2 \beta_2 \left( \frac{\tau 2}{te} \right)^{\beta_2} \exp\left( - \left( \frac{\tau 2}{te} \right)^{\beta 2} \right) \right] \tag{4.38}$$

Figure4.13 displays the resulting generated heat rate.

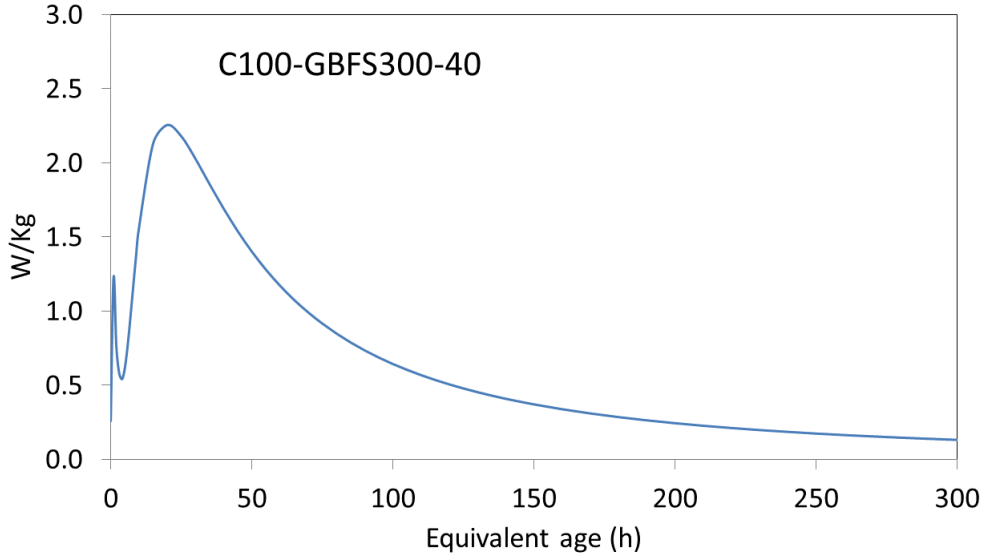


**Figure 4.13 :** C100-GBFS300-0.40 generated heat rate

#### 4.4.7.7 Formwork modeling

As mentioned In the sections 3.2, 3.3, and 3.4, the insulation material used was 10cm EPS with $32kg/m^3$ Density. Based on this, the conduction coefficient of the material was calculated, and by using the Equation 4.29, the equivalent convection coefficient was determined. The obtained value will be utilized in our simulation.

$$h_f = \left( \frac{1}{25} + \frac{0.1}{0.08} \right)^{-1} = 0.8 \tag{4.39}$$

Since thick insulation is used it can be accepted to neglect the effect of other environmental parameters like radiation and irradiation.

### 4.4.8 3-D modeling results

Below are the maximum temperatures recorded for three cases, along with the corresponding maximum temperatures for the side nodes. In Case 1, the maximum temperature was 56.04°C, with a upper node temperature of 54.57°C. In Case 7, the maximum temperature was 41.56°C, with a side node temperature of 39.73°C. In Case 11, the maximum temperature was 46.01°C, with a side node temperature of 44.73°C. The graph for each case is shown in Figure 4.14, 4.15, and 4.16, respectively.

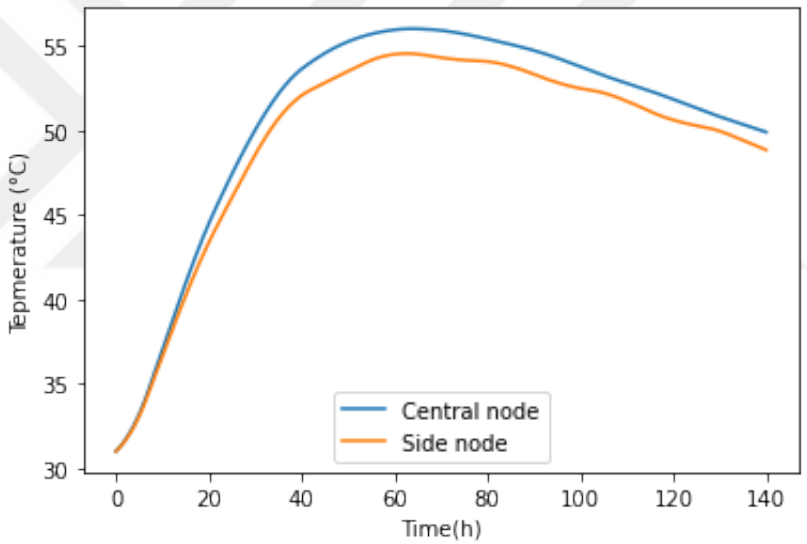


**Figure 4.14 :** Case1 central node and side node temperature development

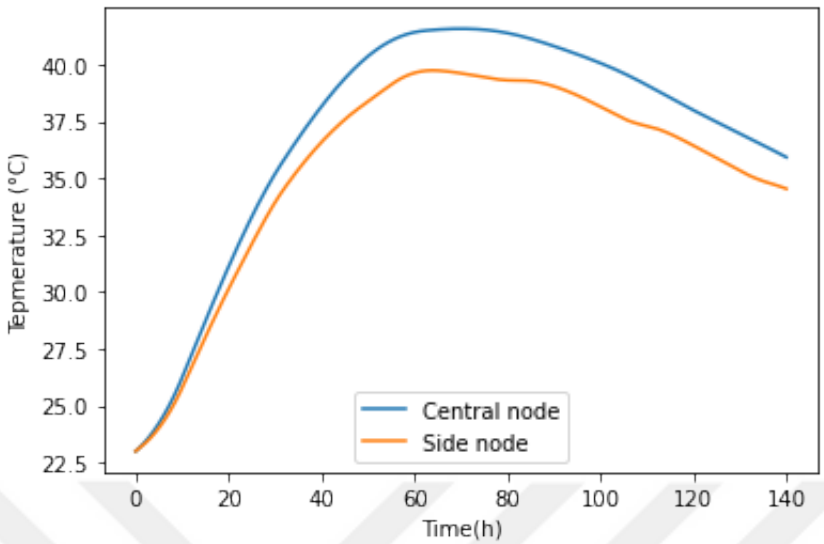


**Figure 4.15 :** Case7 central node and side node temperature development

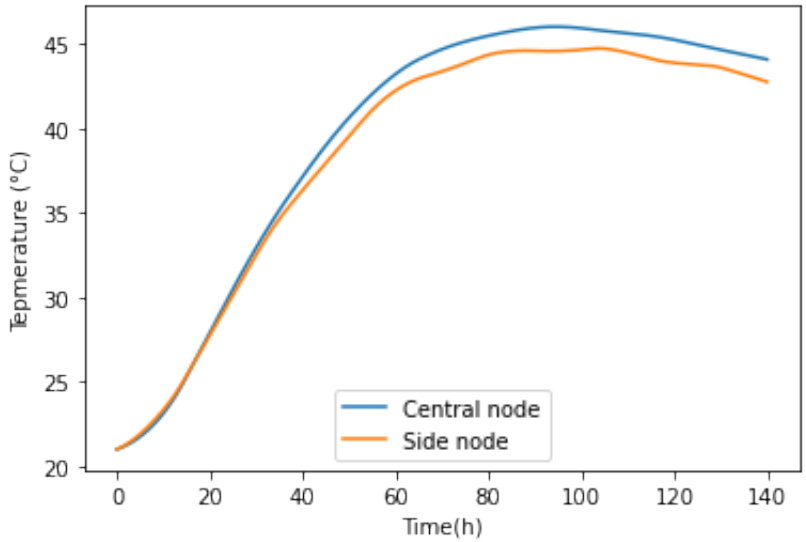


**Figure 4.16 :** Case11 central node and side node temperature development

# 5. VALIDATION

A crucial stage in establishing a numerical model's dependability and accuracy for forecasting the behavior of real-world systems is validation. This chapter describes how 2-D and 3-D numerical models for temperature development within a 1.5m cubic concrete element were validated, also an extra validation have been done to compare our 3-D model wth a previous model which was created by Yun Lin [12]. We contrast the outcomes of our model with experimental information gathered from the Bursa Beton plant. For the purpose of predicting temperature profiles in concrete components, we also contrast the current 2-D, and 3-D models with a prior model, which was designed by Yunus Ballim in 2004 [6] and Lin's model in 2015 [12], respectively. The validation method enables us to assess how well our model predicts temperature development and gives us some assurance that it can properly imitate the behavior of systems in the real world. Results from this chapter's research are essential for establishing.

## 5.1 2-D Model validation

The same input will be utilized for both models during the validation process, and the final outcome will be compared and illustrated in a chart.

The inputs required for the validation process can be located in Table 4.2. Additionally, the activation energy has been selected to be $33256 j/mol$, while the gas constant has been set to $8.314(j/mol.K)$. These values have been carefully chosen to ensure that both models are operating under the same conditions. Using the same parameters and inputs in the validation process will allow for a fair comparison between the two models.

The temperature development profile of the central node is illustrated in Figure 5.1, indicating a significant resemblance between the results obtained from the current model and Ballim's 2-D model. One advantage of this new model, developed in

Python, is that it offers extensive opportunities for future features to be added. Additionally, the running time and outputs that can be obtained from Python surpass those of an Excel worksheet. It is worth noting that the model's validation was achieved by comparing it to a previous model that had already been validated through experiments. Furthermore, Figure 5.2 illustrates the difference between the central node and side node temperature, indicating a strong resemblance between the two results. This similarity serves as further validation of the effectiveness of the current model.

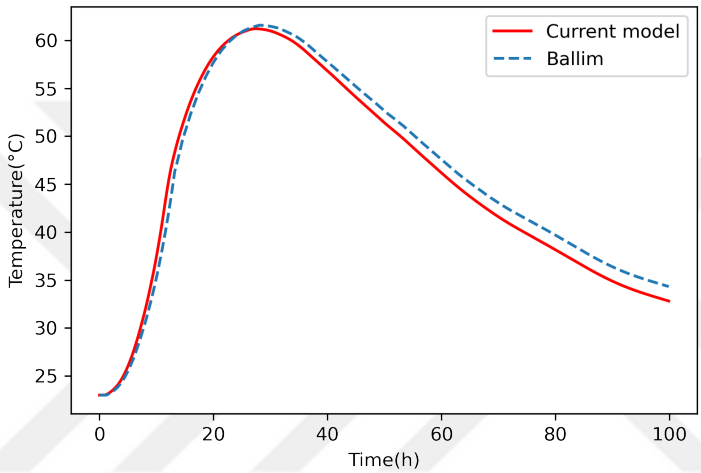


**Figure 5.1 :** Temperature development profile in the central node

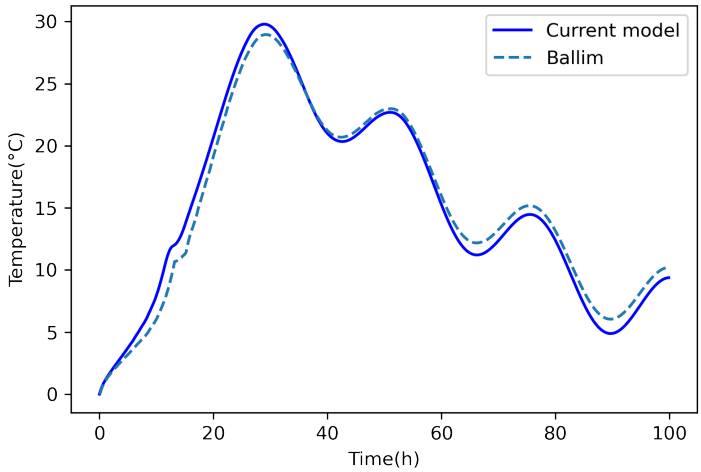


**Figure 5.2 :** Temperature difference between the side node and the centeral node in 2-D modeling

## 5.2 3-D Model validation

To demonstrate the effectiveness of the current model, it was used to simulate the results of an experiment conducted at the Bursa beton factory. The model was provided with input parameters as specified in Table 1. in this simulation the actual time-history temperature is used as ambient temperature which is depicted in figures 4.8, 4.9, and 4.10. The output of the model was then set side by side with the actual results of the experiment. It was observed that there was a high degree of similarity between the two, indicating that the model is capable of accurately predicting the temperature development profile within concrete.

The ability of the current model to predict the behavior of concrete is significant as it can be utilized in various scenarios such as construction projects. By accurately predicting the temperature profile of concrete, the model can help ensure the safety and stability of structures built using concrete. Moreover, the flexibility and extendibility of the model in Python provide ample opportunities to add new features and enhance its capabilities further.

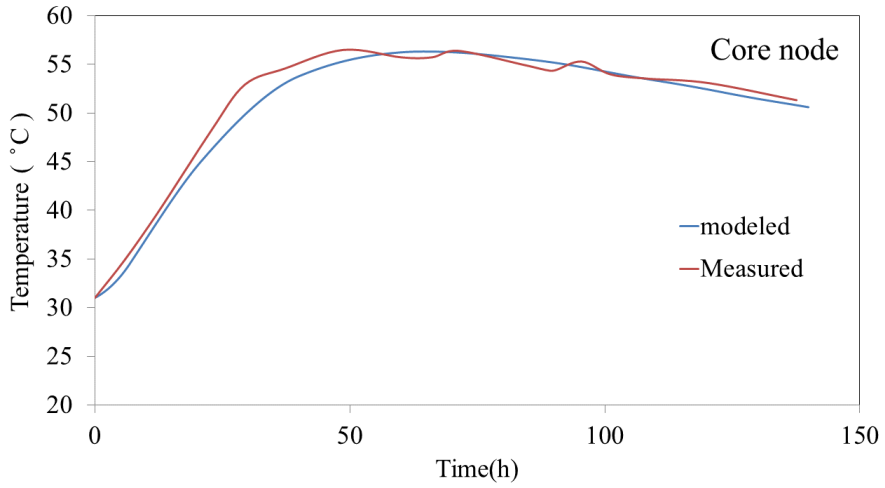


**Figure 5.3 :** Comparison between the central node temperature profile in the model and actual measurement in Bursa beton factory for Case1

The presented graphs depict a comparison between the predicted temperature profile and the actual measured temperature in the Bursa Beton factory. In all three cases(case

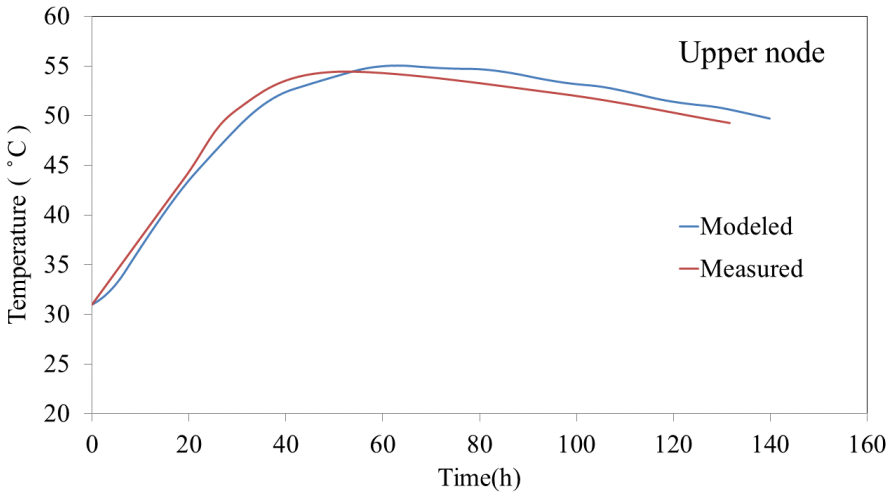


**Figure 5.4 :** Comparison between the upper node temperature profile in the model and actual measurement in Bursa beton factory for Case1

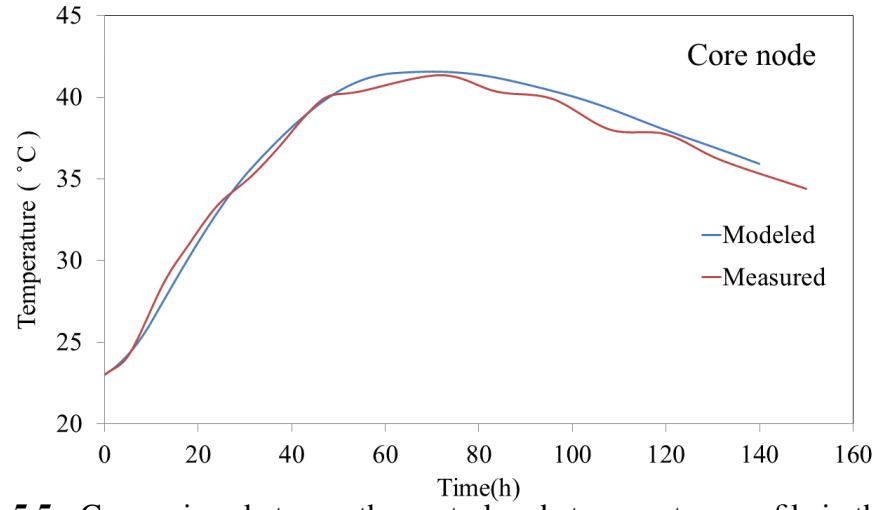


**Figure 5.5 :** Comparison between the central node temperature profile in the model and actual measurement in Bursa beton factory for Case7

1, case 7, and case 11), the results obtained from the model are satisfying, indicating that the model is performing well.

Furthermore, to enhance the credibility and reliability of the current model, an investigation was conducted on the experimental results of a concrete element with a volume of 1.8 cubic meters that was cast in West Virginia University in the United States. The performance of the current model was compared with the previous model used by the author, which employed ANSYS software and the finite element method to simulate temperature development within the element. However, the current model utilizes Python for simulation, which significantly reduces the modeling time and eliminates the need to import the element's shape into the software. The comparison

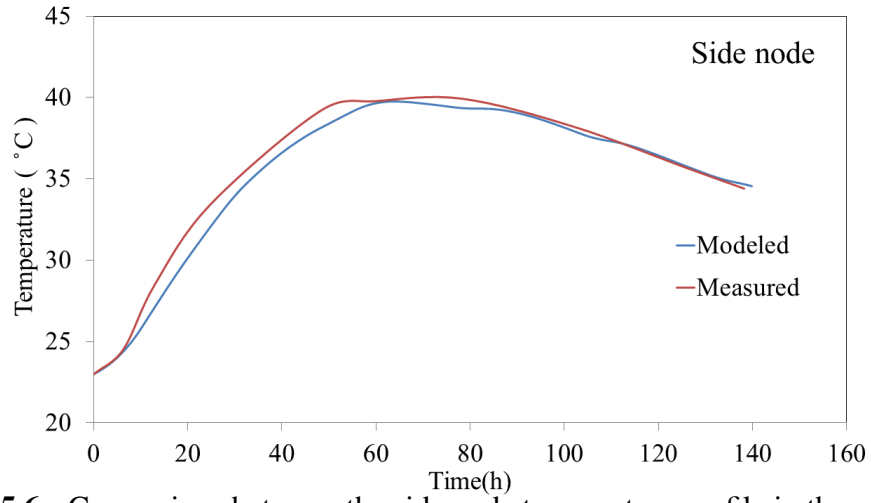


**Figure 5.6 :** Comparison between the side node temperature profile in the model and actual measurement in Bursa beton factory for Case7

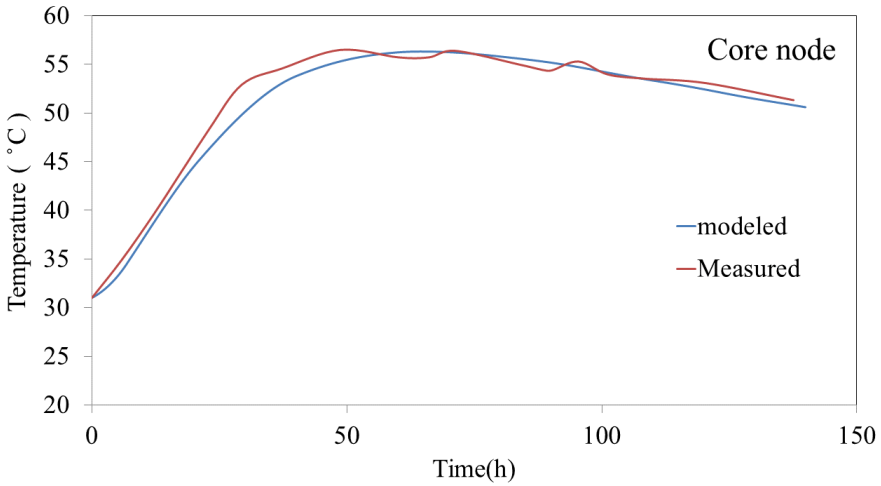


**Figure 5.7 :** Comparison between the central node temperature profile in the model and actual measurement in Bursa Beton factory for Case11

between the two models and the actual experimental data is presented in Figure 5.9 and Figure 5.10.

The graphical representations reveal that the current model, Lin's model, and the data collected from the project site exhibit similarities in both the central and side nodes. Moreover, the current model shows a slight improvement over Lin's model.

The present model, as discussed and illustrated in this chapter, is a reliable instrument for forecasting the temperature inside a concrete building. As a result, it is ideal for conducting sensitivity assessments on mass concrete.

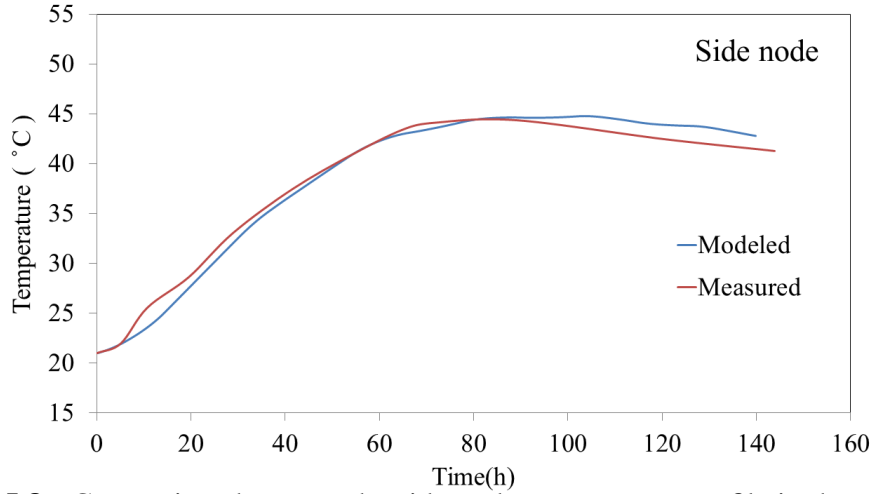


**Figure 5.8 :** Comparison between the side node temperature profile in the model and actual measurement in Bursa beton factory for Case11

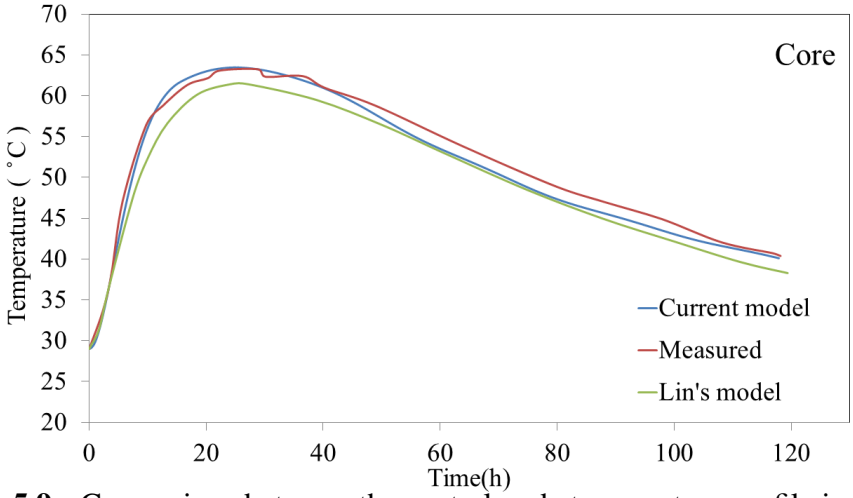


**Figure 5.9 :** Comparison between the central node temperature profile in the model and actual measurement and Lin's model

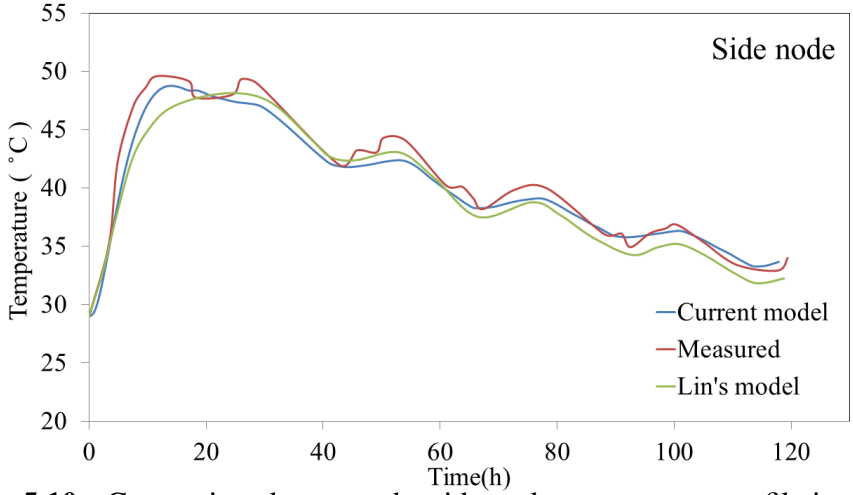


**Figure 5.10 :** Comparison between the side node temperature profile in the model and actual measurement and Lin's model

# 6. SENSITIVITY ANALYSIS

This chapter aims to conduct a sensitivity analysis to evaluate the impact of different parameters on the final result of thermal analysis. The analysis will begin by examining the influence of the percentage of supplementary cementitious material used in blended cement on the final result. Moreover, the effect of varying thermal properties, specifically the thermal conduction coefficient and specific heat capacity, with respect to the degree of hydration will be studied. Additionally, this chapter will investigate the impact of different input parameters, including the initial temperature and element size, on the final result.

Through this sensitivity analysis, we can gain a better understanding of how each input parameter contributes to the final outcome and which parameters have a more significant effect. This information can help optimize the thermal analysis process, resulting in more accurate and reliable predictions of the behavior of concrete structures under different thermal conditions. The model can aid researchers in comprehending which parameters require detailed information and which ones do not have a significant impact on the final outcome. Consequently, this information can assist researchers in designing efficient models that can save computation time.

## 6.1 Supplementary cementitious replacement level

In this section, the impact of varying replacement levels of supplementary cementitious materials on two critical parameters, the extreme temperature at the central node and the temperature difference between the central and side nodes, will be studied.

The investigation will begin by examining the temperature evolution in a concrete sample, using different percentages of cement replacement. Subsequently, the obtained results will be compared with those obtained from the ordinary Portland cement sample. This analysis aims to shed light on the influence of supplementary cementitious materials on the thermal performance of concrete.

An initial temperature of 20°C and an environmental temperature of 5°C are adopted for the investigation of thermal performance in concrete. This selection is in accordance with the standard guidelines that prohibit concrete pouring when the ambient temperature falls below 5°C. [48] Furthermore, a lower environmental temperature promotes greater temperature gradients between the core and side nodes of the concrete sample, which is a critical parameter that influences its thermal behavior, that's why 5°C is chosen for ambient temperature.

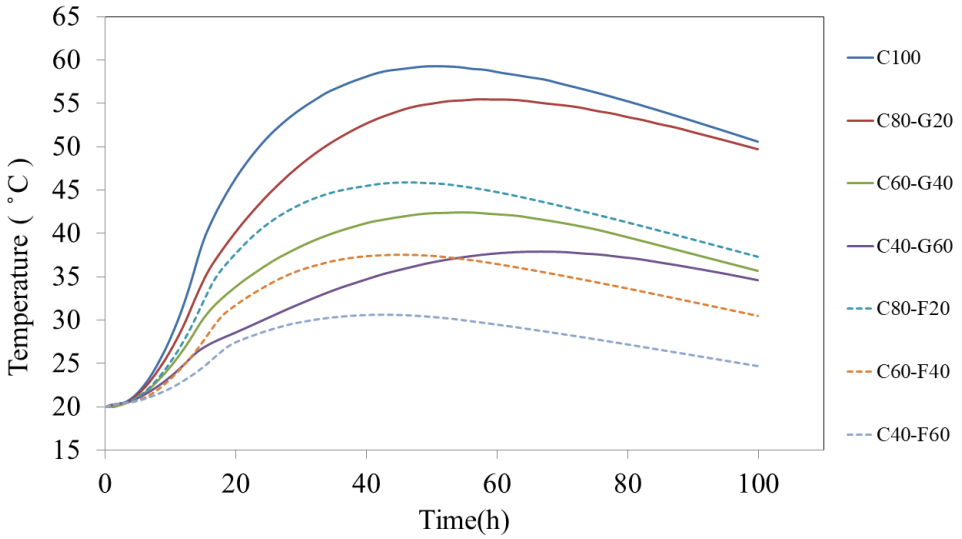


**Figure 6.1 :** Central node temperature profile with different percentages of cement replacement

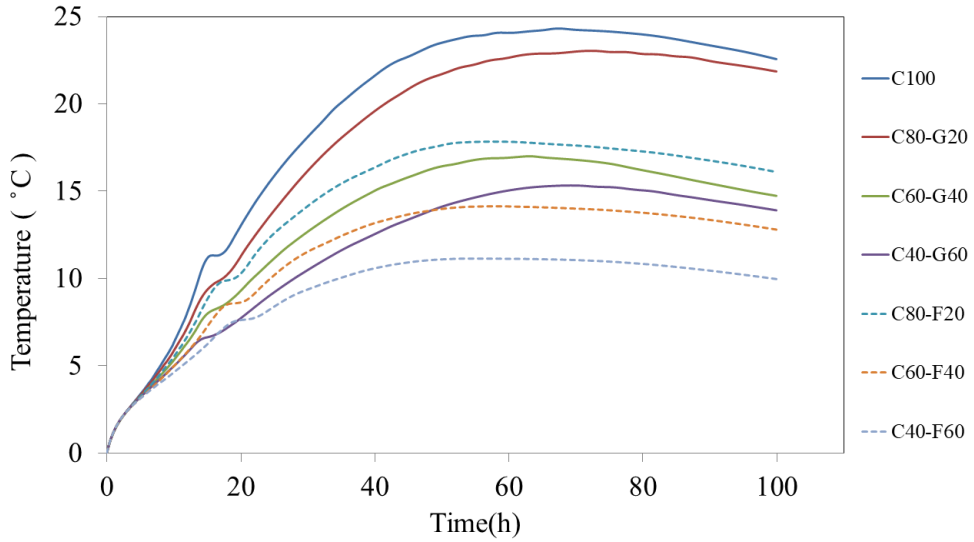


**Figure 6.2 :** Temperature difference between core and side node with different percentages of cement replacement

The figures 6.1 and 6.2 indicate that the incorporation of fly ash and ground blast furnace slag in concrete has notable effects on its thermal behavior. Specifically, the reduction of maximum temperature and temperature difference between the core and side nodes is more pronounced with fly ash compared to slag. For instance, replacing %20 of cement with fly ash can result in a reduction of maximum temperature and temperature difference by %22.53 and %26.57, respectively, whereas these reductions are only %6.37 and %5.19 with ground blast furnace slag. Moreover, the effect of slag is more significant in altering the time at which the sample reaches its maximum temperature, which is beneficial as it allows the concrete sufficient time to attain the appropriate tensile strength. These findings highlight the potential benefits of incorporating fly ash and slag in concrete for improving its thermal performance.

## 6.2 Thermal properties

As stated in sections 4.4.4.1 and 4.4.4.2, the thermal conductivity and specific heat capacity of a concrete element vary during the process of cement hydration, and this relationship is described by equations 4.24 and 4.26. In this investigation, we aim to assess the significance of considering this time-dependent variation for thermal properties in predicting the temperature of concrete elements.

To achieve this objective, we will analyze the impact of varying thermal properties on the final result for mass concrete element, with the size of $2.5m^2$, with different percentages of supplementary cementitious material, replacement percentages will be %0, %20 and %60. For this study, all of the other inputs are going to be considered constant such as ambient temperature, the same inputs as used in section 6.1 is going to be used, also 2-D modeling used for this investigation,

By conducting this study, we can determine which time-dependent variations in thermal properties affect the concrete element temperature development significantly, and which are neglectable.

Firstly, we will study the effect of the thermal conduction coefficient. Figures 6.4 and 6.3 demonstrate that the variation in the thermal conduction coefficient has a negligible impact on the maximum temperature at the central node of the concrete

element. The temperature differential between the side node and the central node, however, is slightly affected, especially when some cement is replaced with ground furnace slag. Overall, it is deemed acceptable to assume a fixed thermal conduction coefficient for mass concrete due to its minimal influence on the final outcome. The summary output is shown in Table 6.1.

The assumption of a fixed value for specific heat capacity can have a considerable impact on the final outcome, particularly in the case of using fly ash as a supplementary cementitious material. For example, replacing %20 of cement with fly ash and assuming a constant value for specific heat capacity can result in the maximum temperature exceeding the standard limit. However, considering a varying value for this parameter leads to a maximum temperature lower than the standard limit of 60°C. In contrast, using slag as a cement replacement material does not exhibit a significant difference in temperature gradient within the concrete element (Figure 6.3), and a fixed value for specific heat capacity can be assumed. Nevertheless, even for low percentages of slag replacement, assuming a constant value for this variable can still influence the final result of the maximum temperature, as depicted in Figure 6.4. So it is crucial to consider the varying specific heat capacity in the modelings. The summary output is shown in Table 6.2.

**Table 6.1 :** Value of max temperature and max Difference between side node and central node (K-var)

| | Mix | Max Difference | | Max temperature | |
|---|---|---|---|---|---|
| | | Fix | K-var | Fix | K-var |
| 1 | C100 | 27.46503 | 26.48222 | 66.6211 | 66.58074 |
| 2 | C80-G20 | 26.11343 | 24.74604 | 50.11906 | 50.06703 |
| 3 | C40-G60 | 16.74031 | 15.61166 | 32.26466 | 32.02657 |
| 4 | C80-F20 | 19.52453 | 18.98633 | 62.47089 | 61.98448 |
| 5 | C40-F60 | 11.875 | 11.34583 | 40.7318 | 39.92487 |

### 6.3 Size effect

To examine the impact of the concrete element size on the maximum temperature in the central node and the maximum temperature difference between the side node and

**Table 6.2 :** Value of max temperature and max Difference between side node and central node (C-var)

| | Mix | Max difference | | Max temperature | |
|---|---|---|---|---|---|
| | | Fix | C-var | Fix | C-var |
| 1 | C100 | 27.46503 | 24.30363 | 66.6211 | 59.23736 |
| 2 | C80-G20 | 26.11343 | 23.04055 | 62.47089 | 55.4632 |
| 3 | C40-G60 | 16.74031 | 15.33294 | 40.7318 | 37.89815 |
| 4 | C80-F20 | 19.52453 | 17.84382 | 50.11906 | 45.88713 |
| 5 | C40-F60 | 11.875 | 11.13214 | 32.26466 | 30.63431 |

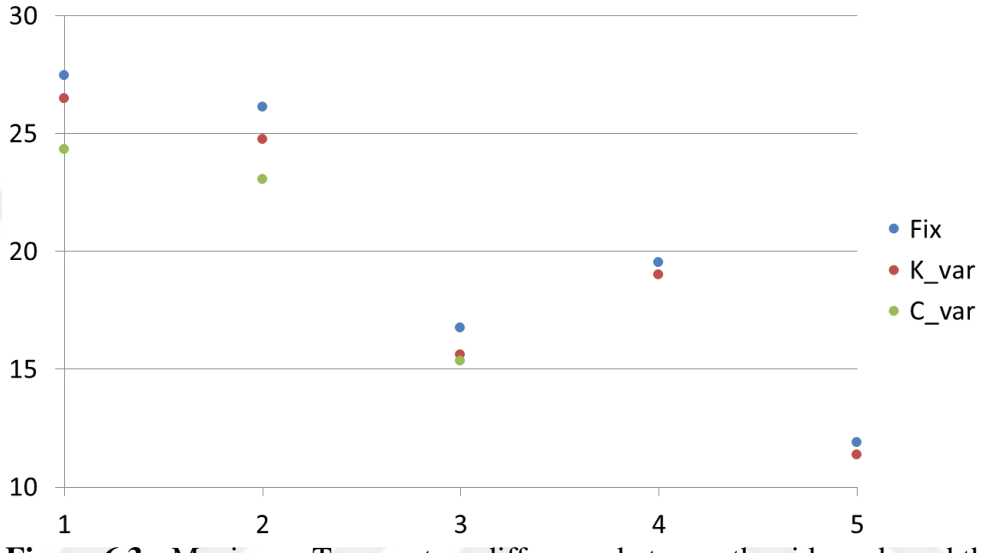


**Figure 6.3 :** Maximum Temperature difference between the side node and the central node

the core, three element sizes, $1m^2$, $1.5m^2$, and $3m^2$, were considered. The results of these analyses are presented in Table 6.3 and illustrated in Figure 6.5 and Figure 6.6.

To investigate how blended cement affects the sensitivity of the thermal behavior of concrete elements to changes in element size, three different types of mixtures mentioned in Table 6.3 were used.

**Table 6.3 :** Size effect sensitive analysis

| Case | Mixture | Max Temperature | | | | Max Temperature difference | | | |
|---|---|---|---|---|---|---|---|---|---|
| | | 1m3 | 1.5m3 | 3m3 | %change | 1m3 | 1.5m3 | 3m3 | %change |
| 1 | C100 | 39.32 | 49.17 | 65.25 | 65.95% | 9.73 | 17.74 | 35.78 | 267.73% |
| 2 | C60-G40 | 28.23 | 34.11 | 46.23 | 63.76% | 6.70 | 11.93 | 23.88 | 256.42% |
| 3 | C60-F40 | 26.24 | 31.58 | 39.68 | 51.22% | 6.49 | 10.63 | 19.66 | 202.93% |

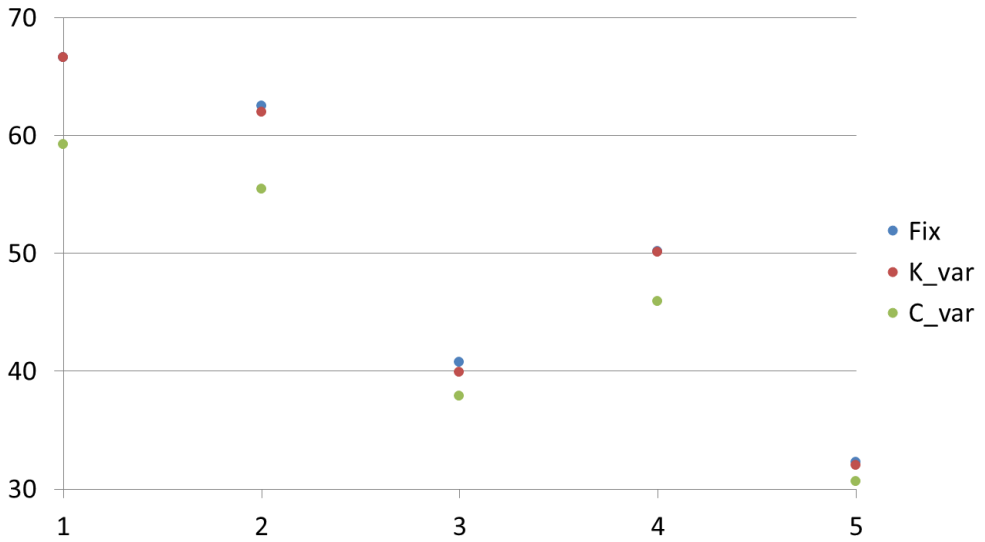


**Figure 6.4 :** Maximum Temperature in central node

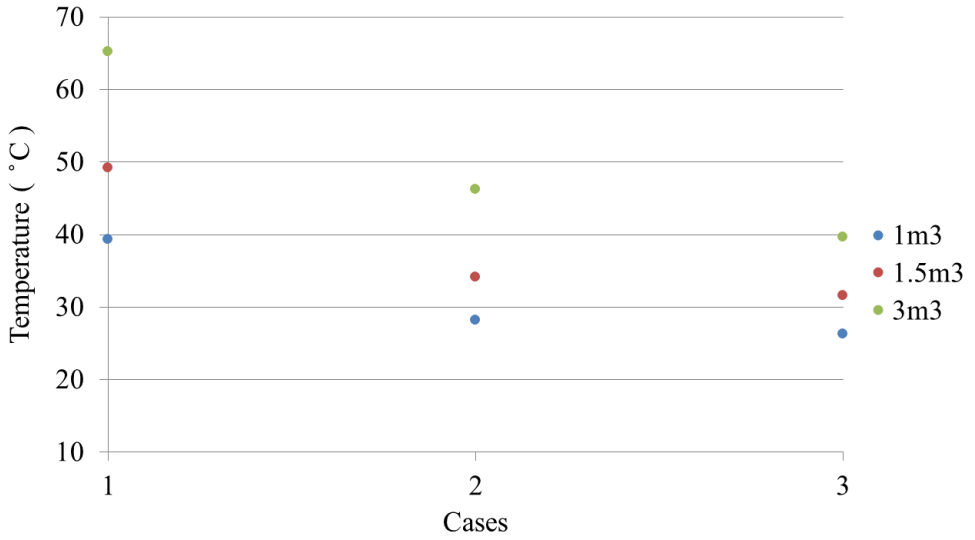


**Figure 6.5 :** Maximum Temperature in central node (Size effect)

The findings presented in Table 6.3 and the corresponding graphs reveal that increasing the element size leads to a rise in the maximum temperature in the core and temperature gradient, although this effect varies for different mixtures., when %100 Portland cement is used (case C100), the thermal behavior of the concrete element is highly sensitive to changes in element size. However, as the amount of supplementary cementitious materials (SCMs) in the blend increases, the sensitivity decreases.

## 6.4 Initial temperature

In this section, we will examine the impact of initial temperature on the final thermal analysis results using a 3-D model of the Bursa Beton factory (case 1). By keeping

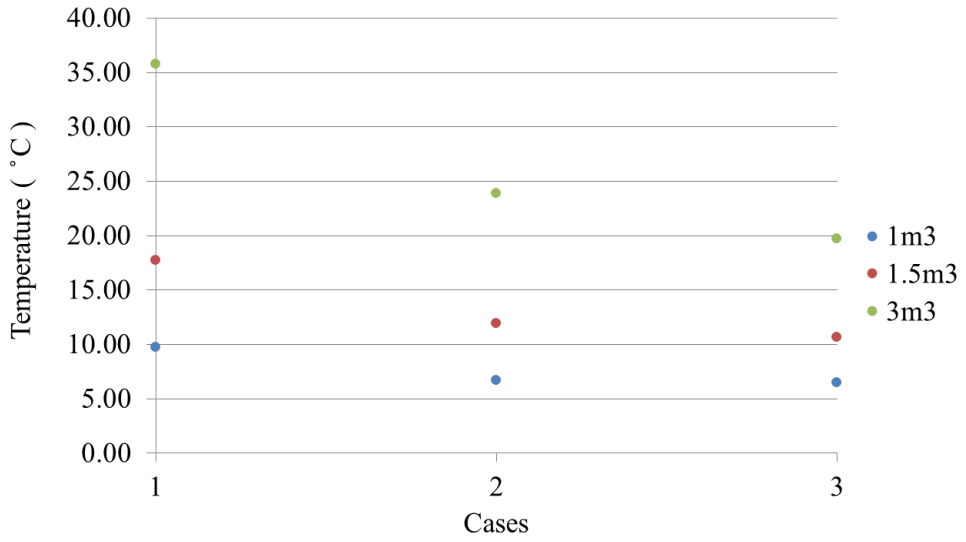


**Figure 6.6 :** Maximum Temperature difference between the side node and the central node (Size effect)

all inputs constant, we will investigate the effect of three different initial temperatures (10°C, 20°C, and 30°C) on the outcomes. the result for maximum temperature is depicted in Figure 6.7, also for the temperature differences between the core and side node it is shown in Figure6.8.

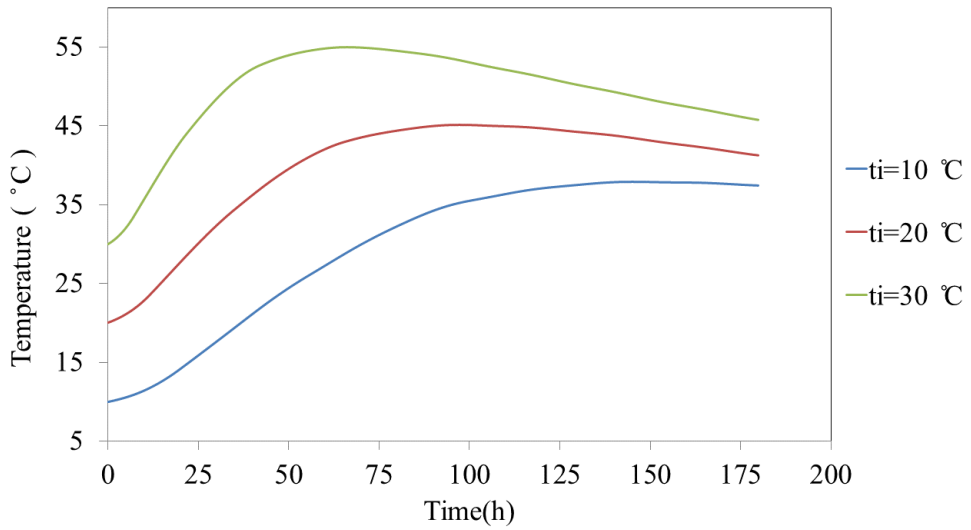


**Figure 6.7 :** The central temperature node with different initial temperatures

From Figures 6.7 and 6.8, it is evident that increasing the initial temperature results in a higher maximum temperature in the core, and the concrete reaches that point at a faster rate, at the same time, increasing the initial temperature leads to higher temperature gradient within the concrete element( this temperature difference it not that high because of using a thick layer of insulation in the experiment). Therefore,

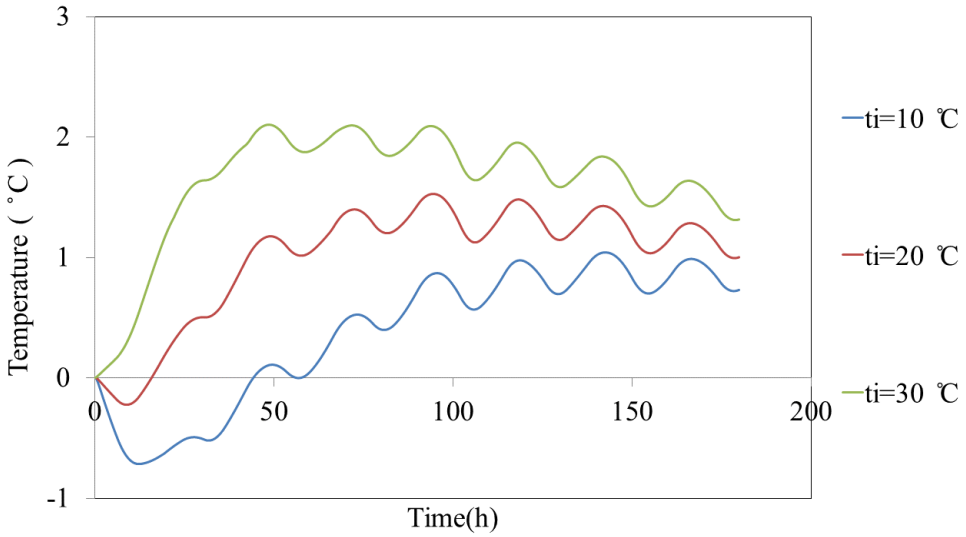


**Figure 6.8 :** Temperature differences between the central node and side node for different initial temperatures

reducing the initial temperature through methods such as pre-cooling can help mitigate the risk of cracking.

# 7. CONCLUSIONS

The modeling and evaluation of temperature development in mass concrete elements is crucial in civil engineering because it ensures the durability and safety of concrete structures. We suggested a unique forecast model for temperature development in mass concrete materials in this work. The model was created to be precise, efficient, and simple to use, with no sketching steps required, unlike modeling in ANSYS or ABAQUS.

The suggested model was validated using both 2D and 3D modeling, and its outcomes were compared to those of existing 2-D and 3-D models like Ballims and Lin. The comparison proved the suggested model's acceptable accuracy in forecasting temperature development in mass concrete components. Furthermore, the 3D modeling was confirmed by testing at the Bursa Beton facility. The validation studies showed the proposed model accurately predicted temperature development in real-world circumstances.

Furthermore, this study also included a sensitivity analysis to investigate the impact of element size and the level of supplementary cementitious material (SCM) replacement on the precision of the model's predictions. The findings revealed that the employment of SCMs had a substantial impact on temperature growth in mass concrete elements, including the maximum temperature achieved in the central node and the time when the peak temperature is reached in the core node. The analysis also revealed the effect of initial temperature on the maximum temperature and the temperature difference between the core and the side nodes in the concrete elements. These findings provide valuable insights for engineers and researchers in the concrete industry, enabling them to optimize the design and construction of concrete structures for enhanced performance and durability.

1-The current Python model, which works well in both 2-D and 3-D versions. For those who are interested in this subject, it can be utilized as an initial prediction model for predicting temperature within the concrete element.

2-The study discovered that the thermal behavior of concrete can be dramatically affected by the addition of fly ash and ground blast furnace slag. Compared to slag, fly ash has a more pronounced impact on lowering the maximum temperature and the temperature differential between the core and side nodes. Slag, on the other hand, can help concrete reach the proper tensile strength by modifying the period at which it reaches its maximum temperature, which has a higher impact. The results generally imply that adding fly ash and slag to concrete can enhance its thermal performance.

3- In order to make precise predictions about the thermal properties of concrete, it is crucial to take the variance in specific heat capacity into consideration. On the other hand, since it barely affects the outcome, using a set value for the thermal conductivity coefficient makes sense. Therefore, rather than concentrating exclusively on the conductivity coefficient, researchers should prioritize finding ways to raise the concrete's specific heat capacity. Overall, these results point to a more significant role for specific heat capacity in the thermal management of concrete.

4- According to the study, the maximum temperature in the core and the temperature gradient both rise in direct proportion to the size of the concrete element, though to a different extent depending on the concrete mixture. When using only Portland cement, changes in element size have a significant impact on how the concrete behaves thermally. However, as the mixture's supplementary cementitious materials (SCMs) content increases, the sensitivity declines.

5-When the initial temperature of a concrete element is raised, the core reaches a higher maximum temperature and it reaches to that point more quickly, and the temperature differential inside the concrete worsens. As a result, there is a higher chance of cracking. Utilizing pre-cooling procedures to reduce the starting temperature is a successful method of reducing this danger.

6- The microclimate can have a considerable effect on the temperature profile of mass concrete. for a comprehensive investigation, the microclimate should be analyzed and the wind speed and solar loading should be obtained.

## REFERENCES


[1] **Liu, L.**, **Ouyang, J.**, **Li, F.**, **Xin, J.**, **Huang, D. and Gao, S.** (2018). Research on the crack risk of early-age concrete under the temperature stress test machine, *Materials*, *11*(10), 1822.

[2] **Schindler, A.K.** (2002). *Concrete hydration, temperature development, and setting at early-ages*, The University of Texas at Austin.

[3] **Neville, A.M.** *et al.* (1995). *Properties of concrete*, volume 4, Longman London.

[4] **Mills, R.** (1966). Factors influencing cessation of hydration in water cured cement pastes, *Highway Research Board Special Report*, (90).

[5] **Fitzgibbon, M.E.** (1976). Thermal cracking in mass concrete, *ACI Journal Proceedings*, *73*(12), 625–630.

[6] **Ballim, Y.** (2004). A numerical model and associated calorimeter for predicting temperature profiles in mass concrete, *Cement and Concrete Composites*, *26*(6), 695–703.

[7] **Azenha, M.** (2004). Behaviour of concrete at early ages. Phenomenology and thermo-mechanical analysis, *MSc Thesis, Faculty of Engineering of the Univeristy of Porto*.

[8] **Kosmatka, S.H.**, **Kerkhoff, B.**, **Panarese, W.C.**, **MacLeod, N.F. and McGrath, R.J.** (2002). Design and control of concrete mixtures, 7th Canadian Edition, *Cement Association of Canada, Ottawa, Canada*.

[9] **Committee, A.** *et al.* (2005). ACI 207.1 R-05—Guide to Mass Concrete, *American Concrete Institute: Farmington Hills, MI, USA*, 30.

[10] **Nawy, E.G.** (2008). *Concrete construction engineering handbook*, CRC press.

[11] **Erdoğan, Y. and Türkmen, İ.** (2016). Mass concrete temperature control in Turkey: A review, *Journal of Building Engineering*, *8*, 152–158.

[12] **Lin, Y. and Chen, H.L.** (2015). Thermal analysis and adiabatic calorimetry for early-age concrete members, *Journal of Thermal Analysis and Calorimetry*, *122*, 937–945.

[13] **Lange, D. and Altoubat, S.** (2003). *Early Thermal Changes, Early Age Cracking in Cementitious Systems. Report of RILEM Technical Committee 181-EAS*.

[14] **Springenschmid, R. and Breitenbücher, R.** (1998). Influence of constituents, mix proportions and temperature on cracking sensitivity of concrete, *Prevention of Thermal Cracking in Concrete at Early Ages*, *15*, 40.

[15] **D Aloia, L.** (2003). Early age kinetics: Activation energy, maturity and equivalent age, *RILEM REPORT*, 127–148.

[16] **Mindess, S.** (1981). Concrete, *Prentice Hall, New Jersey*.

[17] **Association, C.S.** (2019). *CSA A3000-19 Cementitious materials compendium*, Standard, section 4.1.1.1, pages 4-4 to 4-5.

[18] **Douglas, E.**, **Elola, A. and Malhotra, V.M.** (1990). CHARACTERIZATION OF GROUND GRANULATED BLAST-FURNACE AND FLY ASHES AND THEIR HYDRATION IN PORTLAND CEMENT BLENDS, *Cement, concrete and aggregates*, *12*(1).

[19] **Bogue, R.** (1955). *Chemistry of Portland Cement*, Reinhold, New York.

[20] **Schindler, A.K. and Folliard, K.J.** (2005). Heat of hydration models for cementitious materials, *ACI materials journal*, *102*(1), 24.

[21] **Schindler, A.K. and Folliard, K.J.** (2003). Influence of supplementary cementing materials on the heat of hydration of concrete, *Advances in Cement and Concrete IX Conference, Copper Mountain Conference Resort in Colorado*, Citeseer.

[22] **ASTM International** (2005). *Standard Specification for Portland Cement*, ASTM International, West Conshohocken, PA, 2005 edition, `https://doi.org/10.1520/C0150-05`.

[23] **CEN** (2003). EN 196-9 - Methods of testing cement. Heat of hydration. Semi-adiabatic calorimetry, **European Standard EN 196-9**, Comité Européen de Normalisation, `https://doi.org/10.3403/30061492u`.

[24] **Morabito, P.** (1998). Methods to determine the heat of hydration of concrete, *RILEM REPORT*, 1–25.

[25] **McIntosh, J.** (1949). Electrical curing of concrete, *Magazine of Concrete Research*, *1*(1), 21–28.

[26] **Saul, A.** (1951). Principles underlying the steam curing of concrete at atmospheric pressure, *Magazine of Concrete Research*, *2*(6), 127–140.

[27] **Carino, N.J.** (1984). The Maturity Method: Theory and Application, *Journal of Cement, Concrete, and Aggregates*, *6*(2), 61–73.

[28] **D'Aloia, L.** (2003). Early Age Kinetics: Activation Energy, Maturity and Equivalent Age, ***A. Bentur**, editor, Early Age Cracking in Cementitious Systems - Report of RILEM Technical Committee 181-EAS*, RILEM Publications S.A.R.I., Bagneux.

[29] **Copeland, L.**, **Kantro, D. and Verbeck, G.** (1962). Paper IV–3. Chemistry of Hydration of Portland Cement, *Chemistry of Cement: Proceedings of the Fourth International Symposium, Washington, 1960, Symposium Held October 2-7, 1960 at the National Bureau of Standards, Washington, DC*, volume 1, US Government Printing Office, p.429.

[30] **Hansen, P.F. and Pedersen, E.J.** (1977). Maturity computer for controlled curing and hardening of concrete, **Technical Report**.

[31] **Glasstone, S.**, **Laidler, K.J. and Eyring, H.** (1941). *The theory of rate processes: the kinetics of chemical reactions, viscosity, diffusion and electrochemical phenomena*, McGraw-Hill.

[32] **Carino, N.J. and Lew, H.S.**, (2001). The maturity method: from theory to application, Structures 2001: A structural engineering odyssey, pp.1–19.

[33] **Van Breugel, K.** (1998). Prediction of temperature development in hardening concrete, *Prevention of thermal cracking in concrete at early ages*, *15*, 51–75.

[34] **Pane, I. and Hansen, W.** (2005). Investigation of blended cement hydration by isothermal calorimetry and thermal analysis, *Cement and concrete research*, *35*(6), 1155–1164.

[35] **De Schutter, G. and Taerwe, L.** (1995). General hydration model for Portland cement and blast furnace slag cement, *Cement and Concrete Research*, *25*(3), 593–604.

[36] **De Schutter, G.** (1999). Hydration and temperature development of concrete made with blast-furnace slag cement, *Cement and concrete research*, *29*(1), 143–149.

[37] **301, A.C.** (2005). *Specifications for Structural Concrete*, American Concrete Institute.

[38] **Gajda, J. and Vangeem, M.** (2002). Controlling temperatures in mass concrete, *Concrete international*, *24*(1), 58–62.

[39] (2014). *TS 13515, "TS EN 206'nın Uygulamasına Yönelik Tamamlayıcı Standard"*, Turkish Standards Institute.

[40] **Østergaard, L.**, **Stang, H. and Olesen, J.F.**, (2002). Time-dependent fracture of early age concrete, Non-Traditional Cement and Concrete, Brno University of Technology, pp.394–408.

[41] **Rastrup, E.** (1954). Heat of hydration in concrete, *Magazine of concrete research*, *6*(17), 79–92.

[42] **Kim, K.H.**, **Jeon, S.E.**, **Kim, J.K. and Yang, S.** (2003). An experimental study on thermal conductivity of concrete, *Cement and concrete research*, *33*(3), 363–371.

[43] **De Schutter, G.** (2002). Finite element simulation of thermal cracking in massive hardening concrete elements using degree of hydration based material laws, *Computers & Structures*, *80*(27-30), 2035–2042.

[44] **Ruiz, J.**, **Schindler, A.K.**, **Rasmussen, R.**, **Nelson, P. and Chang, G.** (2001). Concrete temperature modeling and strength prediction using maturity concepts in the FHWA HIPERPAV software, *Seventh International Conference on Concrete Pavements. The Use of Concrete in Developing Long-Lasting Pavement Solutions for the 21st CenturyInternational Society for Concrete Pavements*, volume 1.

[45] **Schutter, G.** (2001). *Thermal properties. Early age cracking in cementitious systems. Report 25, A. Bentur*.

[46] **Bentz, D.** (2007). Transient plane source measurements of the thermal properties of hydrating cement pastes, *Materials and structures*, *40*(10), 1073–1080.

[47] **Cervera, M.**, **Faria, R.**, **Oliver, J. and Prato, T.** (2002). Numerical modelling of concrete curing, regarding hydration and temperature phenomena, *Computers & structures*, *80*(18-19), 1511–1521.

[48] **Institute, A.C.** (2016). ACI 306R-16: Guide to Cold Weather Concreting, **Technical Report 306R-16**.

**APPENDICES**

**APPENDIX A :** Bursa Beton factory Experiment result
**APPENDIX B :** Thermal properties sensitive analysis results

**APPENDIX A :** Bursa Beton factory Experiment result

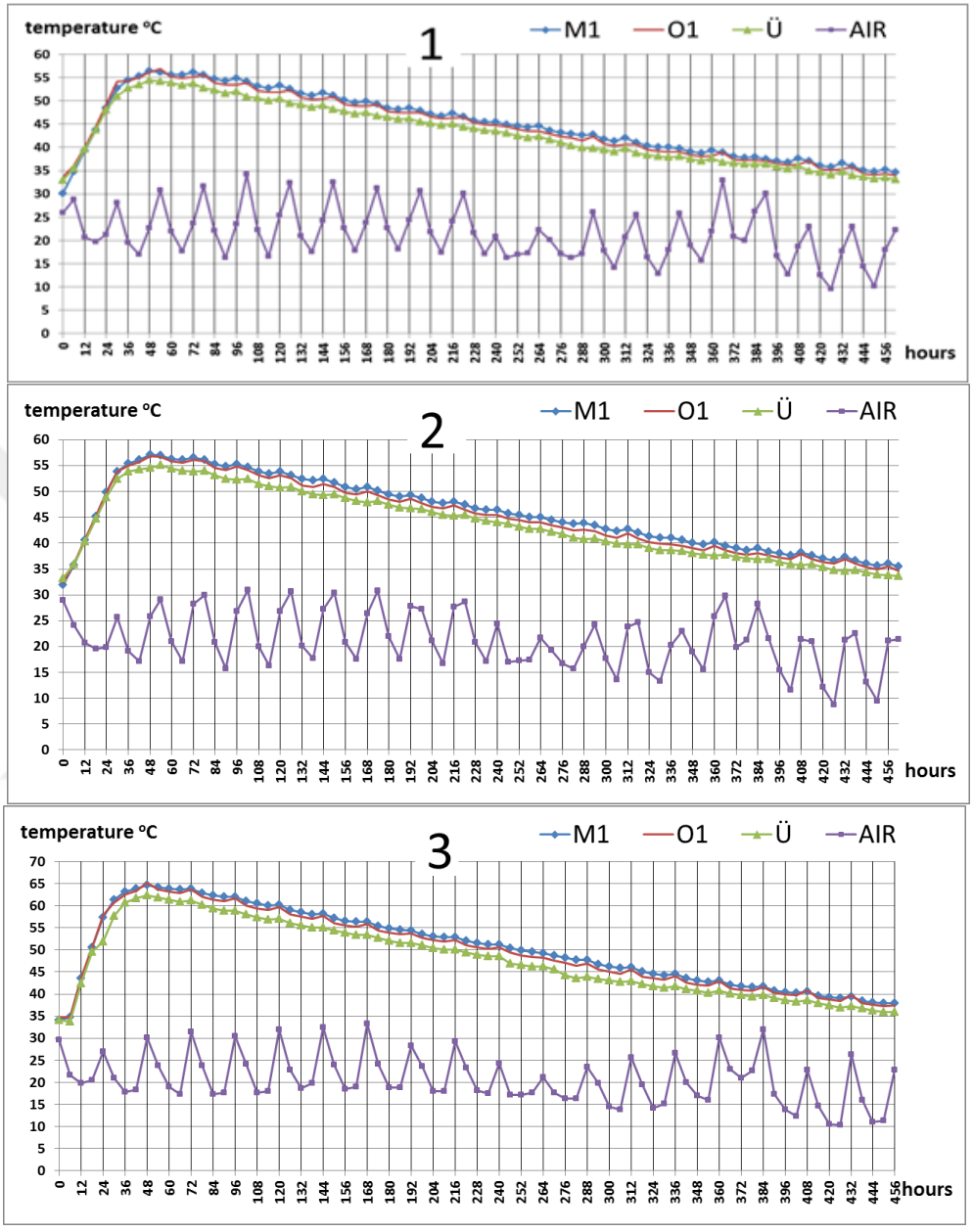


**Figure A.1 :** Phase1 Temperature development

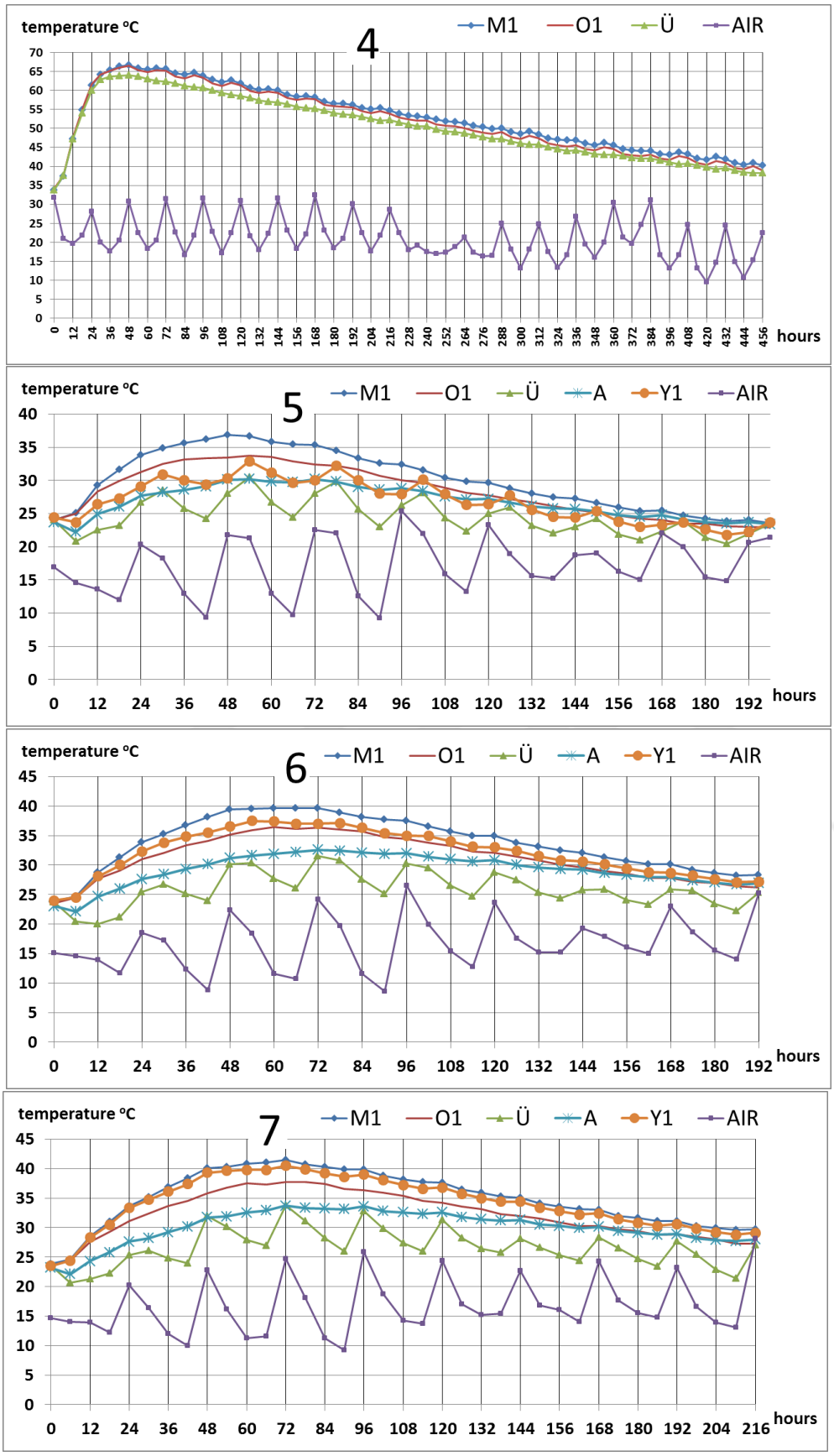


**Figure A.2 :** Phase 1 and 2 Temperature development

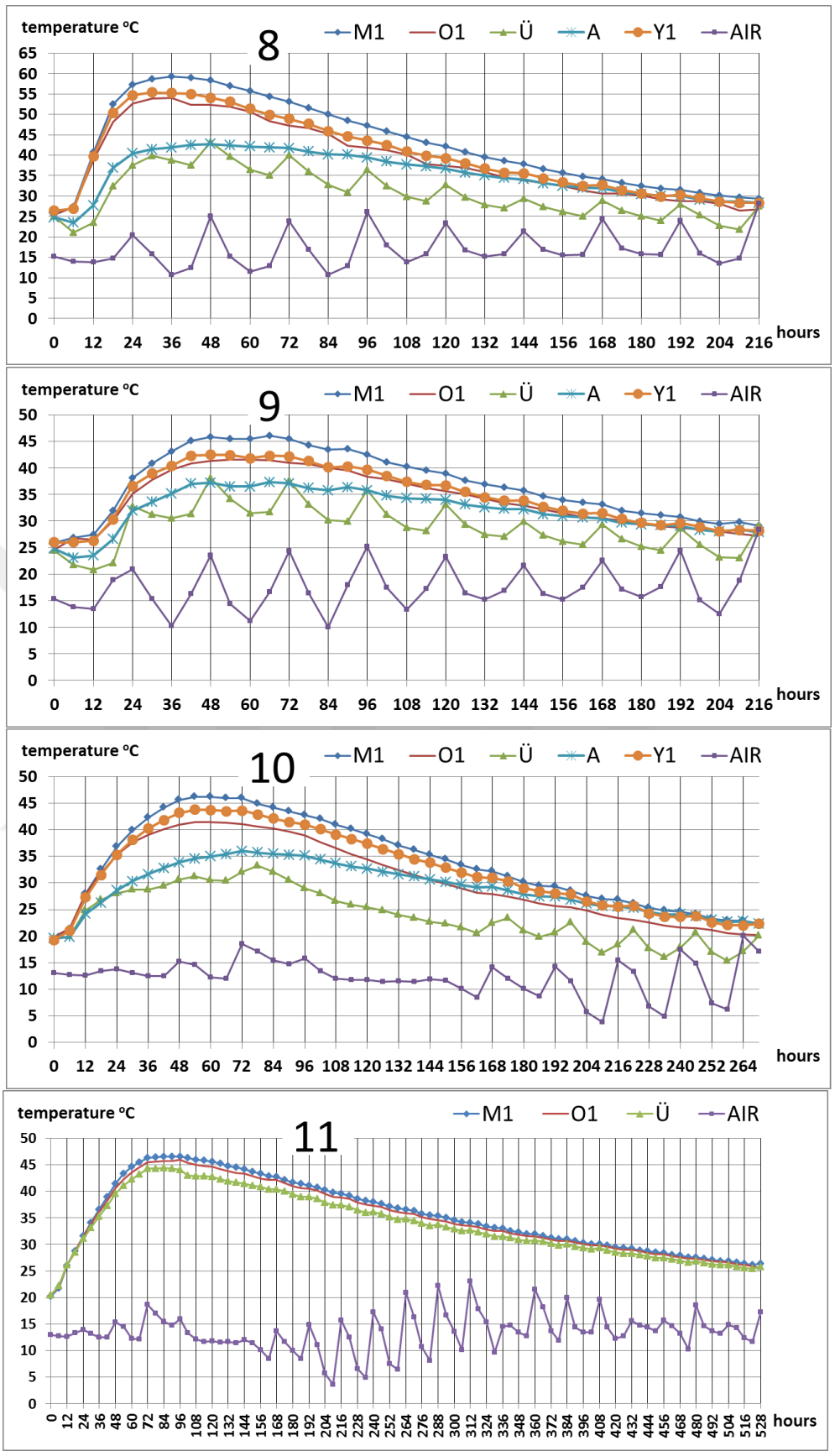


**Figure A.3 :** Phase2 and 3 Temperature development

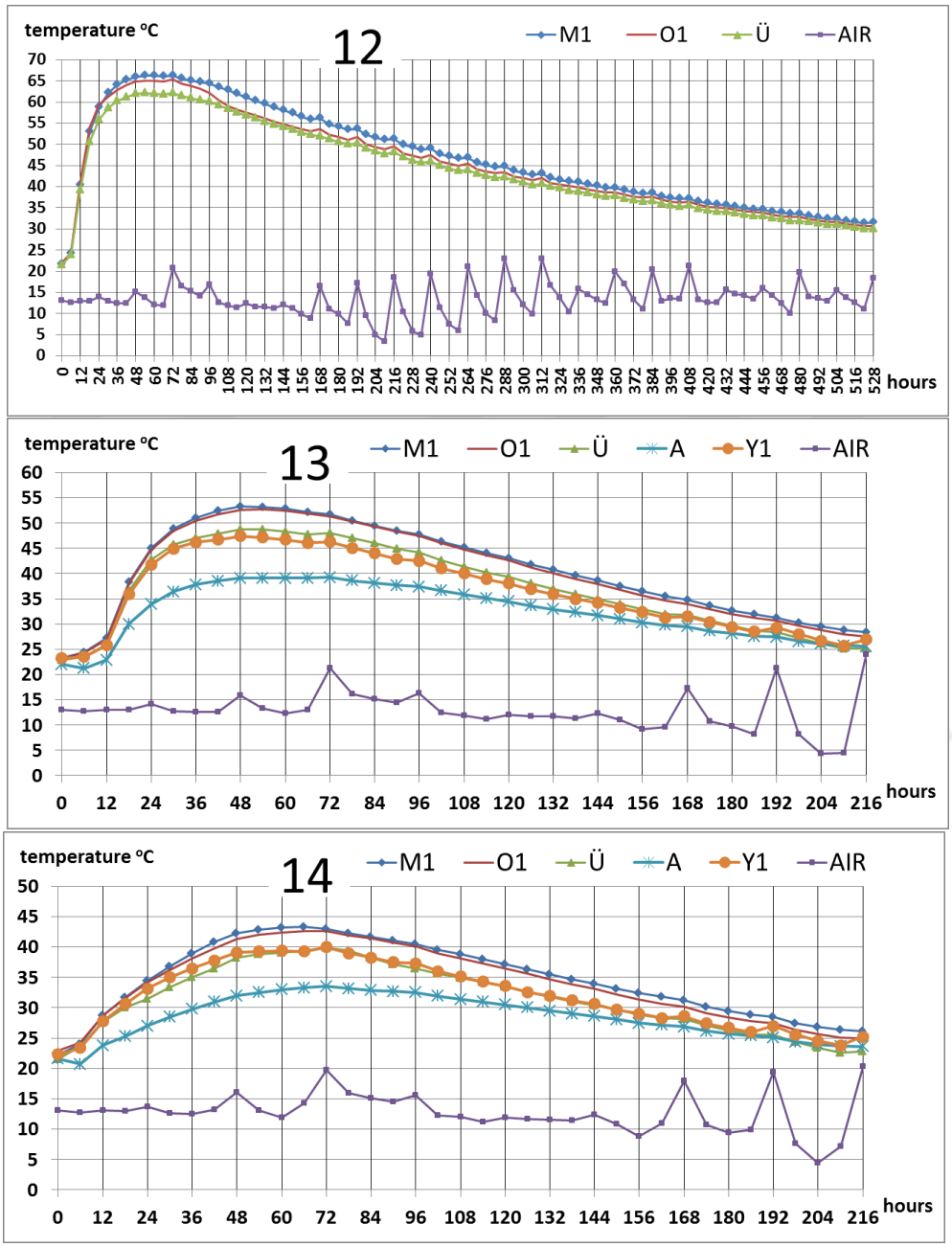


**Figure A.4 :** Phase3 Temperature development

**APPENDIX B :** Thermal properties sensitive analysis results

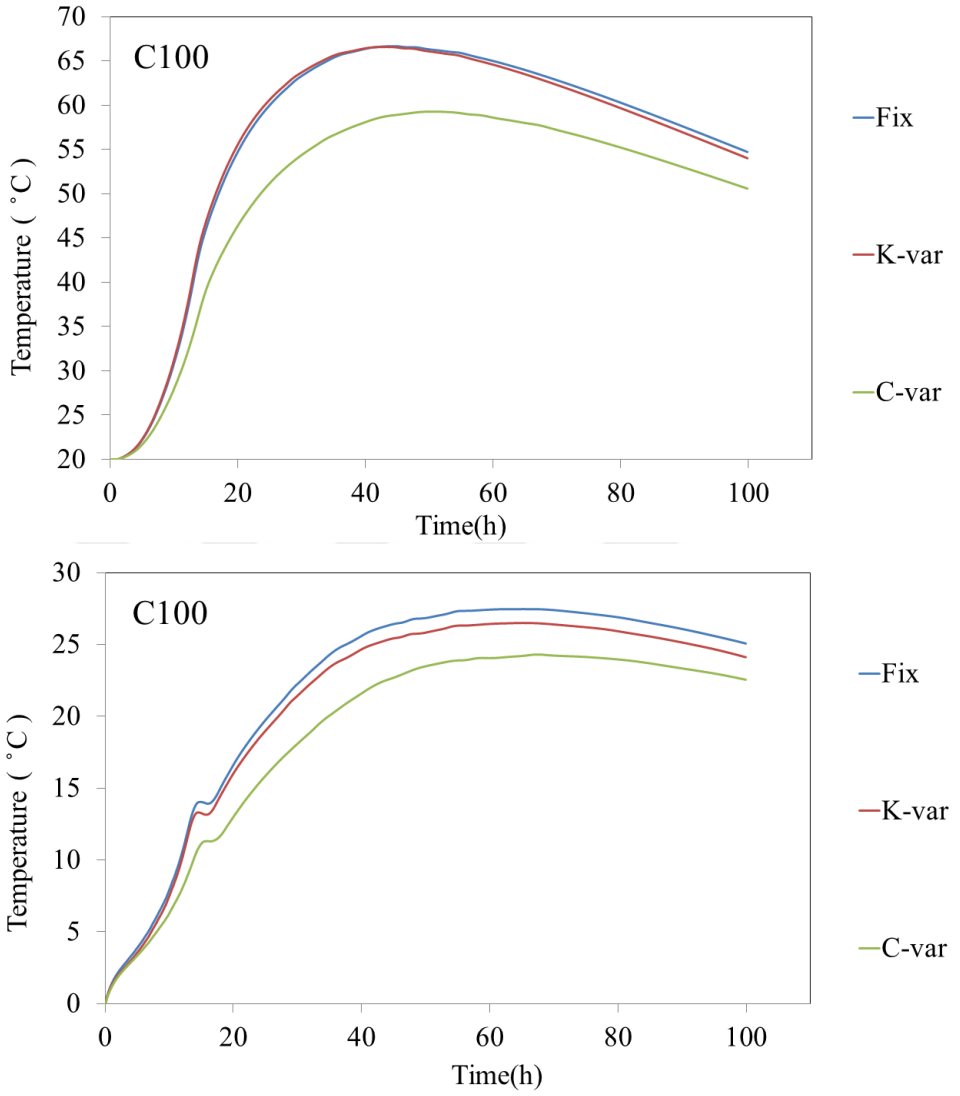


**Figure B.1 :** C100 Thermal properties sensitive analysis results

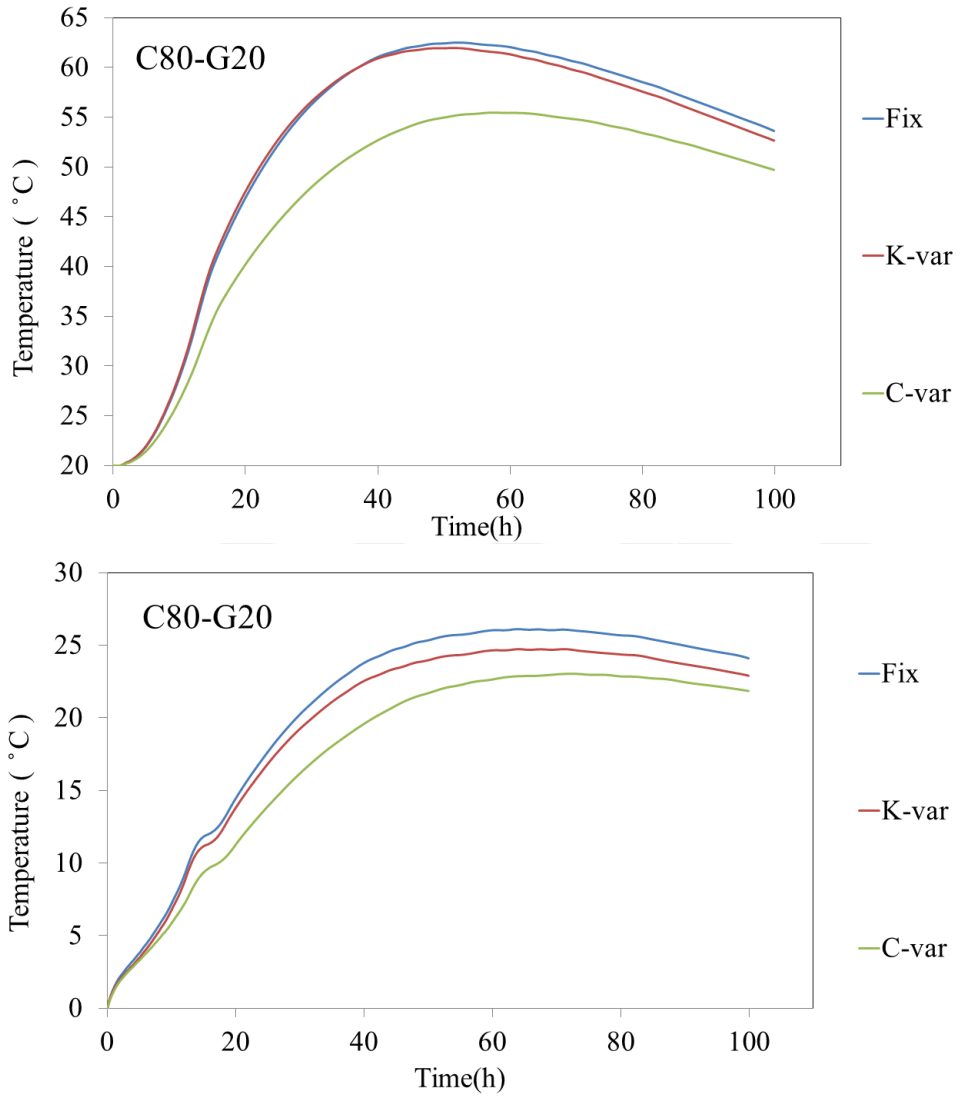


**Figure B.2 :** C80-G20 Thermal properties sensitive analysis results

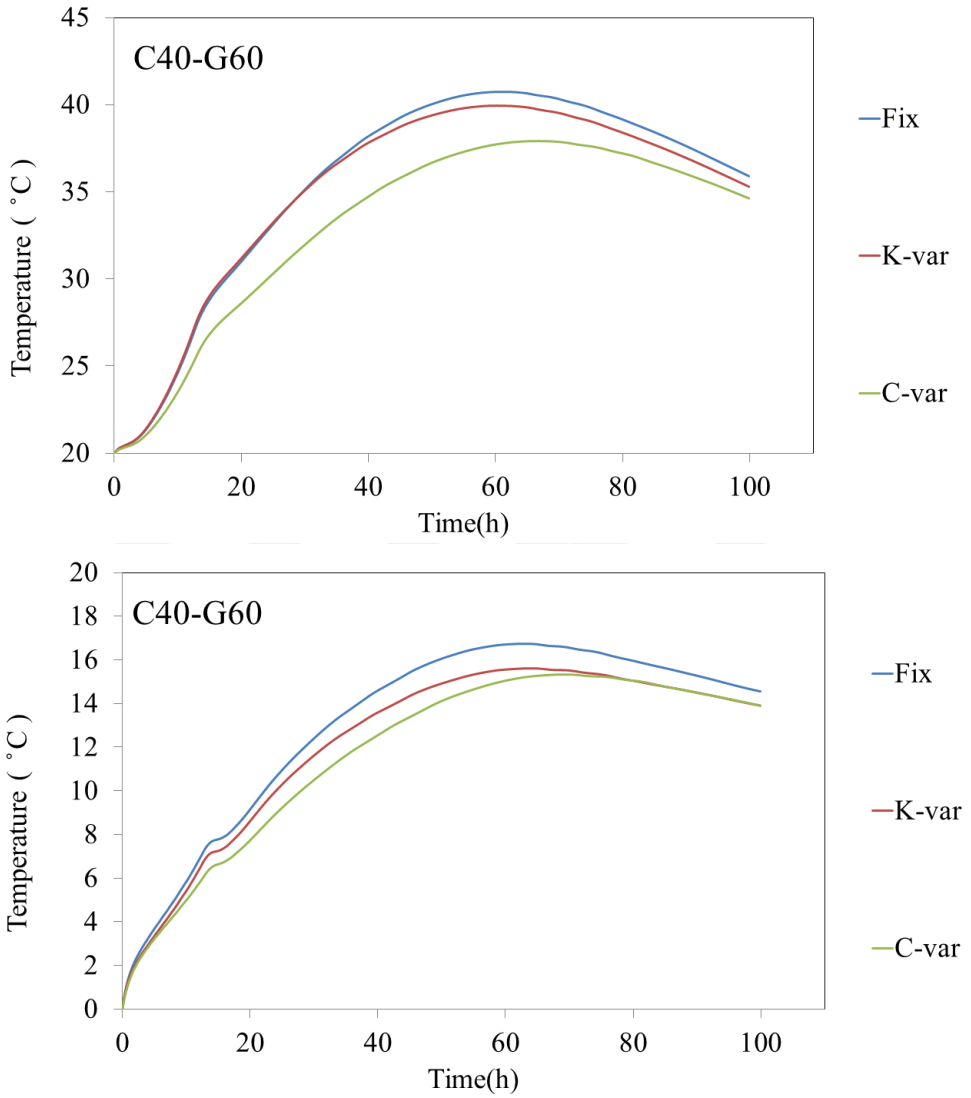


**Figure B.3 :** C40-G60 Thermal properties sensitive analysis results

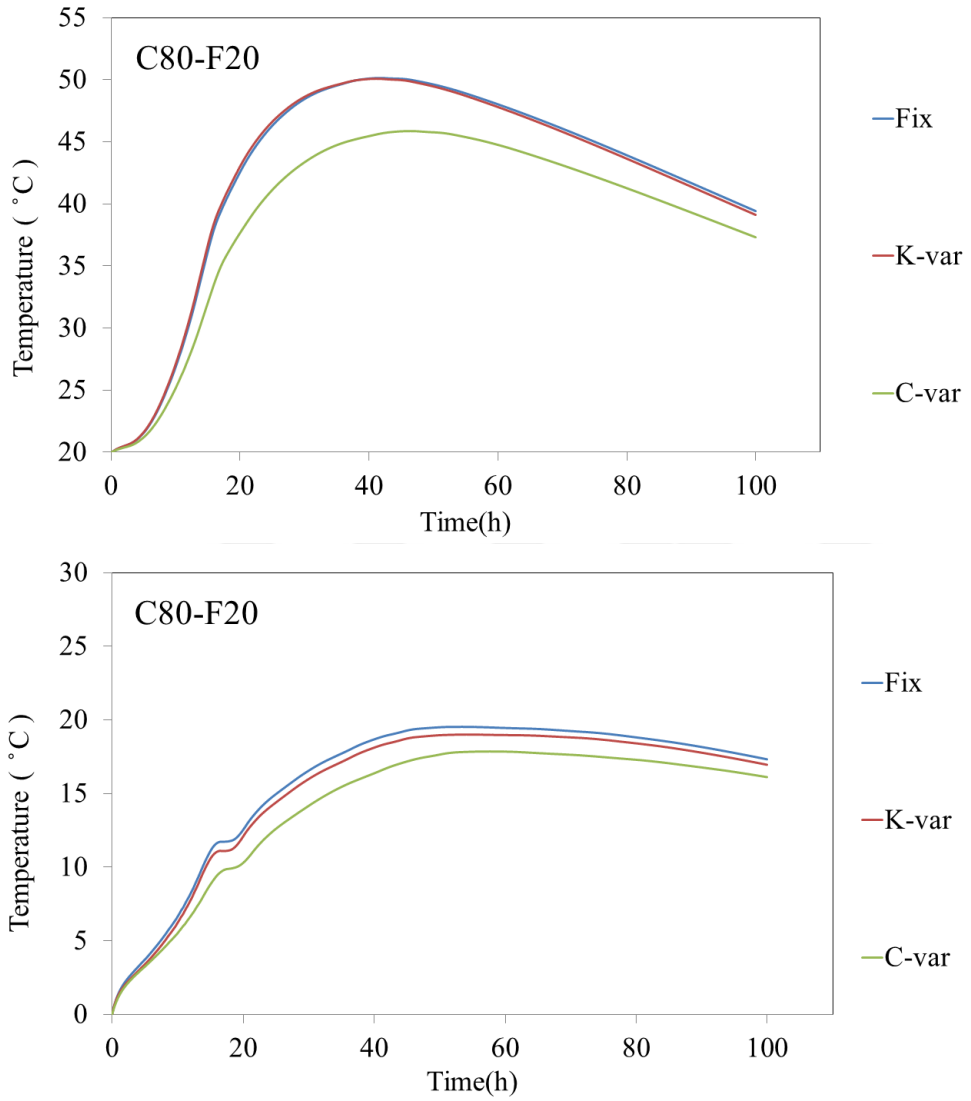


**Figure B.4 :** C80-F20 Thermal properties sensitive analysis results

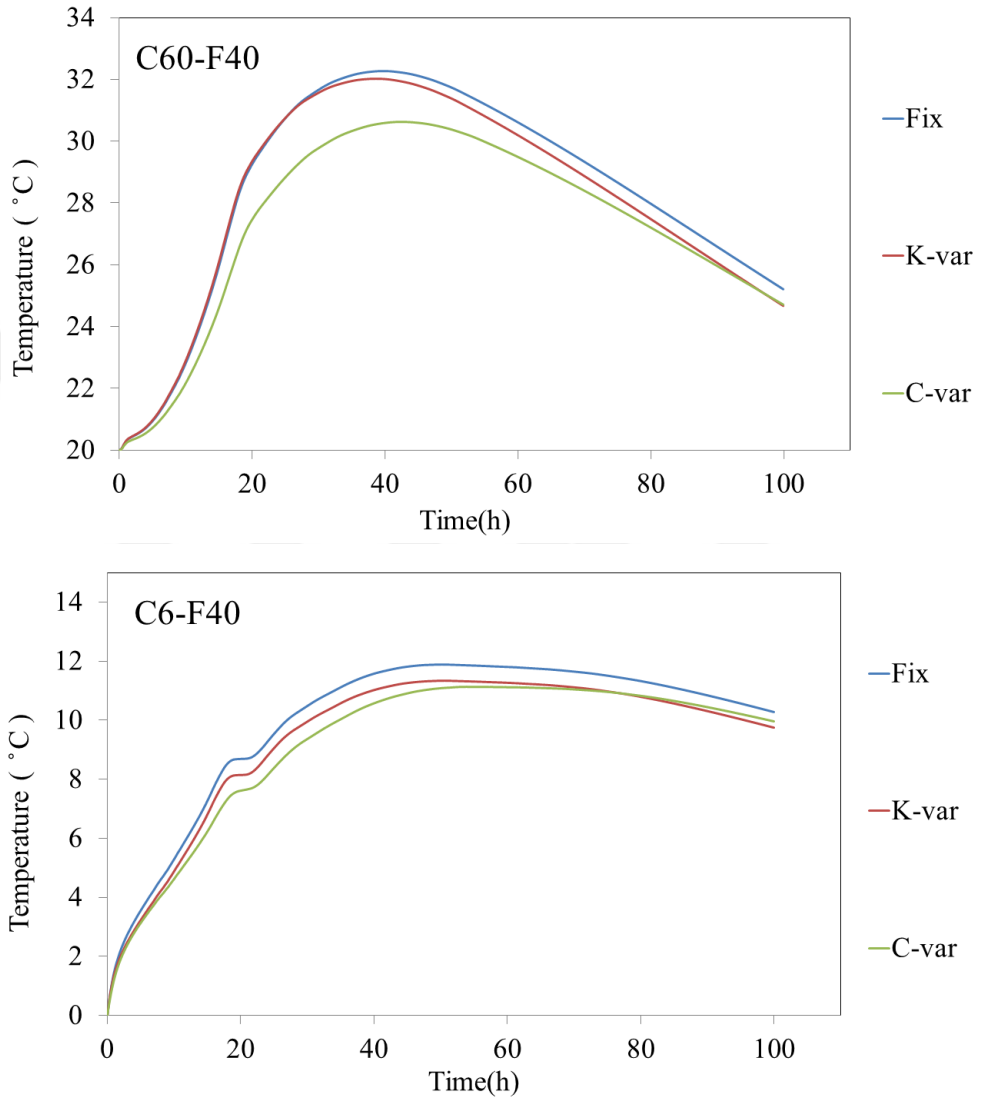


**Figure B.5 :** C40-F60 Thermal properties sensitive analysis results

## CURRICULUM VITAE

**Name SURNAME:** Farzad DANAEI

**EDUCATION:**

- **B.Sc.:** 2015, Univeristy of Tabriz, Civil Engineering, Civil Engineering

**PROFESSIONAL EXPERIENCE AND REWARDS:**

- Master's GPA: 4 out of 4

**PUBLICATIONS, PRESENTATIONS AND PATENTS ON THE THESIS:**

- **Danaei F.**, Ykkaya Y. (2023). Sensitivity Analysis of the Thermal Properties in Early Age Modeling of Mass Concrete *fib Symposium 2023,* june 5-7, 2023 Istanbul, Turkey. (Article Instance)
- **Danaei F.**, Ykkaya Y. (2023). 3-D Modeling the Thermal Behavior of Mass Concrete using Finite Volume Method *2nd INTERNATIONAL GRADUATE RESEARCH SYMPOSIUM IGRS'23* may 16-18, 2023 Istanbul, Turkey. (Presentation Instance)